NAVAL POSTGRADUATE SCHOOL
Monterey, California

AD-A245 144

DTIC
ELECTE
JAN 3 0 1992
S D
D

THESIS

COMPUTATIONAL UNSTEADY FLOW DYNAMICS:

OSCILLATING FLOW ABOUT A CIRCULAR CYLINDER

by

David R. Gordon

December, 1991

Thesis Advisor: T. Sarpkaya

Approved for public release; distribution is unlimited.

92-02385

92 1 29 068

REPORT DOCUMENTATION PAGE

1a. REPORT SECURITY CLASSIFICATION UNCLASSIFIED	1b. RESTRICTIVE MARKINGS

2a. SECURITY CLASSIFICATION AUTHORITY	3. DISTRIBUTION/AVAILABILITY OF REPORT
2b. DECLASSIFICATION/DOWNGRADING SCHEDULE	Approved for public release; distribution is unlimited

4. PERFORMING ORGANIZATION REPORT NUMBER(S)	5. MONITORING ORGANIZATION REPORT NUMBER(S)

6a. NAME OF PERFORMING ORGANIZATION Naval Postgraduate School	6b. OFFICE SYMBOL (if applicable) ME	7a. NAME OF MONITORING ORGANIZATION Naval Postgraduate School

6c. ADDRESS (City, State, and ZIP Code) Monterey, CA 93943-5000	7b. ADDRESS (City, State, and ZIP Code) Monterey, CA 93943-5000

8a. NAME OF FUNDING/SPONSORING ORGANIZATION	8b. OFFICE SYMBOL (if applicable)	9. PROCUREMENT INSTRUMENT IDENTIFICATION NUMBER

8c. ADDRESS (City, State, and ZIP Code)	10. SOURCE OF FUNDING NUMBERS			
	PROGRAM ELEMENT NO.	PROJECT NO.	TASK NO.	WORK UNIT ACCESSION NO.

11. TITLE (Include Security Classification)
COMPUTATIONAL UNSTEADY FLOW DYNAMICS: OSCILLATING FLOW ABOUT A CIRCULAR CYLINDER

12. PERSONAL AUTHOR(S) GORDON, David R.

13a. TYPE OF REPORT Master's Thesis	13b. TIME COVERED FROM 03/91 TO 12/91	14. DATE OF REPORT (Year, Month, Day) December 1991	15. PAGE COUNT 116

16. SUPPLEMENTARY NOTATION The views expressed in this thesis are those of the author and do not reflect the official policy or position of the Department of Defense or the United States Government.

17. COSATI CODES			18. SUBJECT TERMS (Continue on reverse if necessary and identify by block number)
FIELD	GROUP	SUB-GROUP	Numerical, Navier-Stokes, Oscillating Flow, Co-existing Flow, Harmonically Oscillating Flow

19. ABSTRACT (Continue on reverse if necessary and identify by block number)
The numerical experiments, carried out through the use of the vorticity-stream function equations and their finite difference form, on co-existing flows (sinusoidal or non-sinusoidal oscillation plus steady mean flow) are described. A third-order in time, second-order in space, three-level predictor-corrector finite-difference scheme has been used. The Poisson equation for the stream function was solved by a Fast Poisson Solver based on the High Order Difference Approximation with Identity Expansion (HODIE) and the Fast Fourier Transform (FFT) methods provided by the IMSL mathematical library. The results have revealed, for the first time, the existence of a very interesting wake comprised of three rows of heterostrophic vortices at certain Keulegan-Carpenter numbers and relative current ratios. The existence of such a street has been vindicated by physical experiments.

20. DISTRIBUTION/AVAILABILITY OF ABSTRACT [X] UNCLASSIFIED/UNLIMITED [ ] SAME AS RPT. [ ] DTIC USERS	21. ABSTRACT SECURITY CLASSIFICATION UNCLASSIFIED	
22a. NAME OF RESPONSIBLE INDIVIDUAL Professor T. Sarpkaya	22b. TELEPHONE (Include Area Code) (408) 646-3425	22c. OFFICE SYMBOL ME-SL

DD FORM 1473, 84 MAR
83 APR edition may be used until exhausted
All other editions are obsolete
SECURITY CLASSIFICATION OF THIS PAGE
UNCLASSIFIED

COMPUTATIONAL UNSTEADY FLOW DYNAMICS: OSCILLATING FLOW ABOUT A CIRCULAR CYLINDER

by
David R. Gordon
LCDR, USN
B.S., University of California, Berkeley 1978

Submitted in partial fulfillment of the
requirements for the degree of
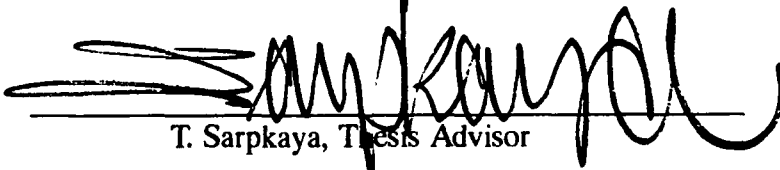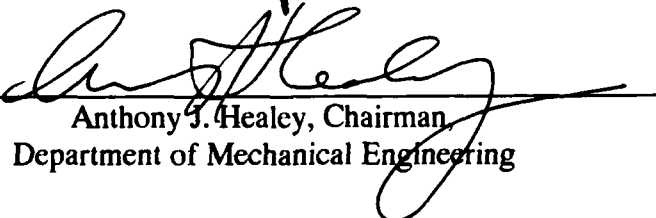
MASTER OF SCIENCE IN MECHANICAL ENGINEERING

from the

NAVAL POSTGRADUATE SCHOOL
December 1991

Author: _____
David R. Gordon

Approved By: _____
T. Sarpkaya, Thesis Advisor

_____
Anthony J. Healey, Chairman
Department of Mechanical Engineering

ABSTRACT

The numerical experiments, carried out through the use of the vorticity-stream function equations and their finite difference form, on co-existing flows (sinusoidal or non-sinusoidal oscillation plus steady mean flow) are described. A third-order in time, second-order in space, three-level predictor-corrector finite-difference scheme has been used. The Poisson equation for the stream function was solved by a Fast Poisson Solver based on the High Order Difference Approximation with Identity Expansion (HODIE) and the Fast Fourier Transform (FFT) methods provided by the IMSL mathematical library. The results have revealed, for the first time, the existence of a very interesting wake comprised of three rows of heterostrophic vortices at certain Keulegan-Carpenter numbers and relative current ratios. The existence of such a street has been vindicated by physical experiments.

TABLE OF CONTENTS

LIST OF TABLES

LIST OF FIGURES

LIST OF SYMBOLS

A   = amplitude of sinusoidal oscillations

A_p = acceleration parameter = $\dfrac{1}{(S/R)}$ = $D\left(\left(\dfrac{dU}{dt}\right)/V^2\right)$

a   = transformation parameter

C_{IL} = inline force coefficient

C_L = transverse force coefficient

C_d^u = Fourier-averaged drag coefficient

C_m = inertia coefficient = $1 + k_{ij}^u$

D   = diameter

F   = force

F_{IL} = inline force

F_L = transverse force

K   = Keulegan-Carpenter Number = $U_m T/D$

K^+ = K by current = $K\left(1 + \dfrac{U_o}{U_m}\right)$ = $K + \dfrac{U_o T}{D}$

k_{ij}^u = Fourier-averaged added mass coefficient

n   = order of polynomial (see Eq 17)

p_s = pressure on cylinder

p_∞ = pressure at outer boundary

$\overline{P}_s$ = pressure coefficient = $\dfrac{P_s - P_\infty}{\rho U_\infty^2}$

R = cylinder radius

Re = Reynolds number $\dfrac{VU}{\upsilon}$, or $\dfrac{U_m D}{\upsilon}$

Re^+ = Re modified by current = $Re\left(1 + \dfrac{U_o}{U_m}\right)$ = $Re + \dfrac{U_o D}{\nu}$

r = radial distance

S = displacement of fluid

S/R = relative displacement of fluid

T = period of oscillations

t = time

U = time dependent velocity

U_m = maximum velocity in pure sinusoidal flow

U_o = collinear steady current velocity

U_∞ = free stream velocity

u = velocity in the x-direction

v = velocity in the y-direction

V   = constant velocity reached at the end of the acceleration period

V_r = current ratio = $\dfrac{U_o}{U_m}$

β = $\dfrac{D^2}{\nu T}$ = $\dfrac{Re}{K}$

$\Delta\xi$ = computational grid spacing

ξ = computational grid coordinate corresponding to the radial direction

τ_s = shear stress

η = computational grid coordinate corresponding to the angular direction

μ = dynamic viscosity

ν = kinematic viscosity

ρ = density

θ = angular position

ψ = stream function

ω = vorticity

ACKNOWLEDGEMENTS

I. INTRODUCTION

The efforts to arrive at coherent descriptions of the interactions between oceans and the structures inserted therein have a long history. The past two decades have seen an explosion of interest in the broad subject of ocean hydrodynamics. As a result of this activity, there is arising an improved and more realistic understanding of the physical characteristics of some time-dependent flows about bluff bodies and their mathematical formulation. On the one hand attention has been focussed on controlled laboratory experiments which allow for the understanding of the separate effects of the governing and influencing parameters, and on the other hand on mathematical and numerical methods which allow for the nearly exact solution of some wave loading situations.

The hydrodynamic loading situations which are well understood are those which do not involve flow separation. Thus, they are amenable to nearly exact analytical treatment. These concern primarily the determination of the fluid forces on large objects in the diffraction regime where the characteristic dimension of the body relative to the wave length is larger than about 0.2. The use of various numerical techniques is sufficient to predict accurately the forces and moments acting on the body, provided that the viscous effects and the effects of separation for bodies with sharp edges are ignored as secondary.

The understanding of the fluid-structure interactions which involve extensive flow separation and dependence on numerous parameters such as

1

Reynolds number, Keulegan-Carpenter number, relative roughness, relative motion of the body, proximity effects, hydroelastic response, etc. is far from complete (Sarpkaya & Isaacson 1981). There are several reasons for this. First, although the physical laws governing the motion (the Navier-Stokes equations) are well understood, valid approximations necessary for numerical and physical model studies are still unknown. Even the unidirectional steady flow about a bluff body remains theoretically unresolved. Much of our understanding of vortex shedding behind bluff bodies came from steady-flow experiments, highly idealized models, and limited numerical solutions. Most of the numerical studies based on the use of the Navier-Stokes equations and some suitable spatial and temporal differencing schemes are limited, out of necessity, to low Reynolds number flows. A second reason why progress has been slow is that the bluff body problems involving wake return are an order of magnitude more complex and there has been only a handful of limited applications of the methods based on Navier-Stokes equations.

The formation of a wake gives rise not only to a form drag, as it would be the case if the motion were steady, but also to significant changes in the inertial forces. The velocity-dependent form drag is not the same as that for the steady flow of a viscous fluid, and the acceleration-dependent inertial resistance is not the same as that for an unseparated unsteady flow of an inviscid fluid. In other words, the drag and inertial forces are interdependent as well as time-dependent. These effects are further compounded by the diffusion and decay of vortices and by the three-dimensional nature of vorticity due to turbulent mixing, finite spanwise coherence, and the random nature of the vortices (which give rise to cycle-to-

cycle variations and numerous flow modes even under controlled laboratory conditions). The stronger and better correlated the returning vortices, the sharper and more pronounced the changes are in pressure distribution on the body and in the integrated quantities such as the lift, drag, and inertia coefficients.

The numerical prediction of the fluid-structure interaction, through the use of finite-difference, finite-element, and discrete-vortex methods, has attracted considerable attention during the past two decades and produced laminar flows difficult to measure and turbulent flows hard to verify. The reasons for this are relatively simple. Numerical solutions based on the full Navier-Stokes equations are not stable at high Reynolds numbers and the instability is non-linearly related to the characteristics of the base flow, the input parameters, and the discretization conditions. Also, the real flow at the computed Reynolds numbers may be turbulent, at least in some regions of the flow, and the numerical experiment does not imitate the physical experiment. Furthermore, the observed physical and numerical instabilities do not necessarily correspond to each other. Assuming that the calculations for a given flow are carried out at sufficiently small Reynolds numbers, where the flow is known to remain stable and laminar, one quickly discovers that it is practically impossible to measure, to any credible degree of accuracy, most or all of the predicted quantities (except the Strouhal number and the photographs of the flow patterns). One may also raise the question as to whether the two-dimensional numerical calculations could or should ever be compared with physical experiments attempting to mimic two dimensionality through the use of various passive or active devices (e.g., end plates on cylinders).

3

Evidently, one's view of the state of the numerical modelling depends to a large extent on one's objectives. For example, if the objective is to obtain some approximate answers and flow kinematics, one might be perfectly satisfied with the existing codes. If the objective is to match the measured and calculated results (e.g., lift and drag coefficients), one might achieve the desired objective by fine tuning a number of model parameters (e.g., the order of approximation of the velocity and/or vorticity gradients, particularly near the wall, mesh size, time step, type of discretization, outer boundary, just to name a few). If one's objectives are to perform numerical experiments for sake of numerical experiments, with no concern with the compatibility of the numerical and experimental results, then one can objectively asses the model instead of attempting to attribute to it artificial powers of prediction.

As far as the turbulent flows are concerned, some or all of the predictions of the numerical calculations for a given flow depend on the closure model used. Some models do better than others for some flows and worse than others for other flows. No model, however sophisticated, has a corner on the numerical market. Evidently, the solution of unsteady turbulent flows at sufficiently high Reynolds numbers will have far reaching theoretical and practical consequences. As noted above, this is not yet the case, and the solutions must necessarily be confined to cases where the accurate prediction of physical experiments is not the real objective. However, it is hoped that even the approximate solutions will have enough information to elucidate the physics of the phenomenon.

It is clear from the foregoing that the objectives of the present investigation are to carry out extensive numerical experiments through the use of the vorticity-stream function form of the Navier-Stokes equations and

their finite difference form, on co-existing flows (sinusoidal or non-sinusoidal oscillation plus steady mean flow). The expectations are that the results will point out the strengths and weaknesses of the code, for the particular type of formulation used, explain the reasons between the various numerical predictions of the same problem, and, hopefully, shed some light on the physics of flows heretofore uncalculated.

II. BACKGROUND STUDIES

A finite difference analysis of the Navier-Stokes equations for a sinusoidally-oscillating ambient flow about a circular cylinder at K (Keulegan-Carpenter Number) = $U_m T/D$ = 5 (Re = 1000) and K = 7 (Re = 700) has been attempted by Baba & Miyata (1987). Their results have shown that the calculations can be carried out only for short times (less than two cycles of flow oscillation) with a non-super computer. Murashige, Hinatsu and Kinoshita (1989) have used a similar method to analyze three cases (K = 5, 7, and 10) at higher Reynolds numbers around 104. The flow was perturbed by artificial means to trigger an asymmetry. At K = 10, a transverse vortex street appeared, in agreement with experimental observations. The numerical simulation of steady flow past a circular cylinder undergoing in-line and/or transverse oscillations through the use of two-dimensional unsteady Navier-Stokes equations was undertaken by Lecointe et al. (1987) for relatively small amplitudes (A/D = 0.13). Justesen (1991) presented extensive results obtained from a numerical solution of a vorticity-stream function formulation of the Navier-Stokes equations for the flow around a circular cylinder in planar oscillating flow at small Keulegan-Carpenter numbers in the subcritical Reynolds number range. Justesen introduced a straining parameter "a" in order to better resolve the large gradients near the cylinder surface. This is in addition to the logarithmic straining, commonly used as part of the transformations, for a better resolution of the gradients near the body. Evidently, Justesen's transformation for a = 0 defaults to the

logarithmic straining. However, "a" becomes another disposable parameter, dependent on at least K and Re. Justesen had to choose judiciously the value of the straining parameter for each K in order achieve drag and inertia coefficients in satisfactory agreement with those obtained experimentally. A systematic numerical variation of the governing parameters for an arbitrary U(t) is extremely difficult.

The in-line oscillations of a cylinder in uniform flow (or the sinusoidally oscillating flow with a steady mean flow) has been the subject of intense interest in recent years (see, e.g., Sarpkaya & Isaacson, 1981 and Sarpkaya & Storm, 1985) in connection with the understanding of the behavior of hot-wire anemometers and the fluid loading of structures subjected to currents, gusts and other types of unsteady flows. The biassing of the shedding of the vortices by the current causes profound changes in both the drag and inertia coefficients, relative to their no-current values. The mobile separation points undergo large excursions, as much as 120 degrees during a given cycle of oscillation over a circular cylinder (Sarpkaya and Butterworth, 1992). These effects are further compounded by the diffusion and decay of vortices and by the three-dimensional nature of vorticity due to turbulent mixing, reduced spanwise coherence, mutual-induction instability, and the random nature of vortices which give rise to cycle-to-cycle variations and numerous flow modes even under controlled laboratory conditions. It is because of these reasons that the present work is dedicated to the numerical analysis of such flows.

III. NUMERICAL REPRESENTATION

A. COMPUTATIONAL METHOD

Here only a brief description of the computational method is presented. A more in depth description is given by Wang (1989) and Putzig (1991).

The fluid is assumed to be two-dimensional, incompressible and viscous. The governing equations for the solution are the Navier-Stokes equations, with the stream function and the vorticity as independent variables. To achieve a higher density of mesh points near the cylinder surface, the computational domain is transformed from the physical plane (polar coordinates, see Figure 1) to a rectangular plane (Figure 2). In the rectangular plane, the mesh is maintained at a uniform grid spacing. It is necessary to have more mesh points closer to the cylinder surface because in this region the gradients of both the vorticity and the stream function are the largest.

A third-order in time, second-order in space, three-level predictor-corrector finite-difference scheme is used to solve the vorticity-transport equation. A Fast Poisson Solver based on the High Order Difference approximation with Identity Expansion (HODIE) and the Fast Fourier Transformation (FFT) provided by the IMSL mathematics library is used to solve for the stream function.

The unsteady Navier-Stokes equations in the polar coordinates, as defined by the vorticity transport equation and the vorticity/stream-function equation are,

8

$$\frac{\partial \omega}{\partial t} - \frac{1}{r}\left[\frac{\partial}{\partial r}(\omega\frac{\partial \psi}{\partial \theta}) - \frac{\partial}{\partial \theta}(\omega\frac{\partial \psi}{\partial r})\right] = \nu\nabla^2\omega \tag{1}$$

and

$$\nabla^2\psi = \omega \tag{2}$$

where

$$\nabla^2 = \frac{\partial^2}{\partial r^2} + \frac{1}{r}\frac{\partial}{\partial r} + \frac{1}{r^2}\frac{\partial^2}{\partial r^2} \tag{3}$$

ω and ψ are the vorticity and the stream function, ν is the kinematic viscosity, t is the time and, r and θ are polar coordinate directions (see Figure 1). The velocity components in the r and θ directions are defined by

$$u = -\frac{1}{r}\frac{\partial \psi}{\partial \theta} \qquad \text{and} \qquad v = \frac{\partial \psi}{\partial r}. \tag{4}$$

The boundary conditions for the physical problem are:

(1) no slip and zero normal velocity on the surface of the cylinder

$$\psi = \frac{\partial \psi}{\partial r} \qquad \text{on} \qquad r = R \tag{5}$$

and (2) the potential flow at infinity is defined as

$$\psi = U(r - \frac{R}{r})\sin\theta \tag{6}$$

9

and $\omega = 0$ at $r = \infty$. U is the external flow and R is the radius of the cylinder.

The coordinate transformations required to go from the physical domain to the computational domain are:

$$r = R \cdot e^{(a\xi)} \qquad \text{and} \qquad \theta = a\eta \qquad (7)$$

where R is the radius of the cylinder and 'a' is a transformation parameter.

The transformation of the non-dimensionalized vorticity-stream function equations and their finite difference form through the use of the central difference approximation for vorticity and a two-step, three-level, predictor-corrector scheme, with a third order accuracy in time, are described in detail in Wang (1989), in Fredrickson (1990) and in Putzig (1991) and will not be repeated here.

B. CALCULATION OF THE FORCE COEFFICIENTS

The in-line and transverse force coefficients are determined from the combined contributions of the shear and pressure forces acting on the cylinder. The viscous forces are calculated from $\tau_s = \mu\omega$. The total in-line force then reduces to

$$F_{IL} = -\int_0^{2\pi} (p_s \cdot \cos(\theta) R d\theta) - \int_0^{2\pi} \mu\omega \sin(\omega) R d\theta \qquad (8)$$

and the total lift force as

10

$$F_L = -\int_0^{2\pi} (p_s \cdot \sin(\theta) R d\theta) - \int_0^{2\pi} \mu\omega \cos(\omega) R d\theta . \tag{9}$$

After dividing the in-line and the lift-force equations by $(0.5\rho U^2 D)$ and defining

$$\overline{p}_s = \frac{2(p_s - p_\infty)}{\rho U_\infty^2} \tag{10}$$

the force coefficients reduce to

$$C_{IL} = -\frac{1}{2}\int_0^{2\pi} (\overline{p}_s \cdot \cos(\theta) R d\theta) - \frac{2}{Re} \cdot \int_0^{2\pi} \mu\overline{\omega}\sin(\omega) R d\theta \tag{11}$$

and

$$C_L = -\frac{1}{2}\int_0^{2\pi} (\overline{p}_s \cdot \sin(\theta) R d\theta) - \frac{2}{Re} \cdot \int_0^{2\pi} \mu\overline{\omega}\cos(\omega) R d\theta . \tag{12}$$

The pressure coefficient is determined from the Navier-Stokes equations in terms of dimensionless vorticity. Once integrated with respect to θ, one has

$$\overline{p}_s(\theta) = \overline{p}_s(0) + \frac{4}{Re}\int_0^{2\pi} \left(\frac{\partial\overline{\omega}}{\partial\overline{r}}\right)_{r=1} d\theta . \tag{13}$$

Equation (13) is substituted into equations (11) and (12) to determine the numerical scheme for the in-line and transverse force coefficients,

11

$$C_{IL} = -\frac{2}{Re} \cdot \int_{0}^{2\pi} \left\{ \left[\int_{0}^{\theta} (\frac{\partial \overline{\omega}}{\partial \overline{r}})_{r=1} d\theta \right] \cos(\theta) + \overline{\omega}\sin(\theta) \right\} d\theta \qquad (14)$$

and

$$C_{L} = -\frac{2}{Re} \cdot \int_{0}^{2\pi} \left\{ \left[\int_{0}^{\theta} (\frac{\partial \overline{\omega}}{\partial \overline{r}})_{r=1} d\theta \right] \sin(\theta) - \overline{\omega}\cos(\theta) \right\} d\theta \ . \qquad (15)$$

The radial derivative of the vorticity on the surface of the cylinder, appearing in Equations (14) and (15), is determined through the use of discrete pointwise approximations of various orders, ranging from second to tenth order. For a second order approximation, one has

$$\left(\frac{\partial \overline{\omega}_i}{\partial \overline{r}}\right)_{r=1} = \frac{-3\omega_i + 4\omega_{i+1} - \omega_{i+2}}{2\Delta\xi} + O(\Delta\xi^2) \ . \qquad (16)$$

For higher order polynomials Equation (16) may be written as

$$\left(\frac{\partial \overline{\omega}_i}{\partial \overline{r}}\right)_{r=1} = \frac{-A\omega_i + B\omega_{i+1} - C\omega_{i+2} + E\omega_{i+4} + \cdots\cdots}{\Delta\xi} + O(\Delta\xi^n) \qquad (17)$$

in which the coefficients A – K are given in Table 1 below.

TABLE 1: COEFFICIENTS OF THE POLYNOMIAL IN EQ. (17)

	n=2	n=4	n=6	n=8	n=10
A	-3/2	-25/12	-49/20	-761/280	-7381/2520
B	2	4	6	8	10
C	-1/2	-3	-15/2	-14	-45/2
D		4/3	20/3	56/3	40
E		-1/4	-15/4	-35/2	-105/2
F			6/5	56/5	252/5
G			-1/6	-14/3	-35
H				8/7	120/7
I				-1/8	-45/8
J					10/9
K					-1/10

C. CALCULATION OF THE DRAG AND INERTIA COEFFICIENTS

If one were to associate the total force with a velocity-square-dependent drag force and an acceleration-dependent inertial force then the coefficient associated with the latter may be interpreted as some measure of the added mass. But one must bare in mind that such a decomposition is far from being unique.

It has been customary to express the fluid force acting on a body moving in a fluid otherwise at rest as

$$F(t) = \frac{1}{2}\rho C_d^u A_p |\{U_o + U(t)\}| \{U_o + U(t)\} + \rho k_{ij}^u V \frac{d}{dt} U(t) \qquad (18)$$

where U_o represents the steady velocity; $U(t)$, the time-dependent oscillations; C_d^u , the Fourier-averaged drag coefficient and k_{ij}^u , the Fourier-averaged added-mass coefficient. It is customary to use an inertia coefficient Cm for a fluid in motion about a body at rest through the use of $C_m = 1 + k_{ij}^u$.

The Fourier averages of the drag and added-mass coefficients over a period of T may be calculated by multiplying both sides of Equation (8) once with U(t) and once with dU/dt to yield

$$C_d^u = \frac{2 \int_0^T F(t) U(t) dt}{\rho A_p \int_0^T |\{U_o + U(t)\}| \{U_o + U(t)\} U(t) dt} \qquad (19)$$

and

14

$$(C_m - 1) = k_{11}^u = \dfrac{\displaystyle\int_0^T F(t)\frac{d}{dt}U(t)\,dt}{\rho\forall\displaystyle\int_0^T\left[\frac{d}{dt}U(t)\right]^2 dt} \qquad (20)$$

which may be evaluated readily, provided that sufficiently reliable data are available for F(t), U_o, U(t), and dU(t)/dt.

A simple dimensional analysis of the flow under consideration shows that the time-averaged force coefficients (C_d^u and k_{ij}^u) are functions of a relative amplitude or Keulegan-Carpenter number, Mach number, Reynolds number, and a parameter involving U_o (e.g., $U_o(T/D)$ or $U_o/[U(t)]_{max}$). There are numerous possibilities regarding the definitions of the relative amplitude or Keulegan-Carpenter number and the Reynolds number. The purpose of the search for a more suitable Keulegan-Carpenter number and/or Reynolds number is to enhance the correlation of the data to reduce the number of the governing parameters, possibly eliminating $U_o(T/D)$ as an independent parameter. The list of possible Reynolds numbers and Keulegan-Carpenter numbers is long and will not be given here. Suffice it to note that the two force-coefficients for the flow about a cylinder may be written as

$$\binom{C_d^u}{k_{ij}^u} = f_i(K, Re, VK) \qquad (21)$$

or as

$$\begin{pmatrix} C_d^u \\ k_{ij}^u \end{pmatrix} = f_i(K^+, Re^+, VK) \qquad (22)$$

in which

$$K = \frac{U_m T}{D}, \qquad Re = \frac{U_m D}{v}, \qquad VK = \frac{U_o T}{D}$$

$$K^+ = K\left(1 + \frac{U_o}{U_m}\right) = K + \frac{U_o T}{D}$$

$$Re^+ = Re\left(1 + \frac{U_o}{U_m}\right) = Re + \frac{U_o D}{v} . \qquad (23)$$

The purpose of the present calculations was not to provide a detailed comparison between the measured and calculated forces but rather to attempt to establish a relationship between the shedding of vortices and the relative magnitude of the current. The particular values of K and V_r chosen for the calculations (K = 4 to 6, V_r = 0.0 – 1.2) was one for which some experimental data were available at comparable β, Re, and V_r values.

IV. DISCUSSION OF RESULTS

The numerical experiments were carried out through the use of a VAX–2000, a VAX–3520, a CRAY Supercomputer and the IMSL Mathematical Library. The solution procedure and technique have been validated for several types of unsteady flows, i.e., impulsively-started, suddenly-stopped, and uniformly-decelerated flows before applying it to co-existing flows (oscillatory flow or sinusoidally-oscillating flow with mean velocity). Excellent agreement with flow visualization and experimentally determined drag and lift coefficients has been obtained for both symmetric and asymmetric wake solutions. It is this validation that led to the exploration of the characteristics of sinusoidally- and non-sinusoidally-oscillating flows superimposed on a mean velocity.

The sinusoidal oscillation was specified by $U = U_o + U_m \sin(2\pi t/T)$ in which U_o is the steady mean velocity and U_m is the amplitude of sinusoidal oscillations. The non-sinusoidal oscillation was represented by

$$U = U_o + U_m [320166\cos(\theta) - 76230\cos(3\theta) + 22869\cos(5\theta)$$

$$- 5445\cos(7\theta) + 847\cos(9\theta) - 63\cos(11\theta)] / (262144) \qquad (23)$$

in which $\theta = \omega t - \pi/2$. This profile, without the mean velocity U_o, was first used by Justesen and Spalart (1990) in connection with the turbulence modeling of oscillatory boundary layers. They have referred to it as the "steep" velocity variation since it yields a quasi-steady interval and an interval with a very large pressure gradient in each half-cycle (see Figure 3).

17

As noted by Jensen and Spalart, the coefficients in equation (23) were determined by requiring that the first ten derivatives be zero at t = 0.

The flow was perturbed by changing the direction of the ambient flow sinusoidally (with an amplitude of one-half of a degree) during the first cycle of the oscillation. The amplitude of the sine wave was the only free parameter. It is worth noting that this type of disturbance gradually returns the perturbed quantity to its initial state.

Numerical experiments have been carried out in the range of K = 4 to 6, β = 200, Re = 800 to 1200, $\Delta t \approx 0.002$ and for various values of $V_r = U_o/U_m$, as shown in Table 2.

TABLE 2: THE RANGE OF THE GOVERNING PARAMETERS

V_r / K =	4	5	6	7	8
0.0			X		
0.20			X*		
0.40	X		X*		
0.50	X	X			
0.60	X*	X	X*	X	X
0.65	X				
0.70	X*		X*		
0.80	X		X		
1.00			X		
1.20			X		

*The calculations have been carried out for both the sinusoidal and non-sinusoidal oscillations at the indicated K and V_r values.

18

Evidently, this is a rather limited exploration of a highly complex problem and requires much more numerical and experimental work. The purpose of the present calculations was not to provide a detailed comparison between the measured and calculated forces but rather to attempt to establish a relationship between the shedding of vortices and the relative magnitude of the current.

Figures 4 through 9 show at time $t/T = 9.0$, for $K = 4$ and $V_r = 0.4$, the in-line force, the transverse force, a close-up view of the streaklines, the complete streaklines, the streamlines, and the vorticity field, respectively; Figures 10–15 show the same plots, for $K = 4$ and $V_r = 0.5$; Figures 16–21 the same plots, for $K = 4$ and $V_r = 0.6$; Figures 22–27 show similar plots, for $K = 4$ and $V_r = 0.65$; Figures 28–33 show the corresponding plots, for $K = 4$ and $V_r = 0.7$; and Figures 34–39 show the same plots, for $K = 4$ and $V_r = 0.8$. Figures 40–45, 46–51, 52–57, and 58–63 show the plots cited above, at time $t/T = 9.0$, for $K = 6$ and $V_r = 0.6$, 0.7, 1.0, and 1.2, respectively. Figures 64–69 and 70–75 show the force and vortex plots for the steep-sine oscillations for $K = 4$ and $V_r = 0.6$ and 0.7, respectively. Finally, Figures 76–81 and 82–86 show similar plots for $K = 6$ and $V_r = 0.6$ and 0.7, respectively.

The streaklines show that for relatively small values of V_r , the wakes are on both the upstream and downstream sides of the cylinder and exhibit highly irregular and often highly stretched vortices. As V_r increases, the wake begins to occupy more and more, the downstream side of the cylinder (see Figure 13). The most interesting feature of the flow, however, is not the position but the shape of the wake. Figure 13 shows that the width of the wake increases and the vortices begin to arrange themselves along three

19

rows. Figures 18–20 for $V_r = 0.6$, Figures 24–26 for $V_r = 0.65$, and Figures 30–32 for $V_r = 0.7$ show that the wake is comprised of three rows of heterostrophic vortices. They differ only in detail from one V_r to another in the narrow range of V_r from about 0.6 to 0.7. At lower V_r values (see Figures 6–8 for $V_r = 0.4$ and Figures 12–14 for $V_r = 0.5$), where the sinusoidal oscillation is relatively important, the shedding of the vortex couples become more and more alternating. One pair goes to one side of the cylinder, the next pair goes to the central street, and the third pair goes to the other side of the street. Then the events repeat themselves. At higher V_r values, however, (see Figures 37 for $V_r = 0.8$) the central vortex pairs become weaker and fairly stretched out. The vortex pairs rotate and orient themselves as if they were going to be part of an ordinary Karman vortex street.

The lift coefficient plots show (see Figures 17, 23, 29, and 35) the increasing asymmetry of the wake with V_r for V_r larger than about 0.7. At lower V_r values (see Figures 16 and 22) the in-line force coefficient remains essentially constant and periodic. At larger V_r values (see Figure 34), however, the in-line force becomes increasingly asymmetrical.

Table 3 and Figure 87 show a comparison of the calculated and experimental drag and inertia coefficients for $K = 4$ for representative values of V_r. The computed values were based on an eighth order polynomial representation of the radial vorticity gradient. As expected, the inertia coefficients agree extremely well. As far as the drag coefficients are concerned, the agreement is not as good, but certainly better than expected in view of the fact that β was 200 in the calculations and about 600 in the experiments. Nevertheless, the trend of the data is well predicted.

TABLE 3. COMPARISON OF MEASURED AND CALCULATED FORCE COEFFICIENTS FOR K = 4 AND VARIOUS VALUES OF V_r

V_r:	0.4	0.6	0.8	1.0
C_m^u (exp)	1.9	1.8	1.7	1.5
C_m^u (cal)	1.92	1.86	1.83	1.60
C_d^u (exp)	0.73	0.85	0.87	0.91
C_d^u (cal)	0.52	0.72	0.86	0.85

Figure 88 is a representative sample of the flow visualization obtained with K = 4 and V_r = 0.7 at t/T = 20. The symmetric growth and motion of the vortices are clearly visible. This figure should be compared with Figures 30. The similarity is rather striking in spite of the fact that β was 200 in the calculations and about 650 in the experiments.

As noted previously, the calculations were carried out for larger values of K in order to determine as to whether the unusual vortex wake seen in Figures 30–32 is a consequence of a unique combination of K and V_r values or whether it would occur at any K value as long as V_r is chosen judiciously. The results have shown that (see Figures 40–63) the three-row vortex street occurs only for K = 4 in a suitable range of V_r values (about 0.6–0.7). For example, a comparison of Figures 31 and 49 shows that the wakes for K = 4 and K = 6 are significantly different for identical values of V_r.

The calculations through the use of the "steep-sine" oscillation and a steady current have shown (see Figures 64–86) that the three-row vortex wake does not occur and that the wake is comprised of a series of relatively active and inactive vortical regions. The inactive regions result from the periods of rapid acceleration and the active regions from the time intervals during which the velocity is nearly steady (see Figure 3). More significantly, however, figures such as Figure 82 show that the repetitive but non-sinusoidal nature of the flow causes dramatic changes in the in-line (see Figures 46 and 82) as well as the transverse force. Parts of the cycle become "inertia dominated" and parts of the cycle become "drag dominated." Had the flow been non-repetitive and non-sinusoidal (e.g., Gaussian), the drag and inertia dominated regions even at high K values would have randomly occurred throughout the history of the motion. It is because of this reason that it has not been easy to evaluate the ocean data or possible to compare it with the laboratory data, obtained under idealized conditions. It does not appear that this situation will change in the near future.

V. CONCLUSIONS

The investigation reported here warranted the following conclusions:

1.   Even the higher order finite difference formulations of the governing equations based on the vorticity/stream-function formulation of the Navier Stokes equations can be solved for only relatively small Reynolds numbers. This is primarily due to stability and computer constraints.

2.   The numerical experiments with pulsating flows (oscillation plus steady mean flow) for K = 4 and K = 6 yielded total force coefficients in good agreement with those obtained experimentally.

3.   For K = 4 and relative current velocities of about 0.6–0.7, the vortices shed nearly symmetrically at each cycle and gave rise to a most unusual three-row vortex street, where each row is comprised of a pair of heterostrophic vortices. For relative current velocities larger than about one, the vortex wake returned to the asymmetric mode, as is encountered in a regular Karman vortex street.

4.   For K larger than about 4, the three-row vortex street did not occur either for sinusoidally- or non-sinusoidally–oscillating co-existing flow, showing that the three-row vortex wake is indeed quite unique. It remains to be seen as to whether it occurs at much larger Reynolds numbers (larger β) for K = 4 and V_r = 0.6–0.7.

5.   Extensive flow visualization studies yielded vortex patterns in close agreement with those predicted numerically at the corresponding relative current velocities.

6.   The foregoing numerical experiments could not have been possible had it not been due to the availability of a VAX-3520 and a CRAY supercomputer. It is also realized that calculations at higher Reynolds numbers and for larger numbers of cycles of flow oscillation will require extremely large CPU times even on a supercomputer.

APPENDIX
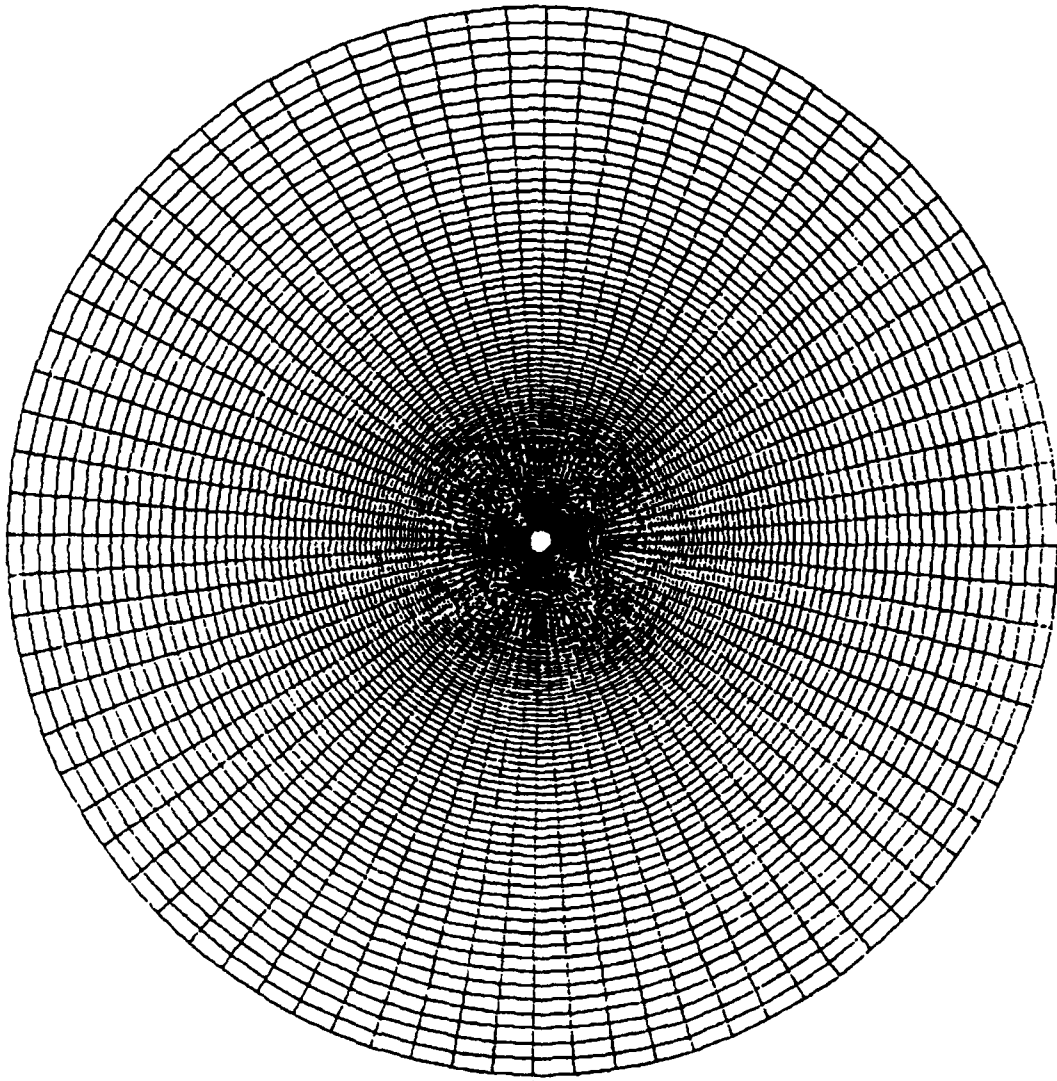
Figure 1. Grid in the Physical Domain
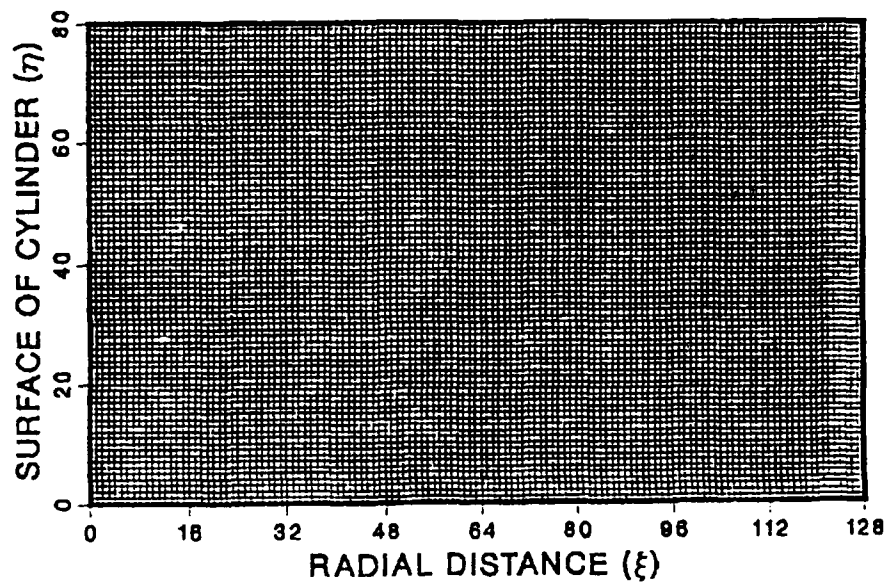
Figure 2. Grid in the Computational Domain
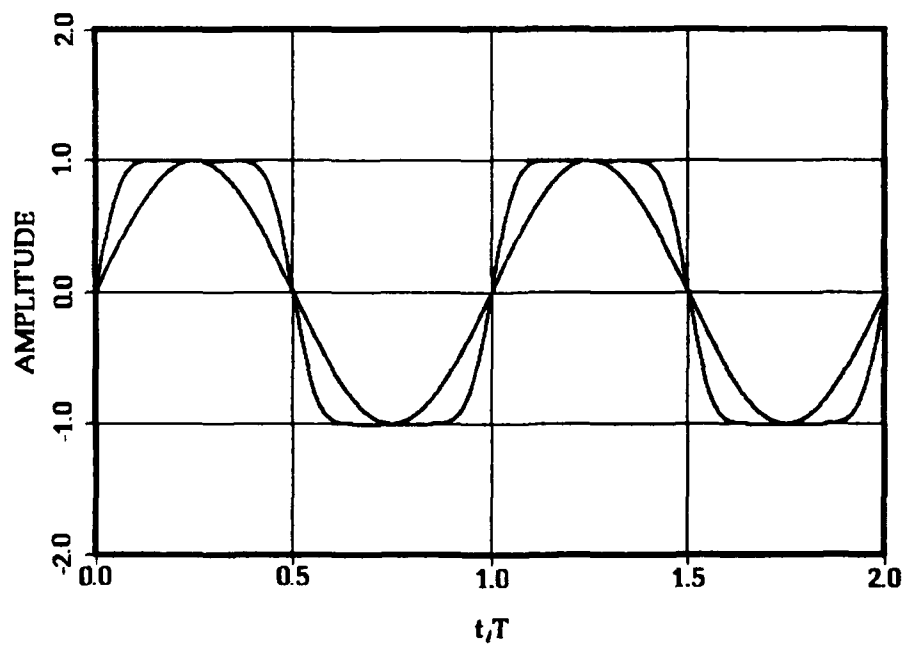
Figure 3. "Steep Sine" Curve Compared With Sine Curve

25
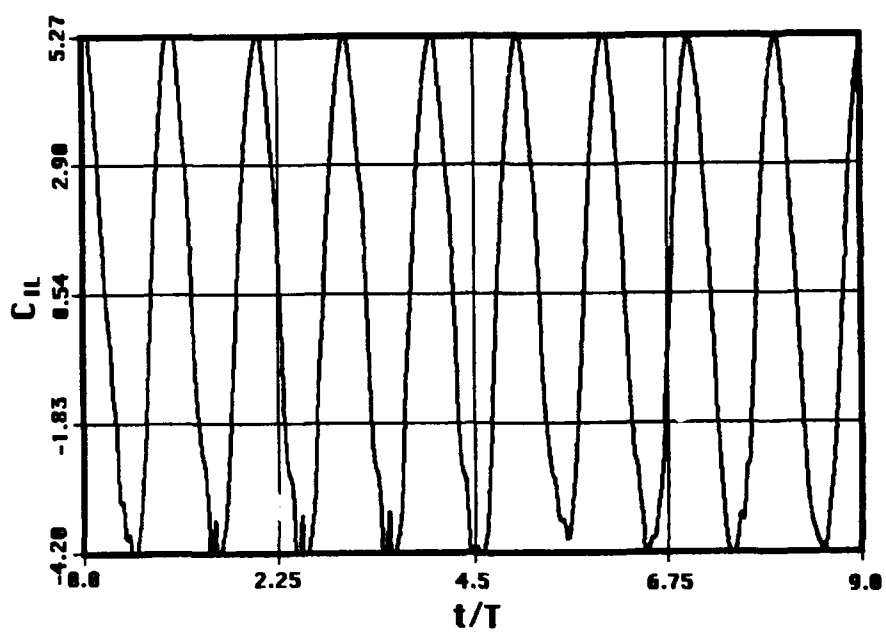
Figure 4. Inline Force Coefficient, K = 4, Re = 800, V_r = 0.4
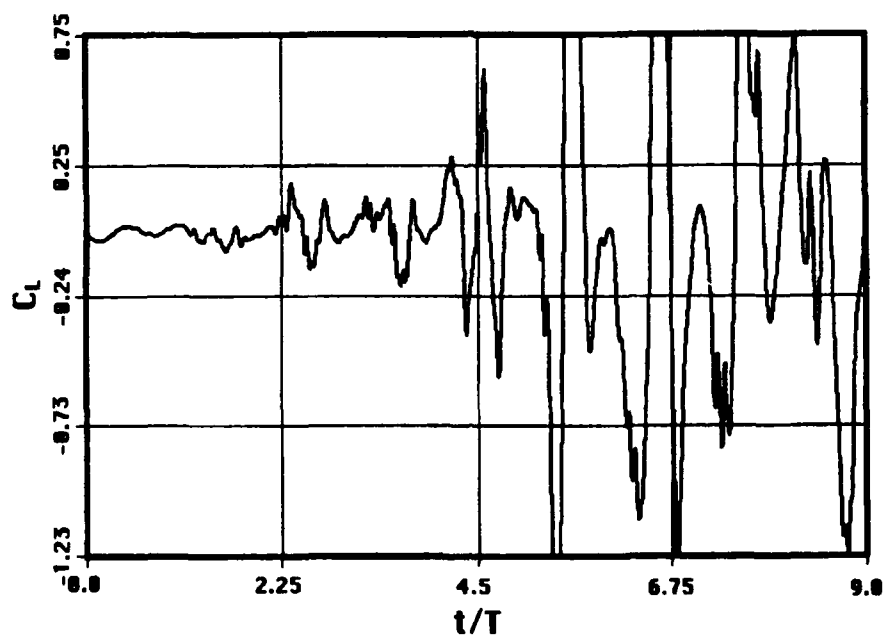
Figure 5. Transverse Force Coefficient, K = 4, Re = 800, V_r = 0.4

26

Figure 6. Closeup View of Streaklines, K = 4, Re = 800, V_r = 0.4, t/T = 9.0

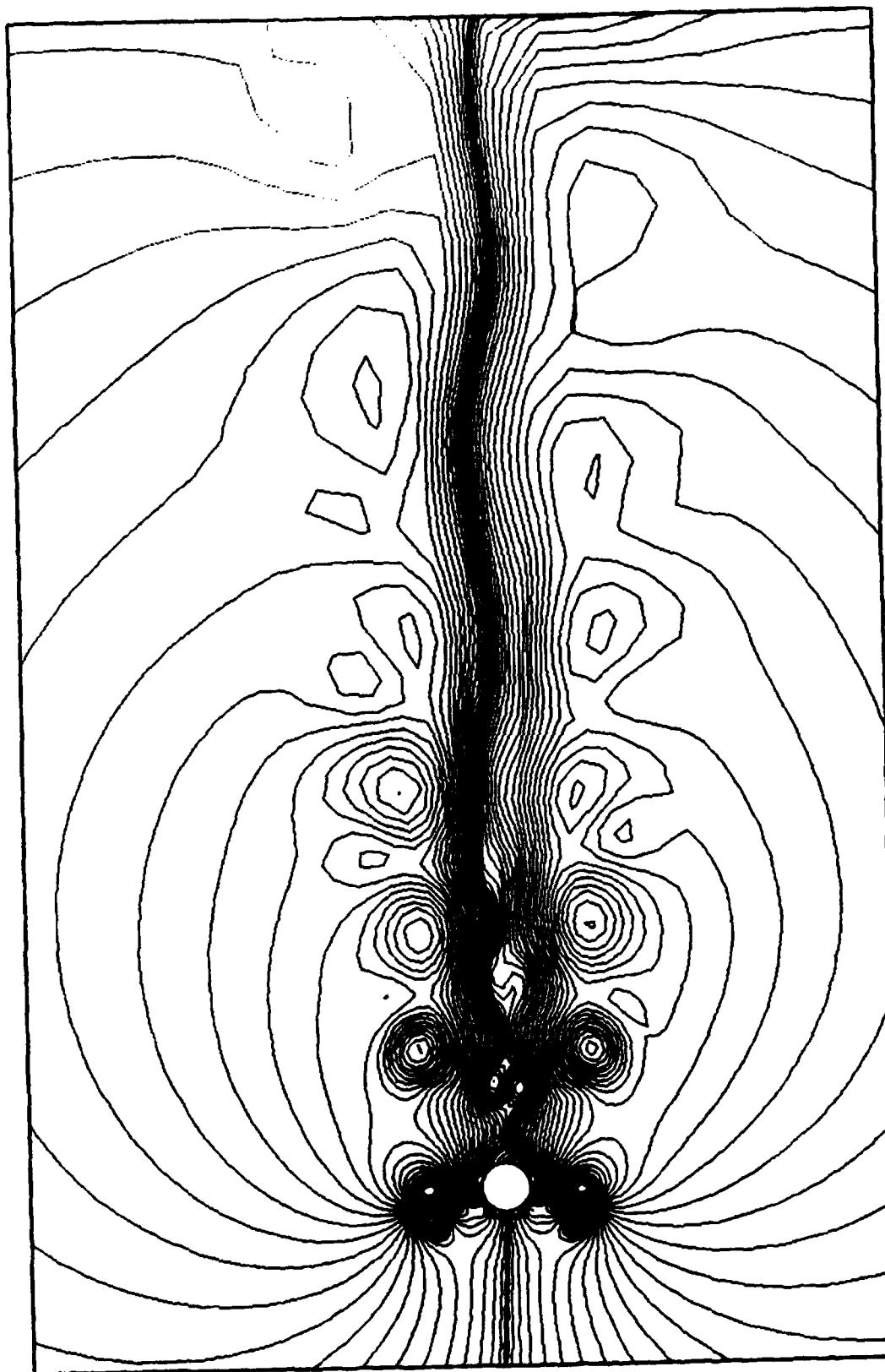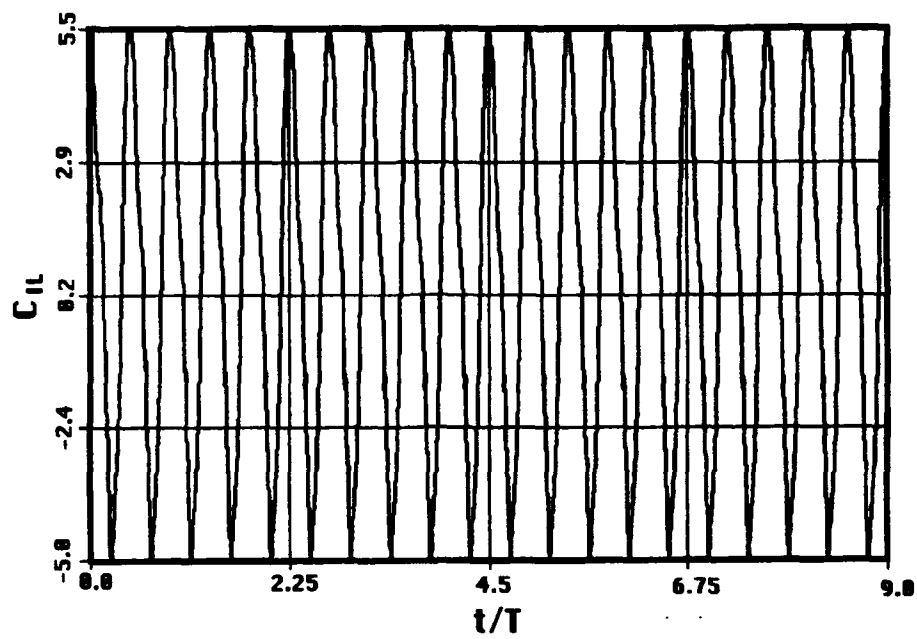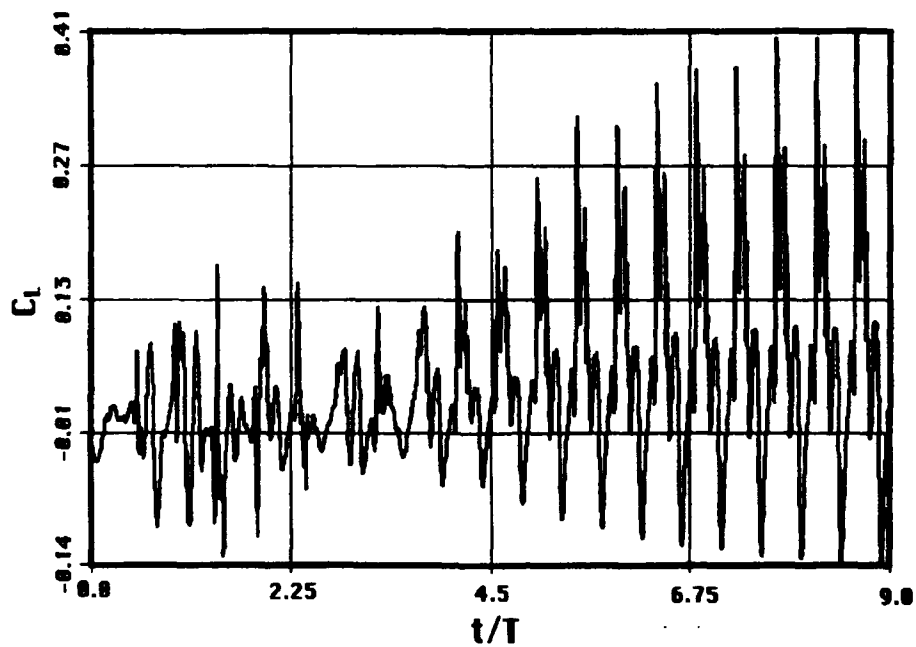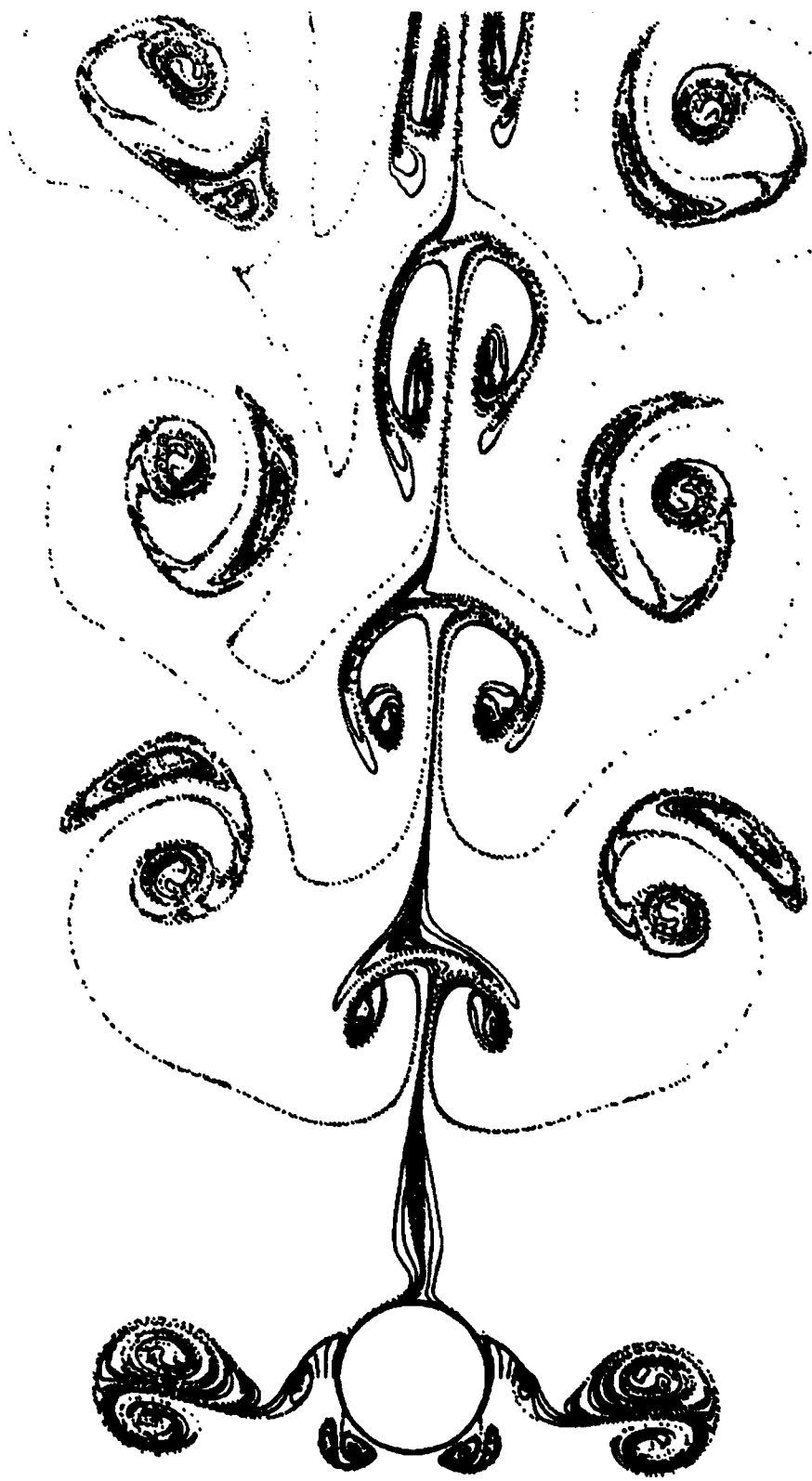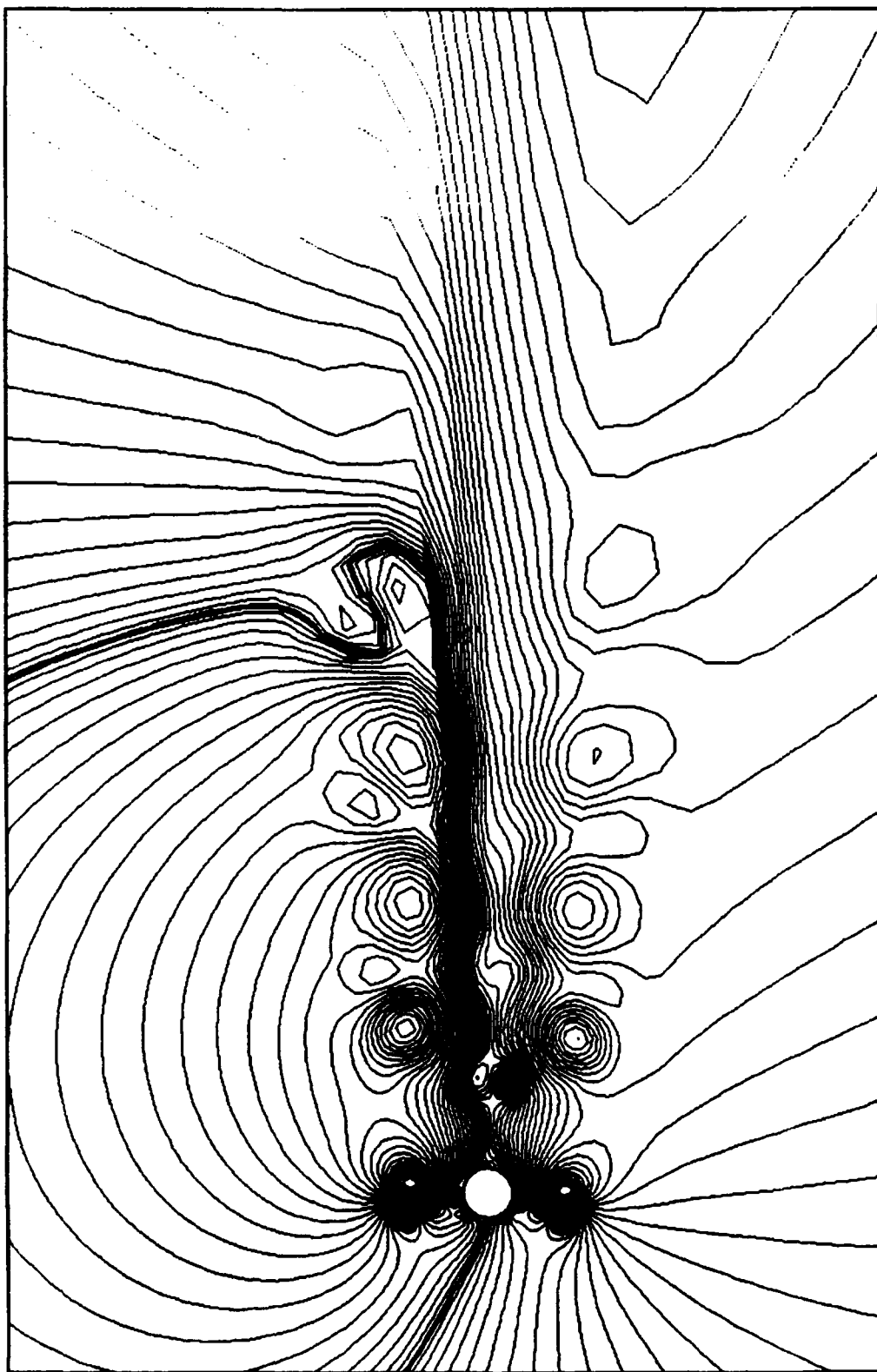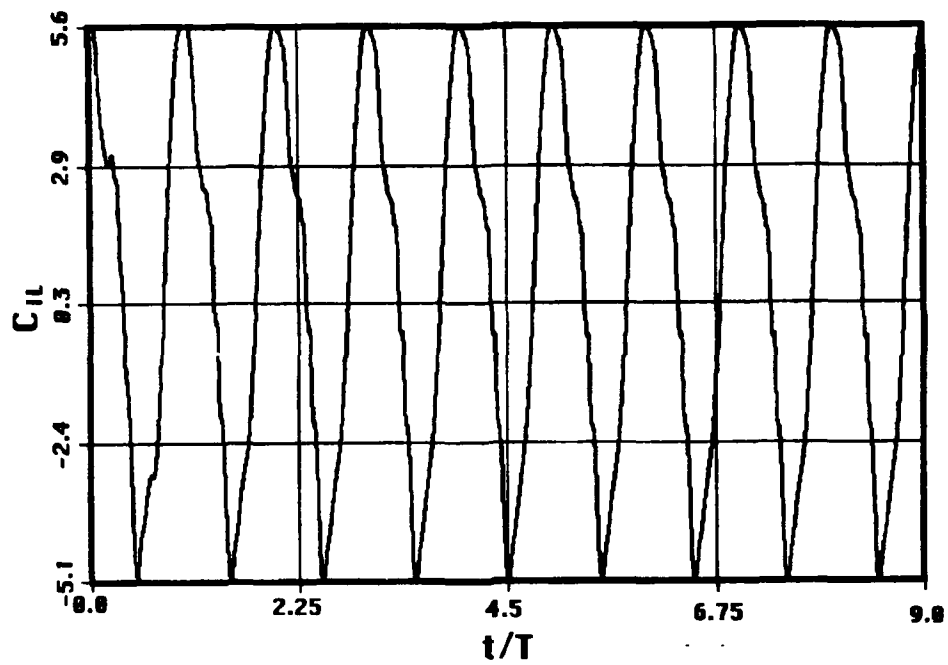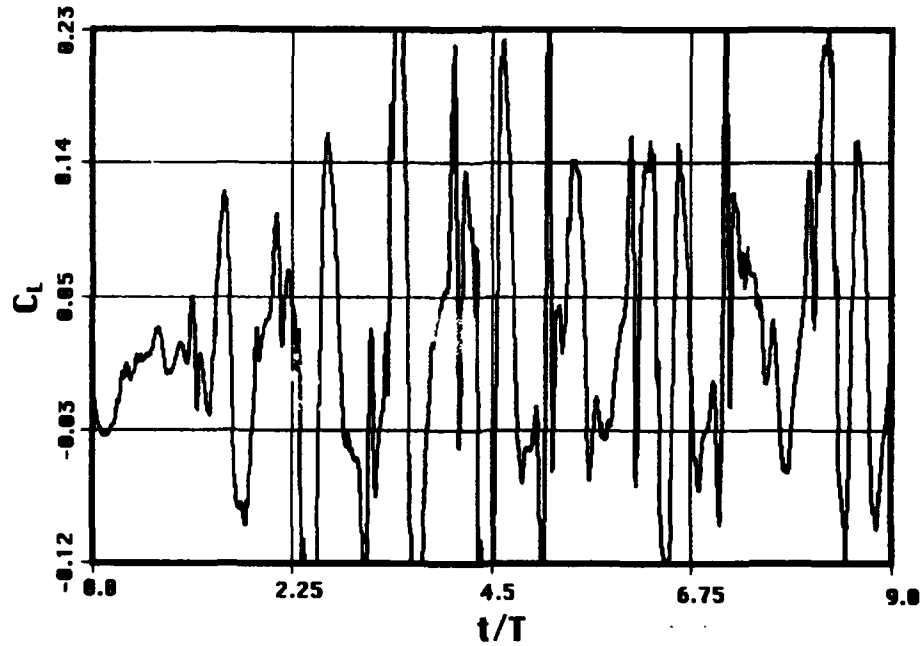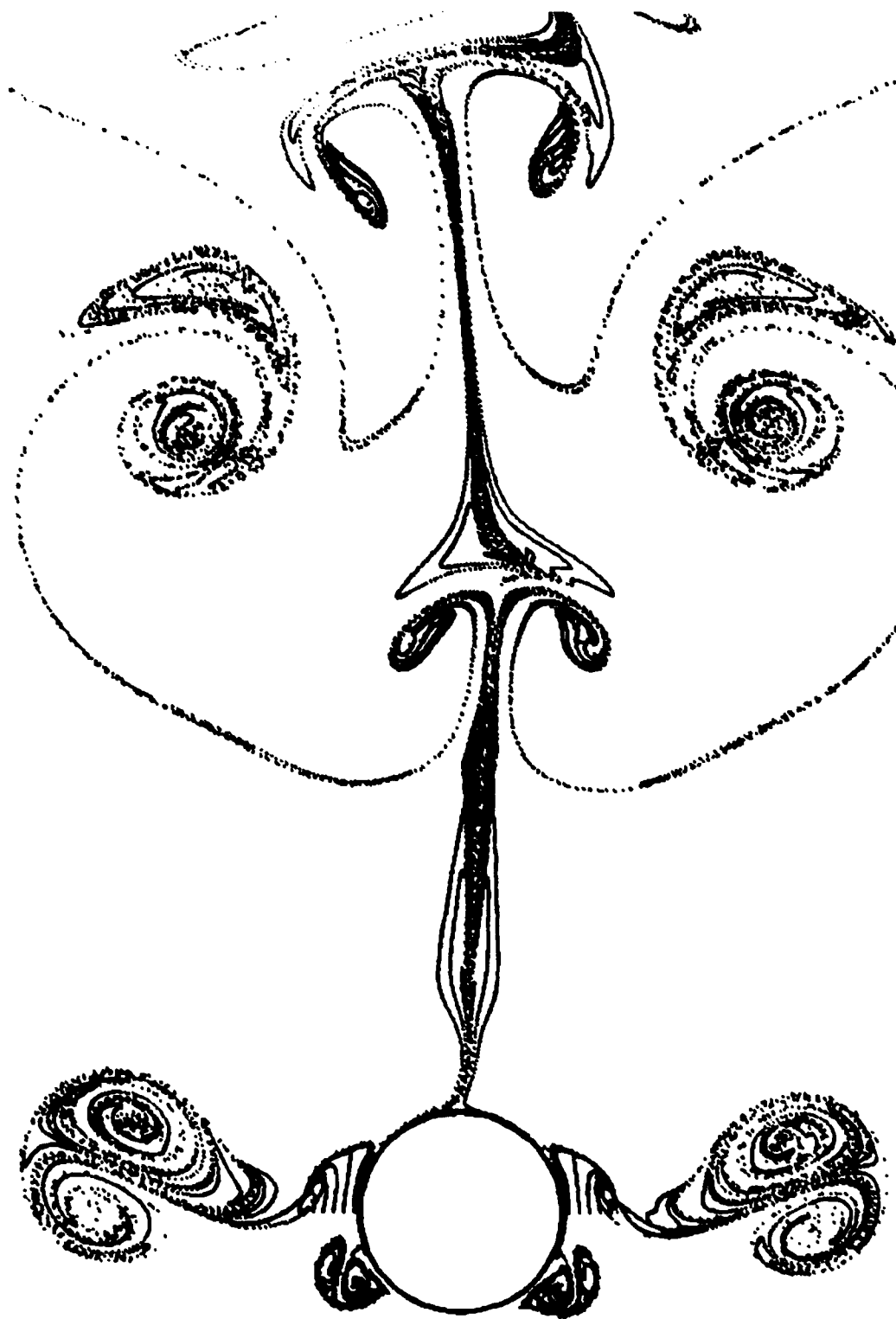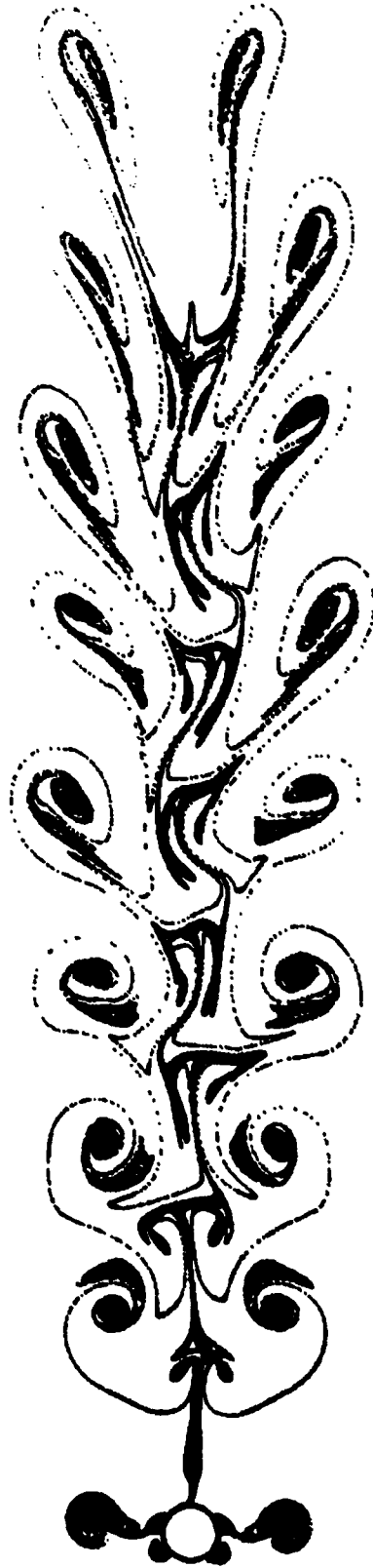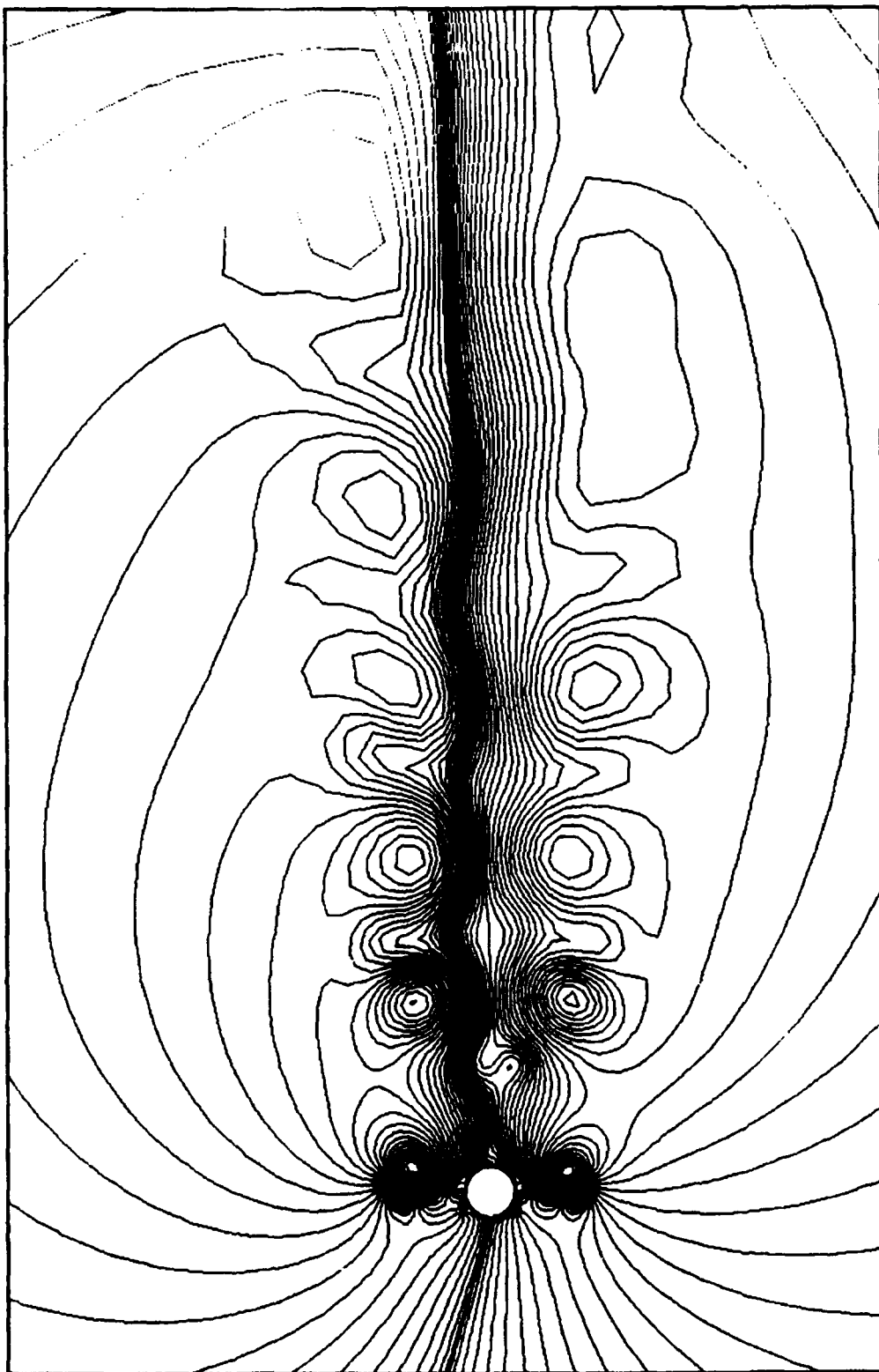Figure 7. Streaklines, K = 4, Re = 800, V_r = 0.4, t/T = 9.0
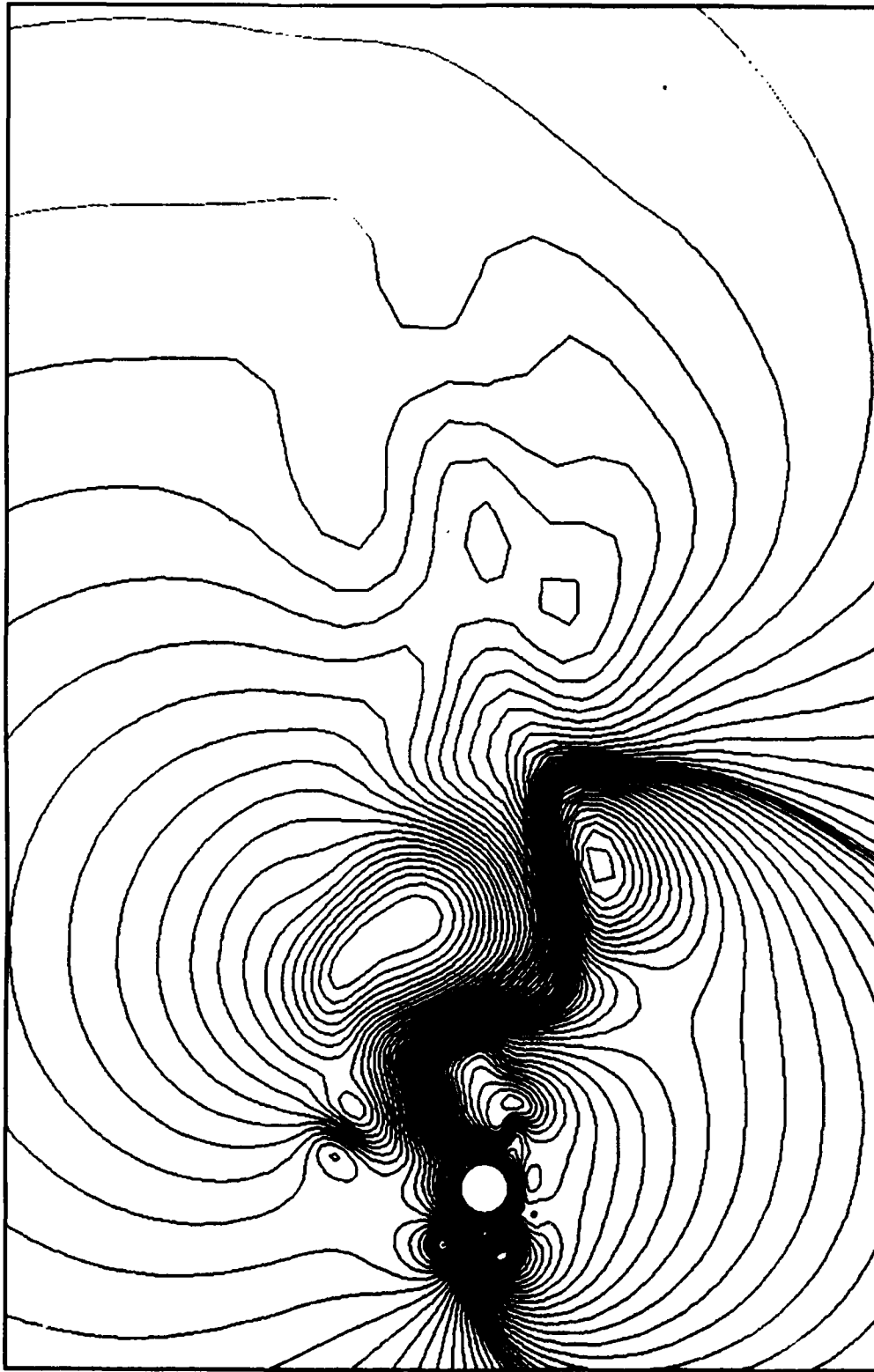
Figure 8. Streamlines, K = 4, Re = 800, V_r = 0.4, t/T = 9.0

29

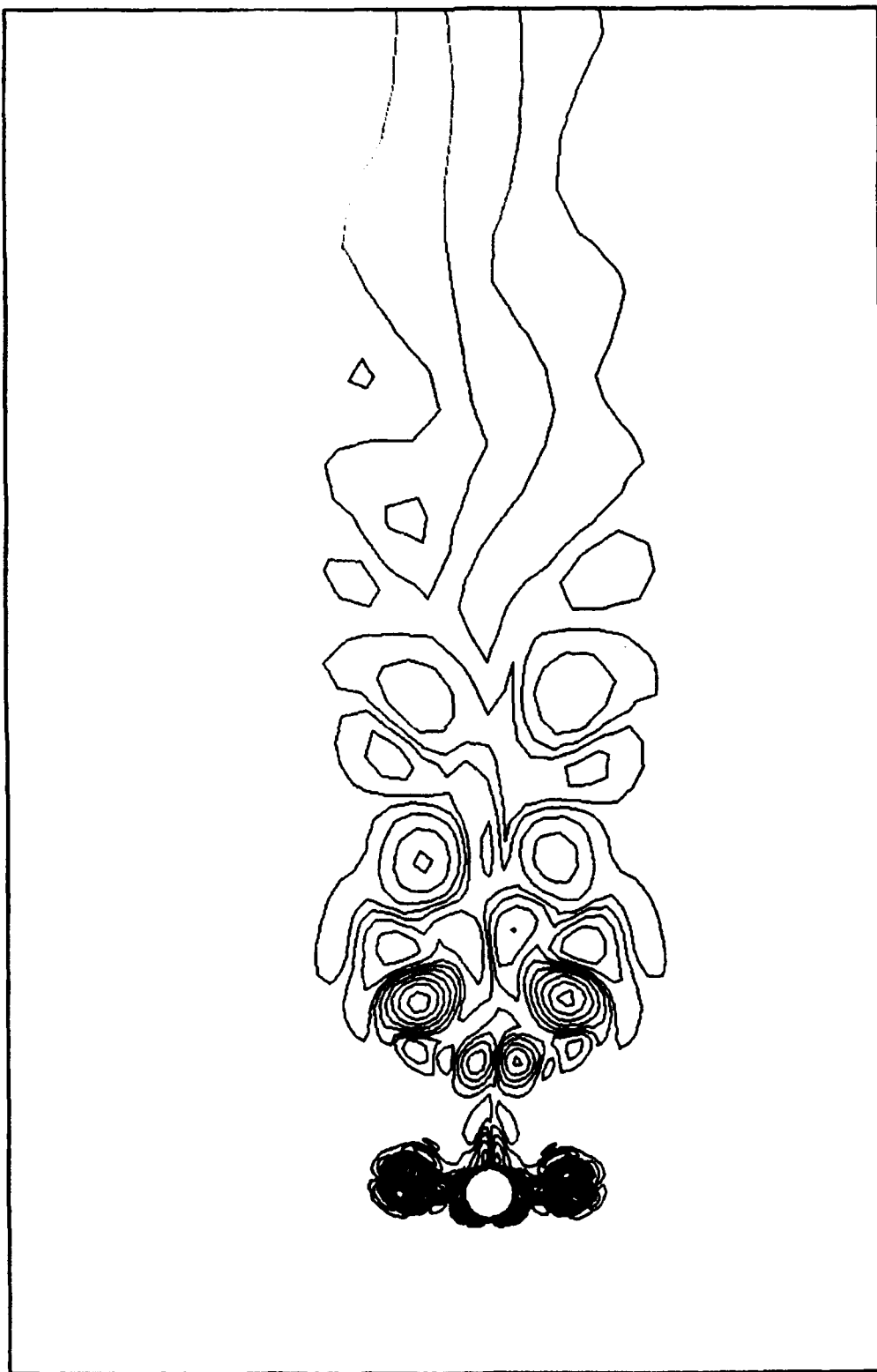Figure 9. Vorticity Contours, K = 4, Re = 800, V_r = 0.4, t/T = 9.0

30
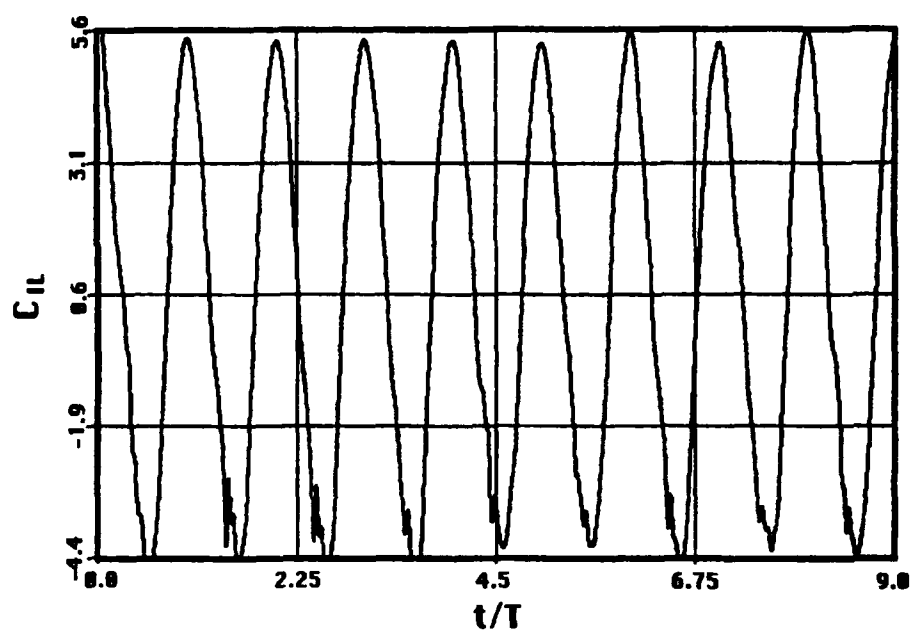
Figure 10. Inline Force Coefficient, K = 4, Re = 800, V_r = 0.5
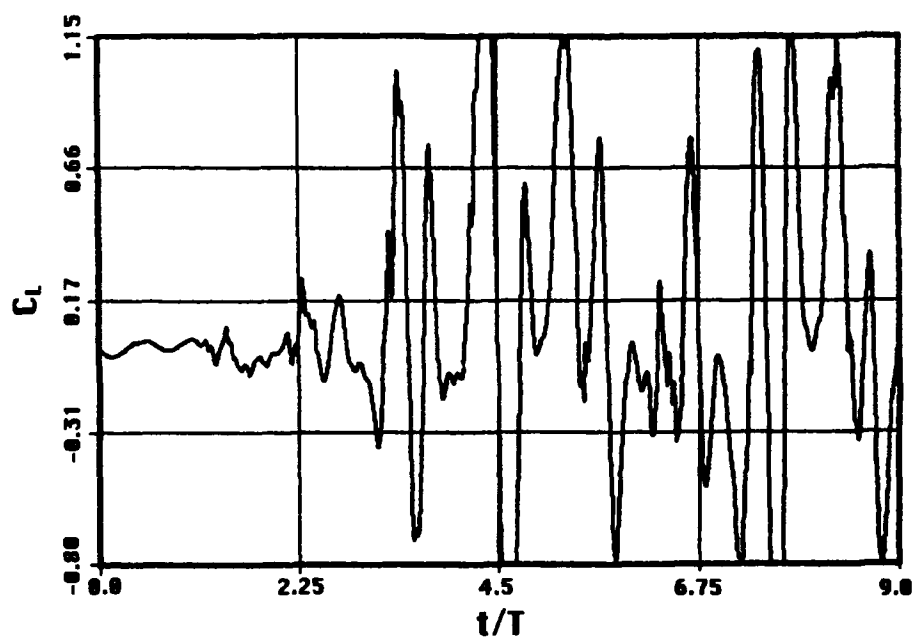
Figure 11. Transverse Force Coefficient, K = 4, Re = 800, V_r = 0.5

31
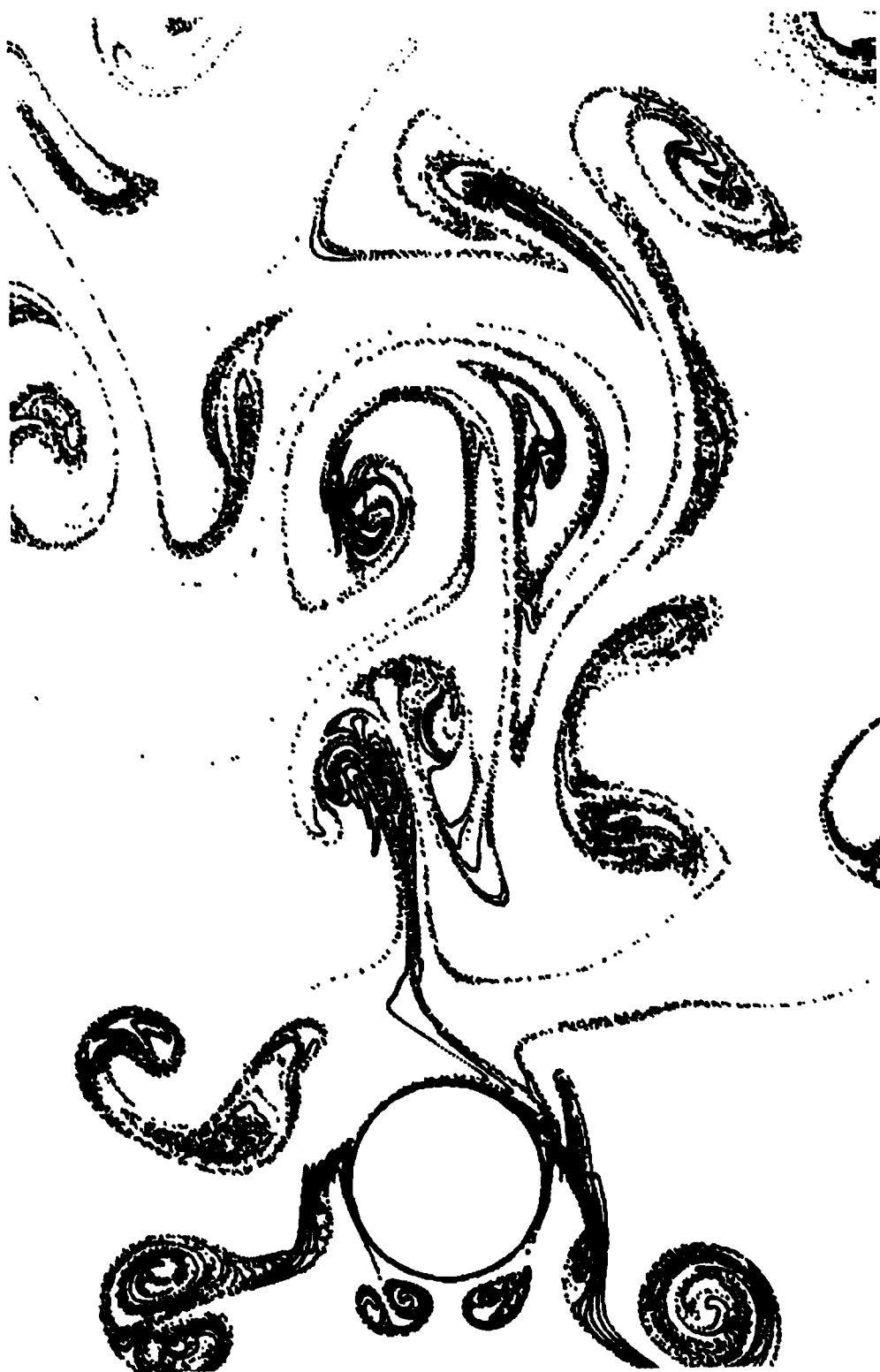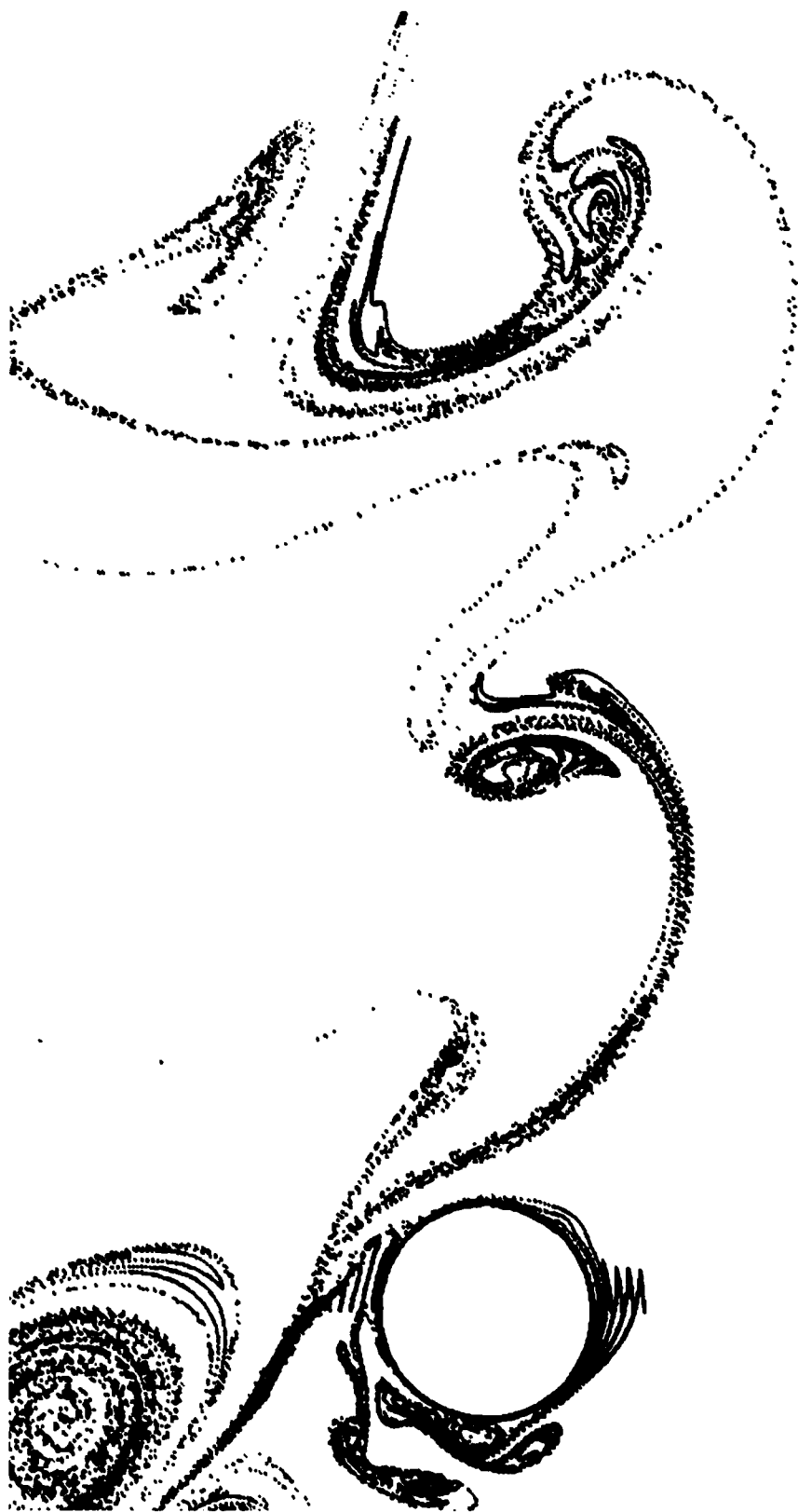
Figure 12. Closeup View of Streaklines, $K = 4$, $Re = 800$, $V_r = 0.5$, $t/T = 9.0$

Figure 13. Streaklines, K = 4, Re = 800, V_r = 0.5, t/T = 9.0
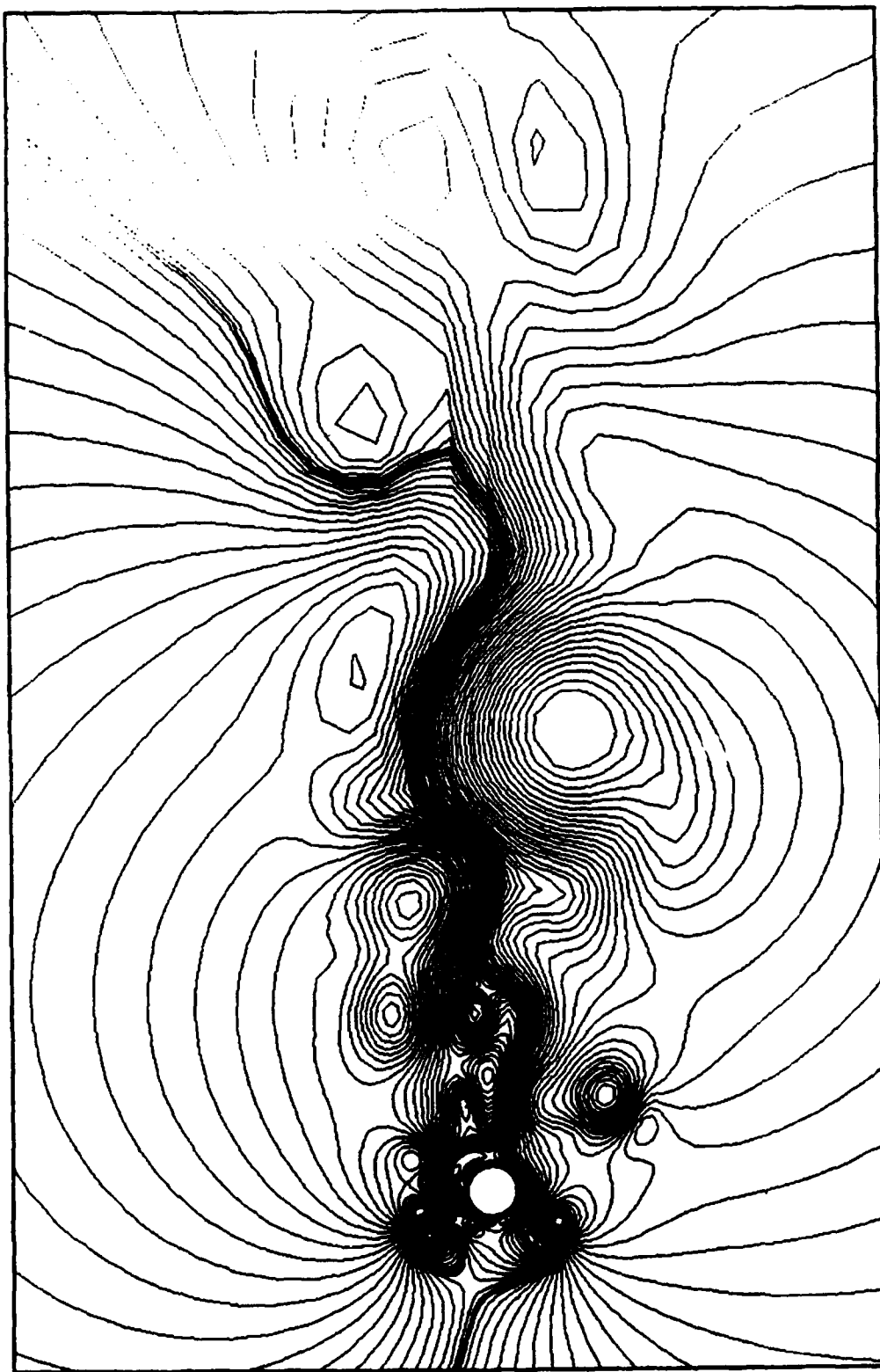
Figure 14. Streamlines, K = 4, Re = 800, V_r = 0.5, t/T = 9.0

34

Figure 15. Vorticity Contours, K = 4, Re = 800, V_r = 0.5, t/T = 9.0
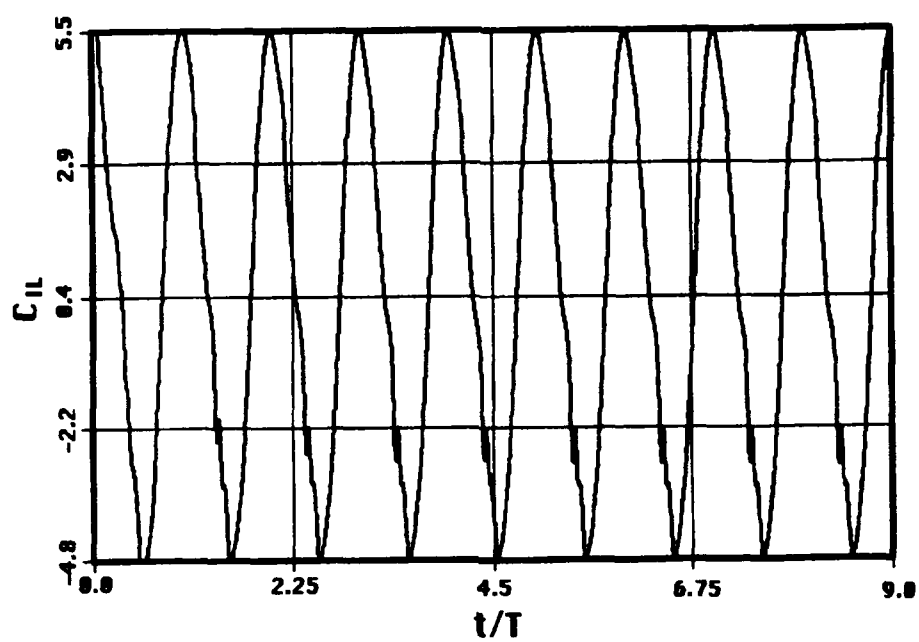
Figure 16. Inline Force Coefficient, K = 4, Re = 800, V_r = 0.6
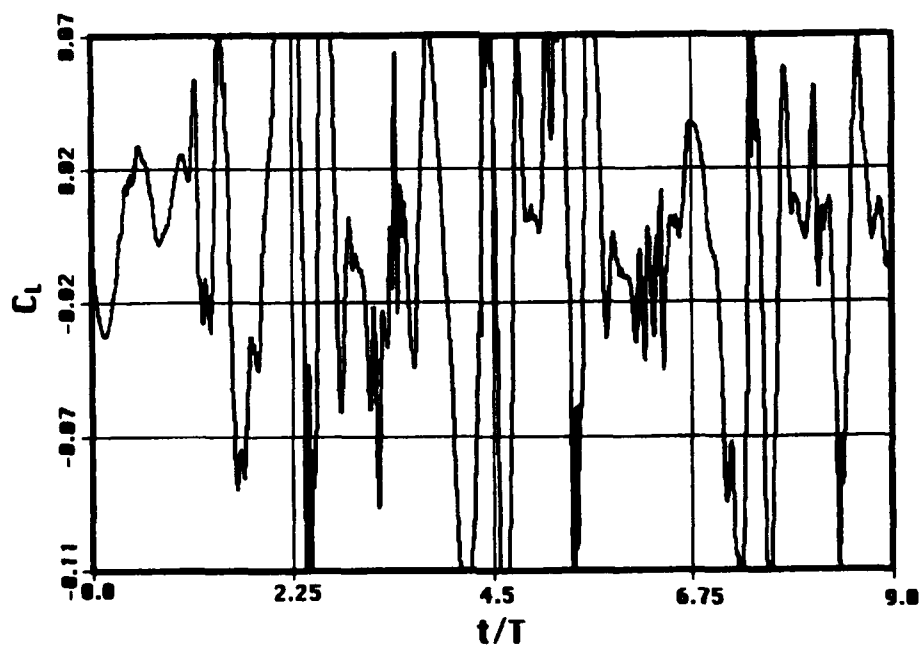
Figure 17. Transverse Force Coefficient, K = 4, Re = 800, V_r = 0.6.

36
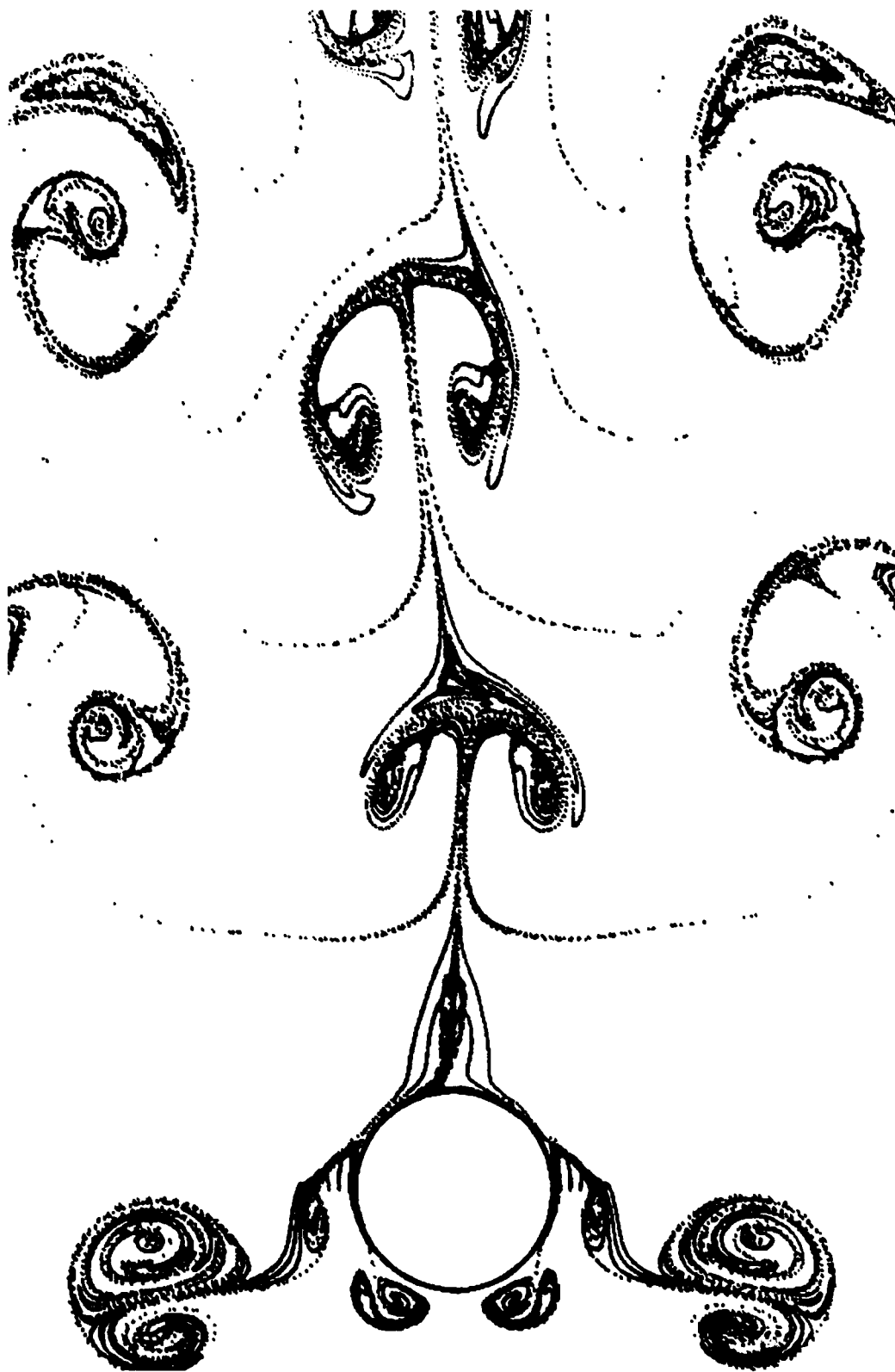
Figure 18. Closeup View of Streaklines, K = 4, Re = 800, V_r = 0.6, t/T = 9.0

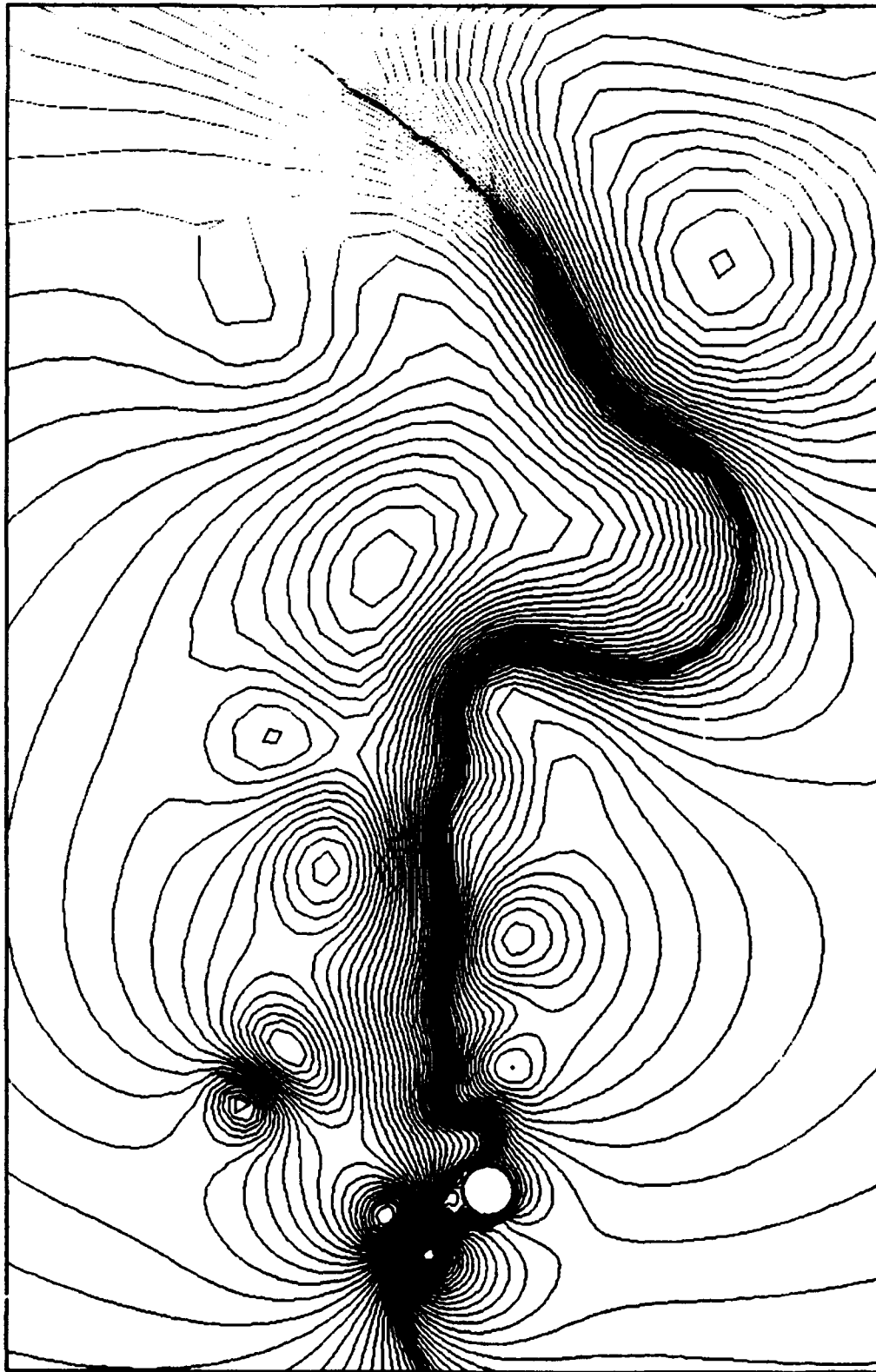Figure 19. Streaklines, K = 4, Re = 800, V_r = 0.6, t/T = 9.0
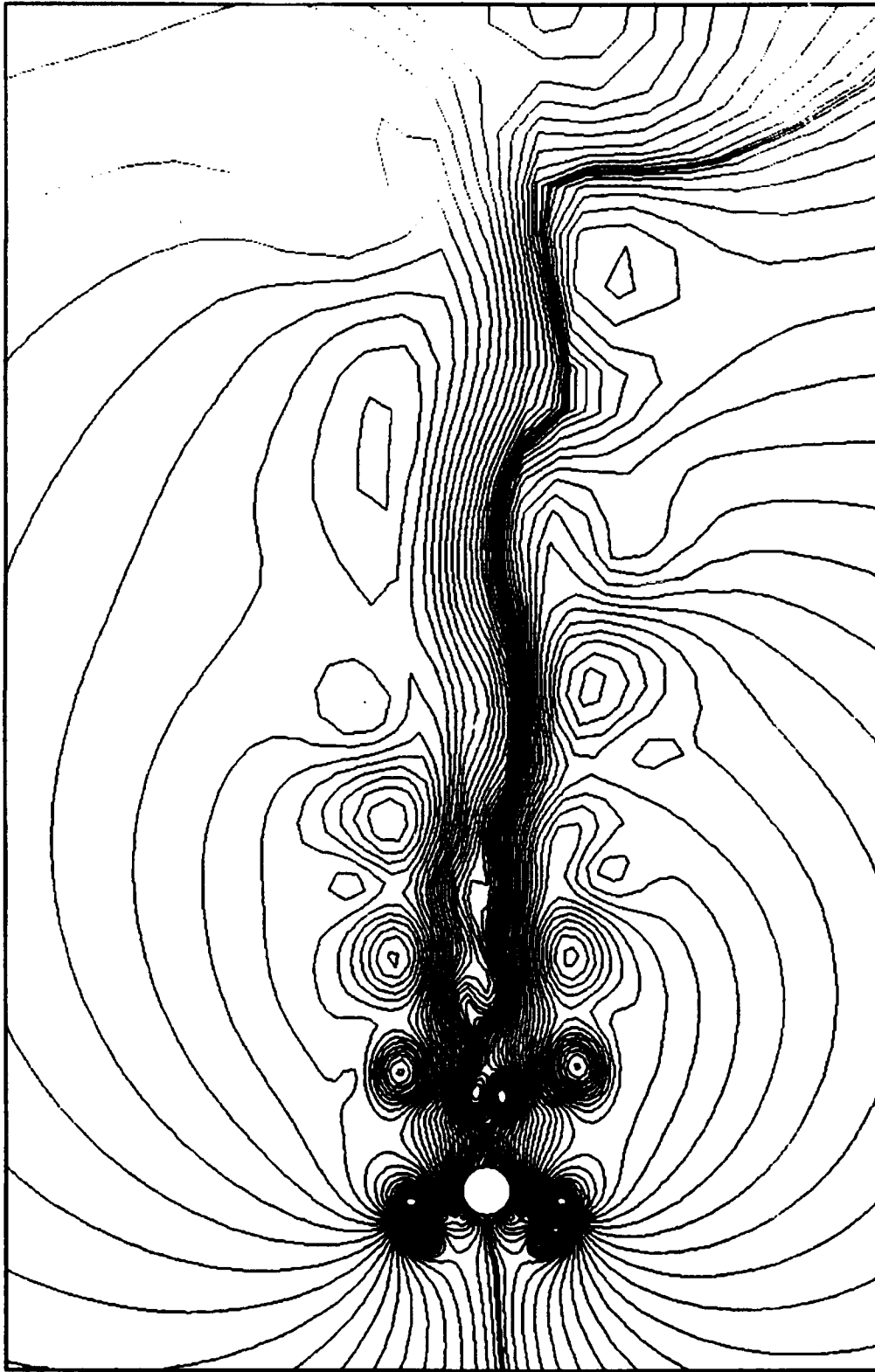
Figure 20. Streamlines, K = 4, Re = 800, V_r = 0.6, t/T = 9.0
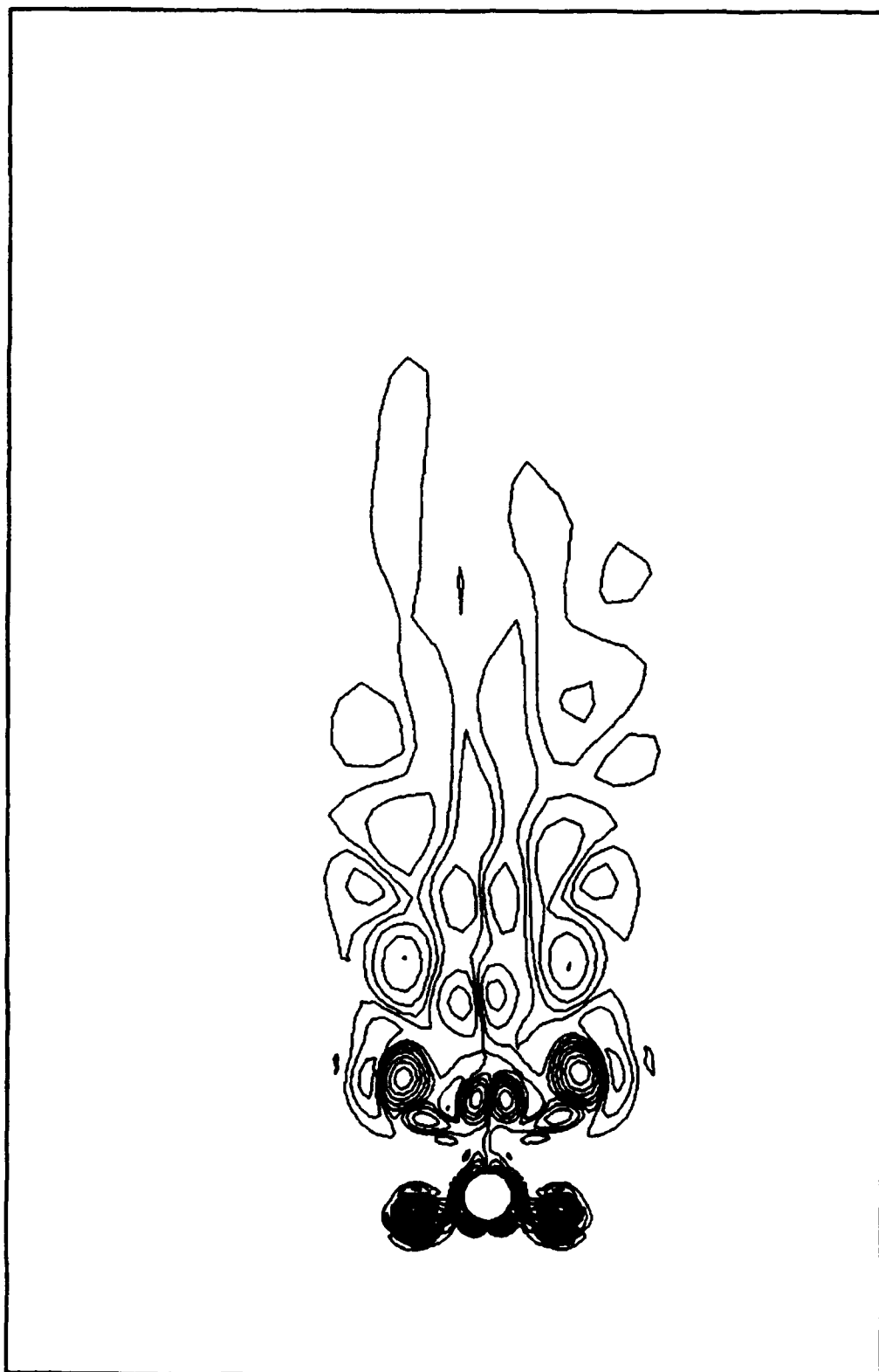
Figure 21. Vorticity Contours, K = 4, Re = 800, V_r = 0.6, t/T = 9.0
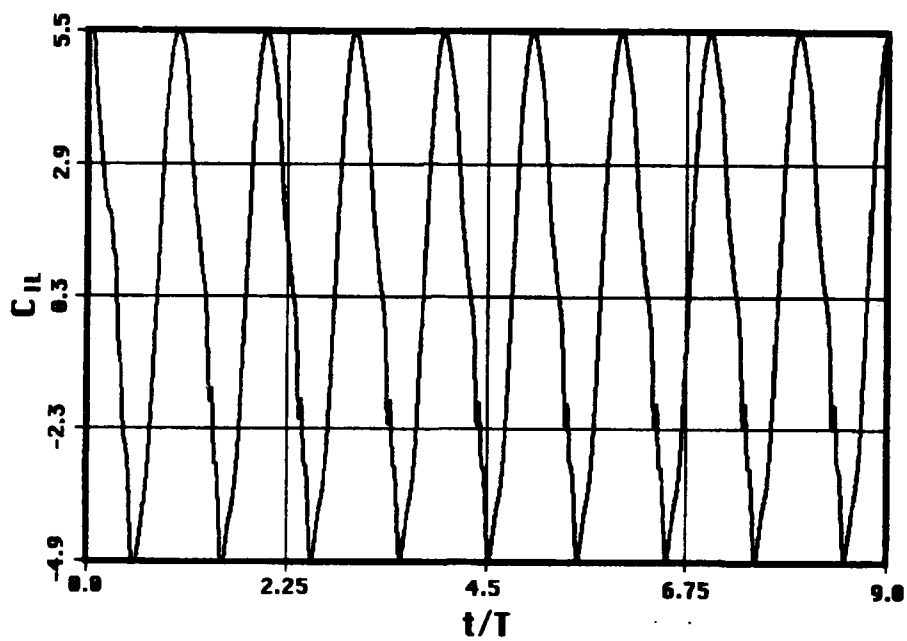
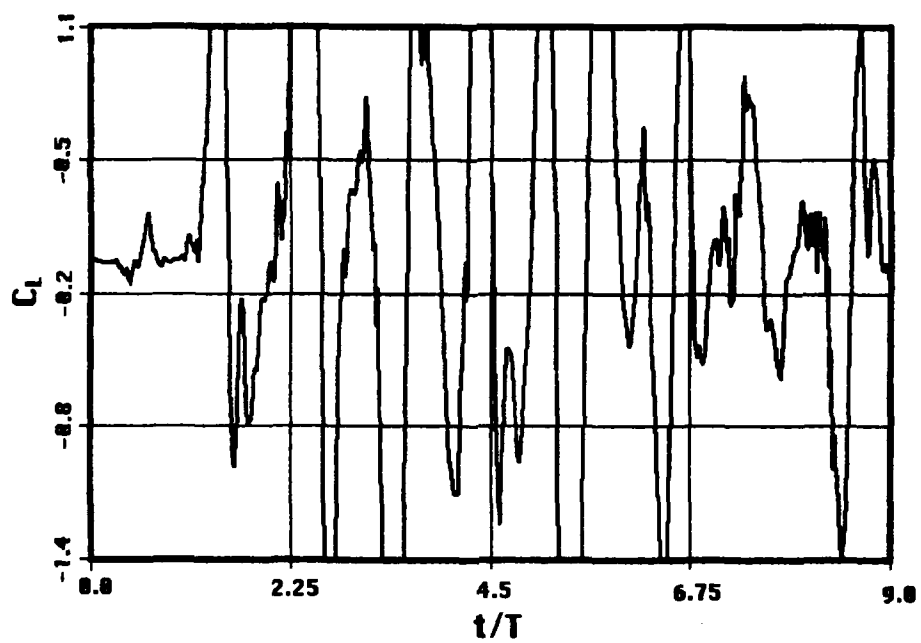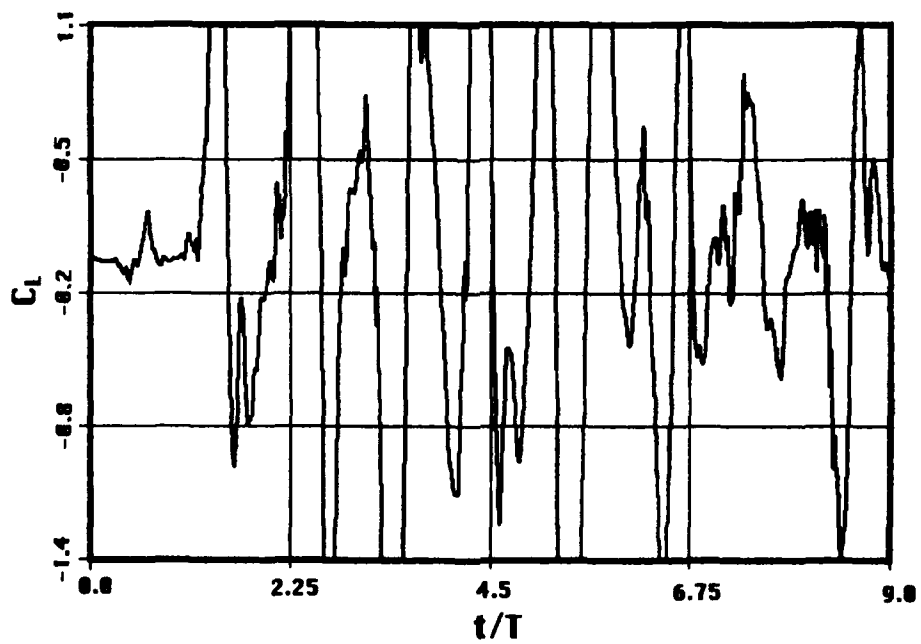Figure 22. Inline Force Coefficient, K = 4, Re = 800, V_r = 0.65
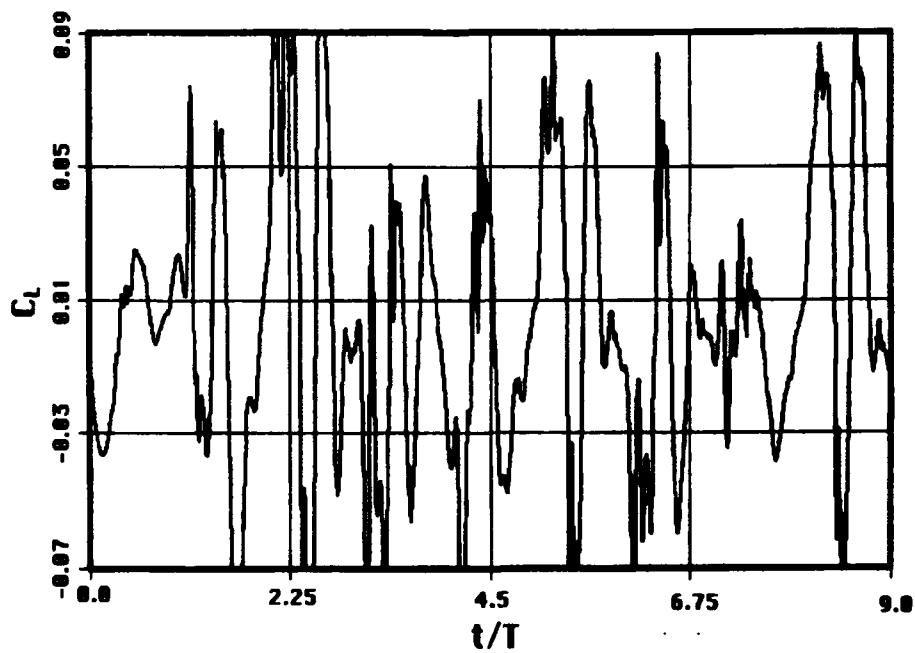
Figure 23. Transverse Force Coefficient, K = 4, Re = 800, V_r = 0.65

41
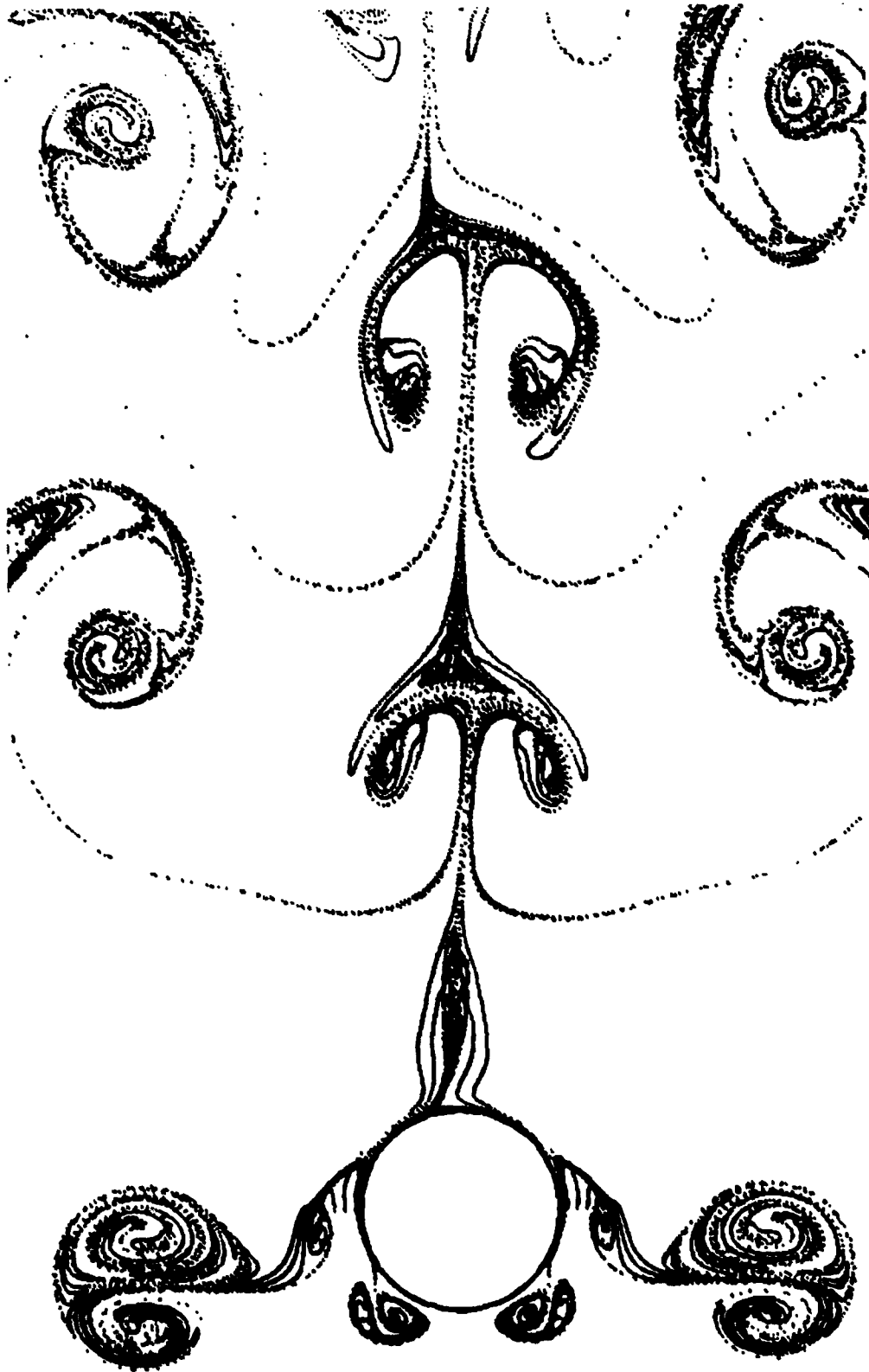
Figure 24. Closeup View of Streaklines, K = 4, Re = 800, V_r = 0.65, t/T = 9.0

Figure 25. Streaklines, K = 4, Re = 800, V_r = 0.65, t/T = 9.0

Figure 26. Streamlines, K = 4, Re = 800, V_r = 0.65, t/T = 9.0
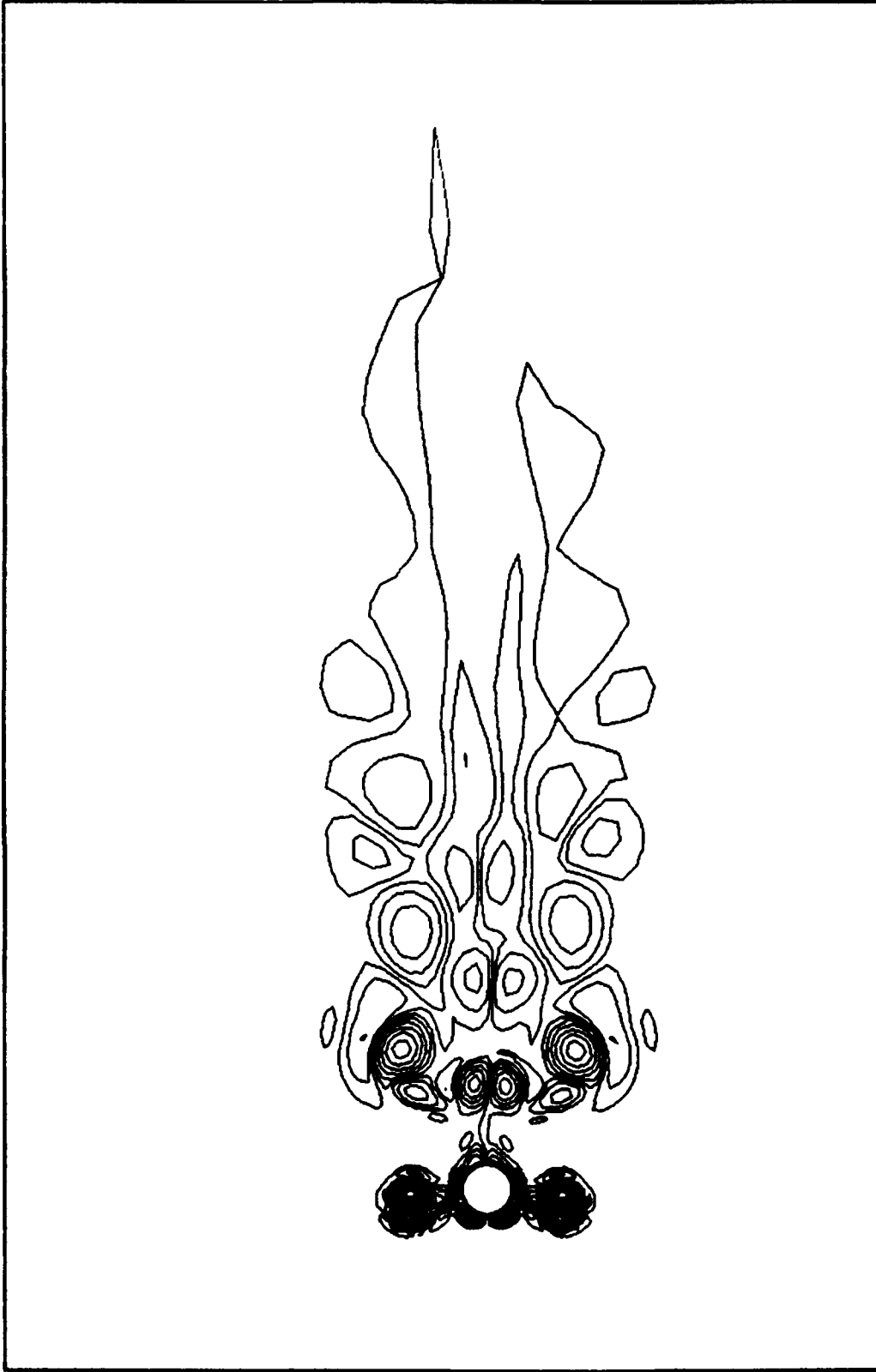
Figure 27. Vorticity Contours, K = 4, Re = 800, V_r = 0.65, t/T = 9.0

45

Figure 28. Inline Force Coefficient, K = 4, Re = 800, V_r = 0.7

Figure 29. Transverse Force Coefficient, K = 4, Re = 800, V_r = 0.7

46

Figure 30. Closeup View of Streaklines, $K = 4$, $Re = 800$, $V_r = 0.7$, $t/T = 20.0$

Figure 31. Streaklines, K = 4, Re = 800, V_r = 0.7, t/T = 20.0

48

Figure 32. Streamlines, K = 4, Re = 800, V_r = 0.7, t/T = 20.0

49
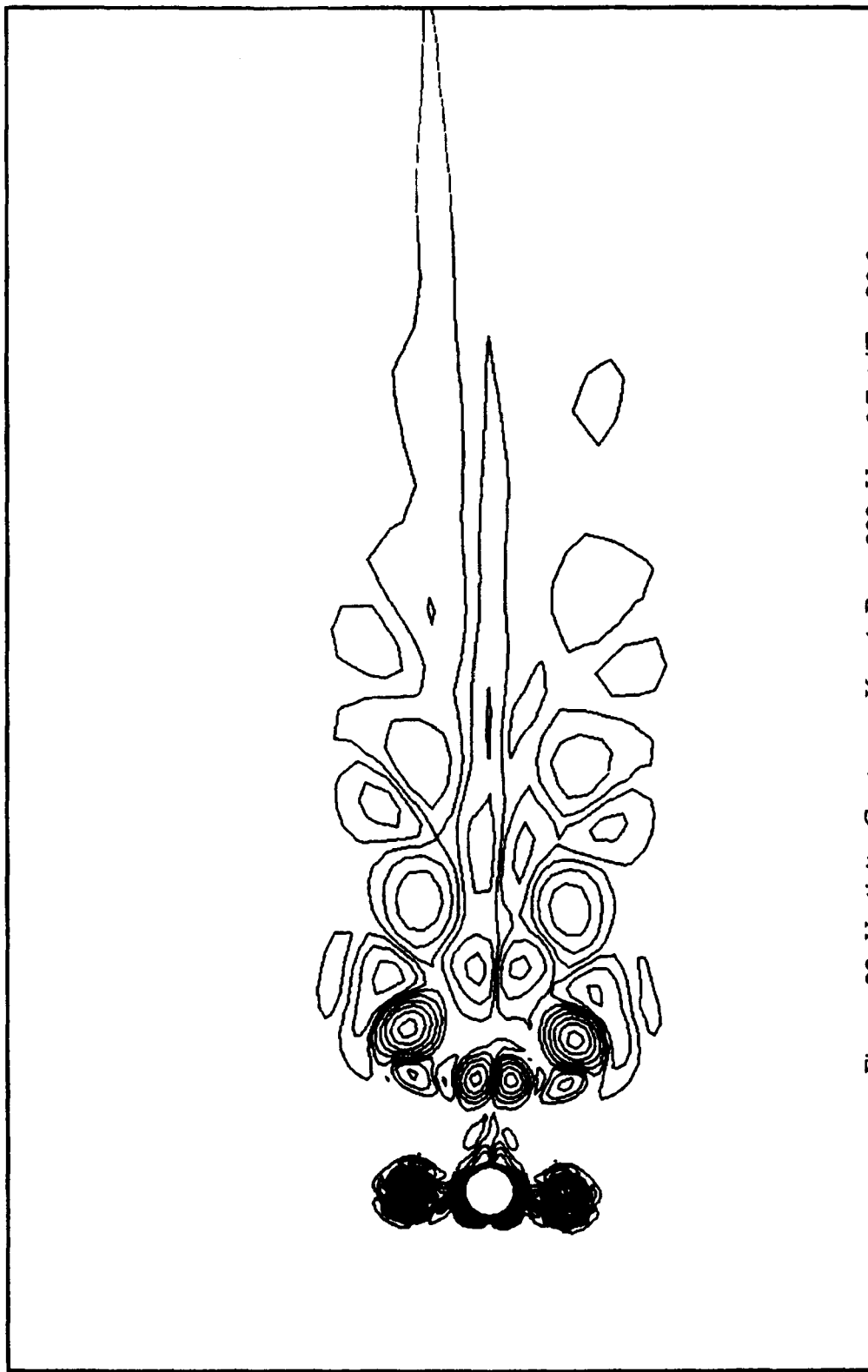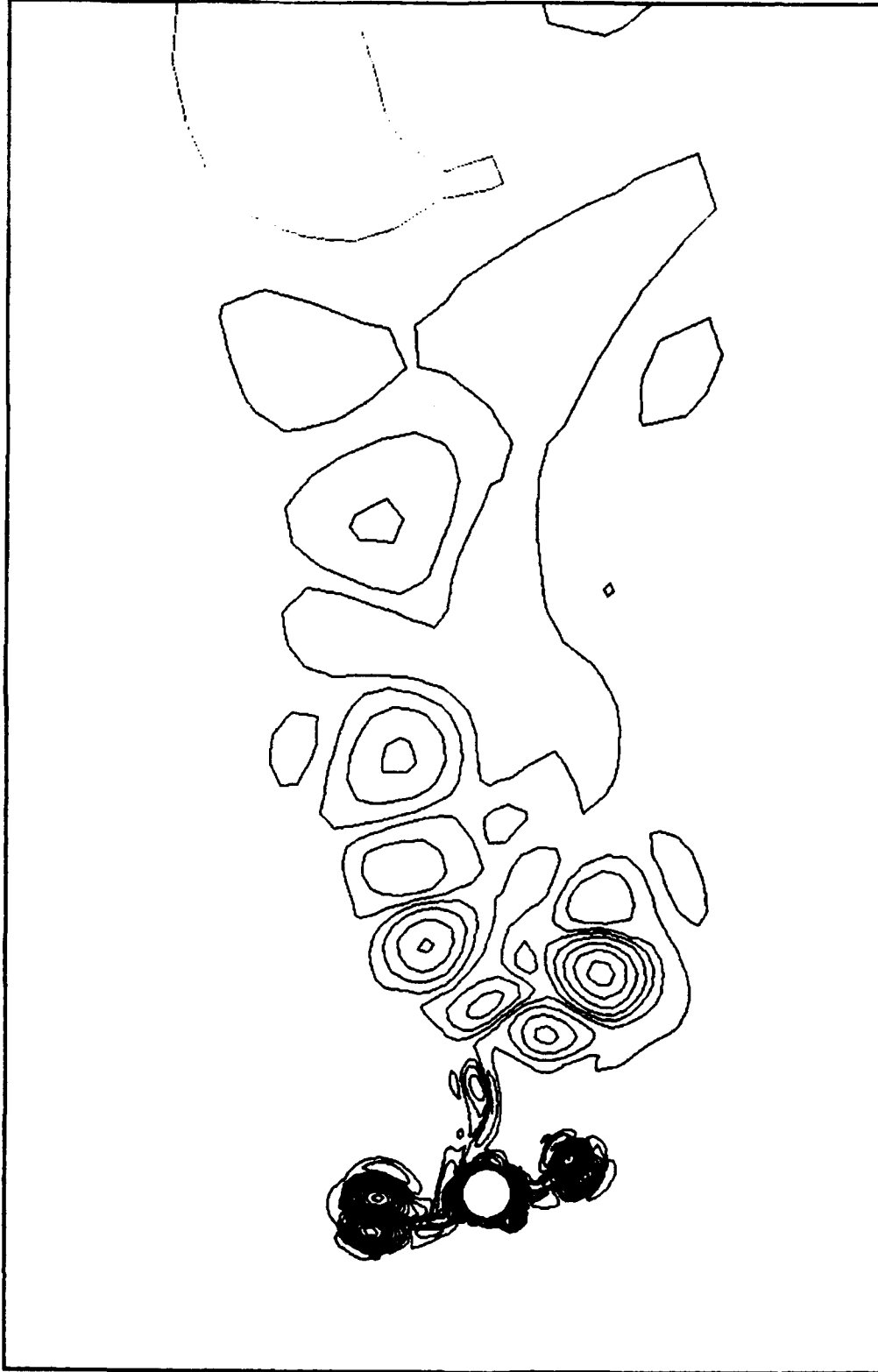
Figure 33. Vorticity Contours, K = 4, Re = 800, V_r = 0.7, t/T = 20.0

Figure 34. Inline Force Coefficient, K = 4, Re = 800, V_r = 0.8

Figure 35. Transverse Force Coefficient, K = 4, Re = 800, V_r = 0.8

51

Figure 36. Closeup View of Streaklines, K = 4, Re = 800, V_r = 0.8, t/T = 9.0

Figure 37. Streaklines, $K = 4$, $Re = 800$, $V_r = 0.8$, $t/T = 9.0$

Figure 38. Streamlines, $K = 4$, $Re = 800$, $V_r = 0.8$, $t/T = 9.0$

54

Figure 39. Vorticity Contours, K = 4, Re = 800, V_r = 0.8, t/T = 9.0

55
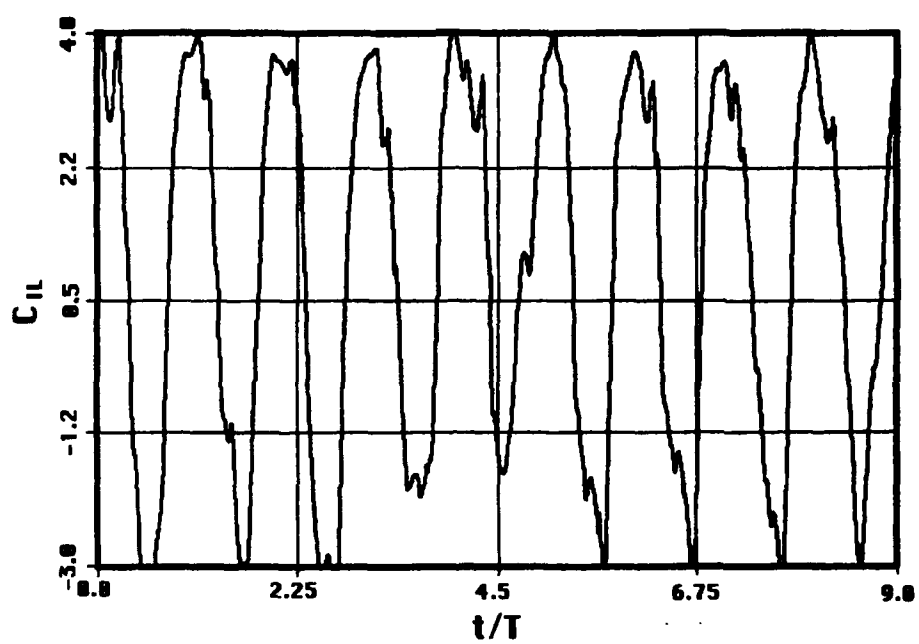
Figure 40. Inline Force Coefficient, K = 6, Re = 1200, V_r = 0.6
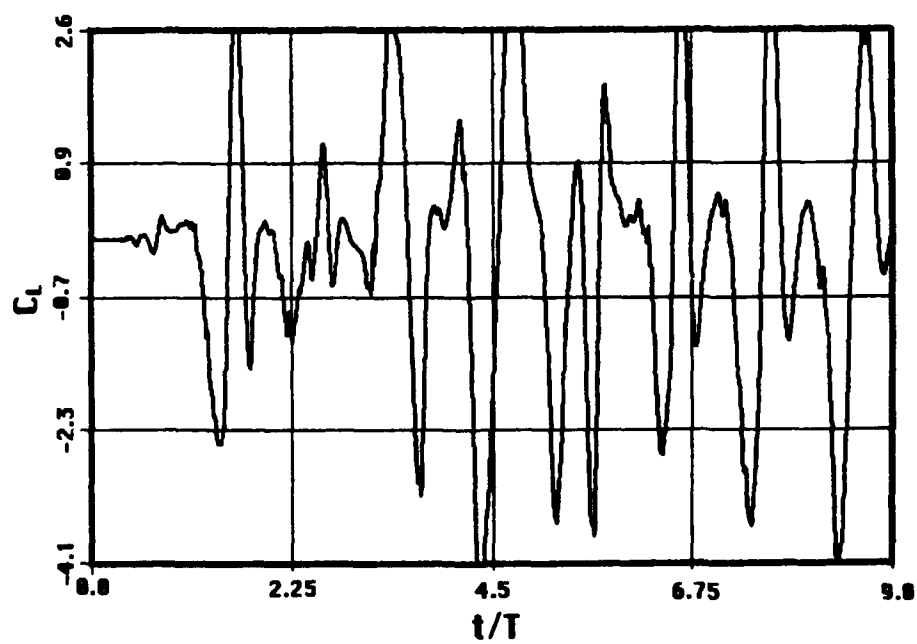
Figure 41. Transverse Force Coefficient, K = 6, Re = 1200, V_r = 0.6

56

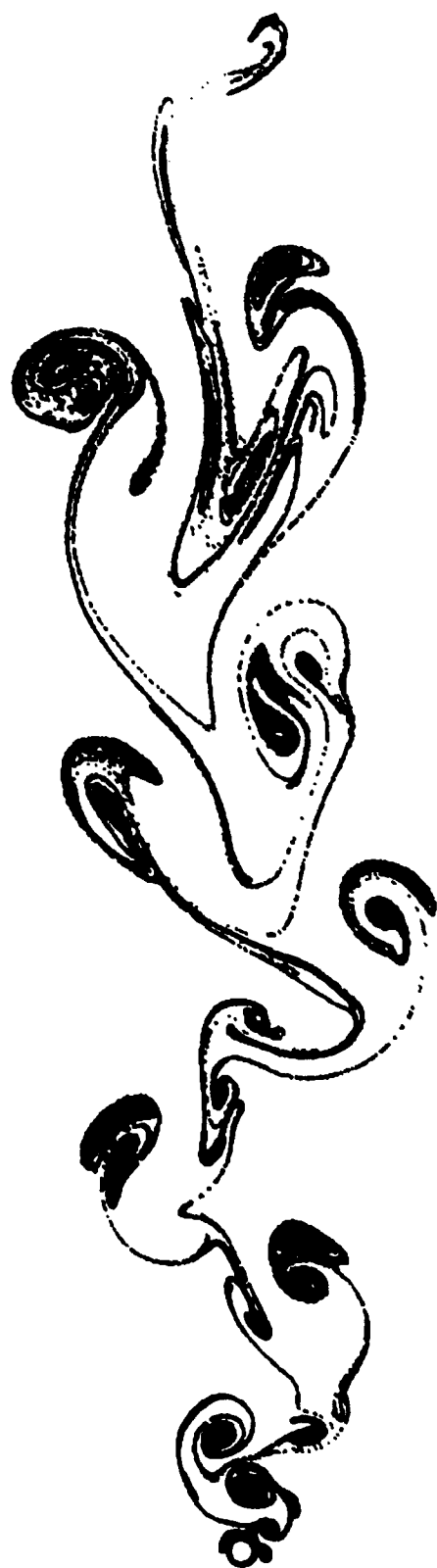Figure 42. Closeup View of Streaklines, $K = 6$, $Re = 1200$, $V_r = 0.6$, $t/T = 9.0$

57

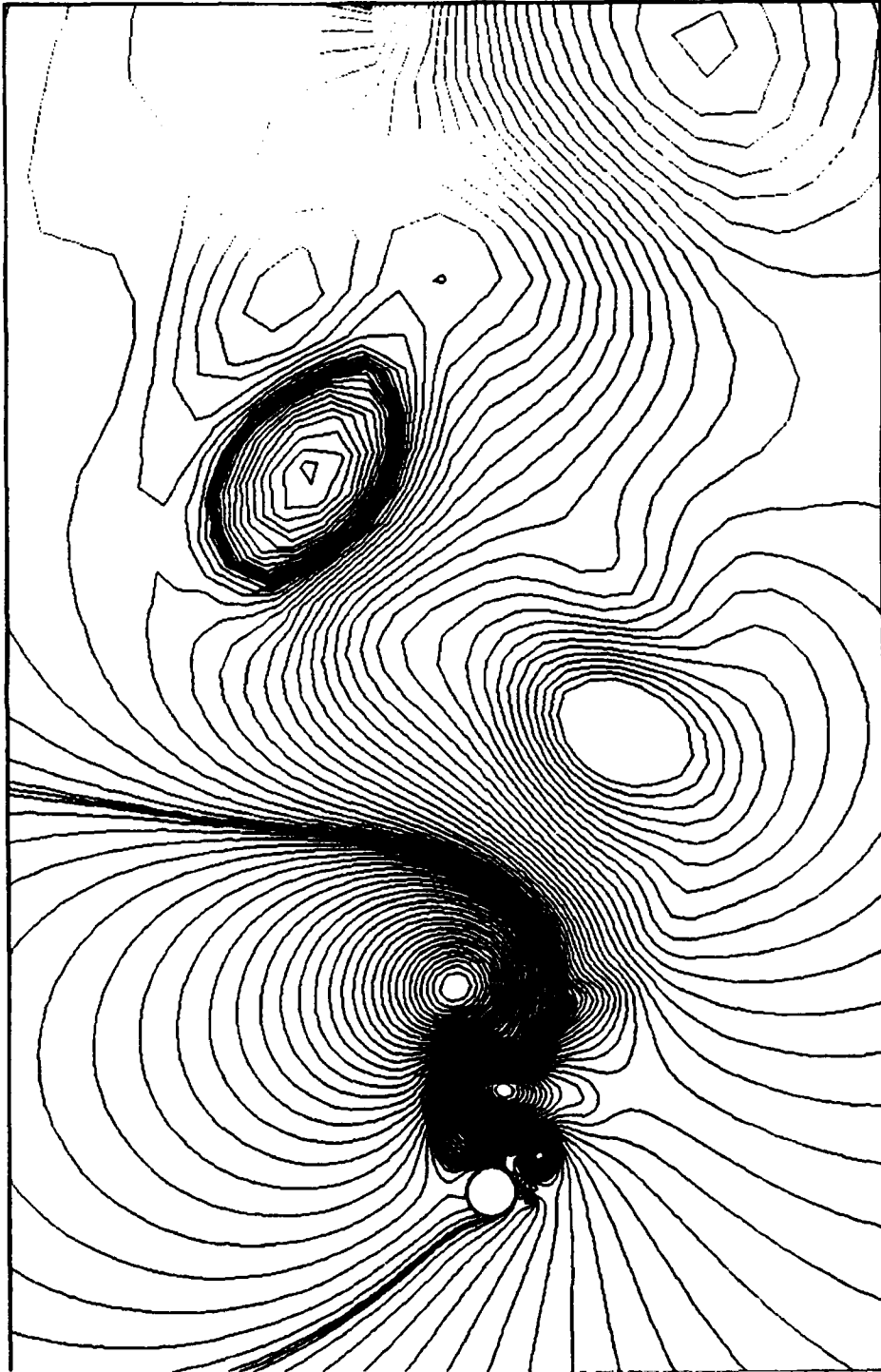Figure 43. Streaklines, K = 6, Re = 1200, V_r = 0.6, t/T = 9.0

Figure 44. Streamlines, K = 6, Re = 1200, V_r = 0.6, t/T = 9.0

59
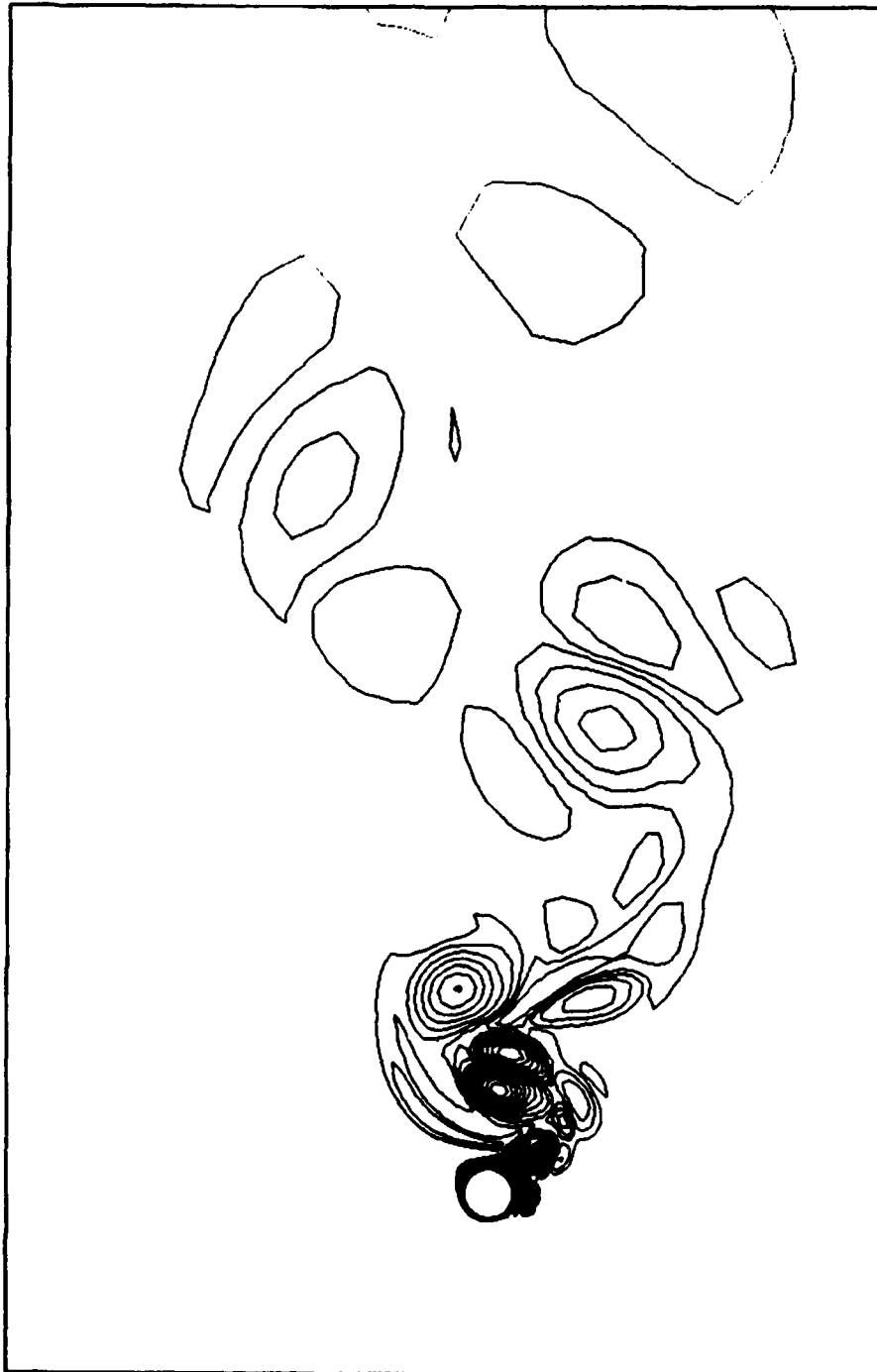
Figure 45. Vorticity Contours, K = 6, Re = 1200, V_r = 0.6, t/T = 9.0
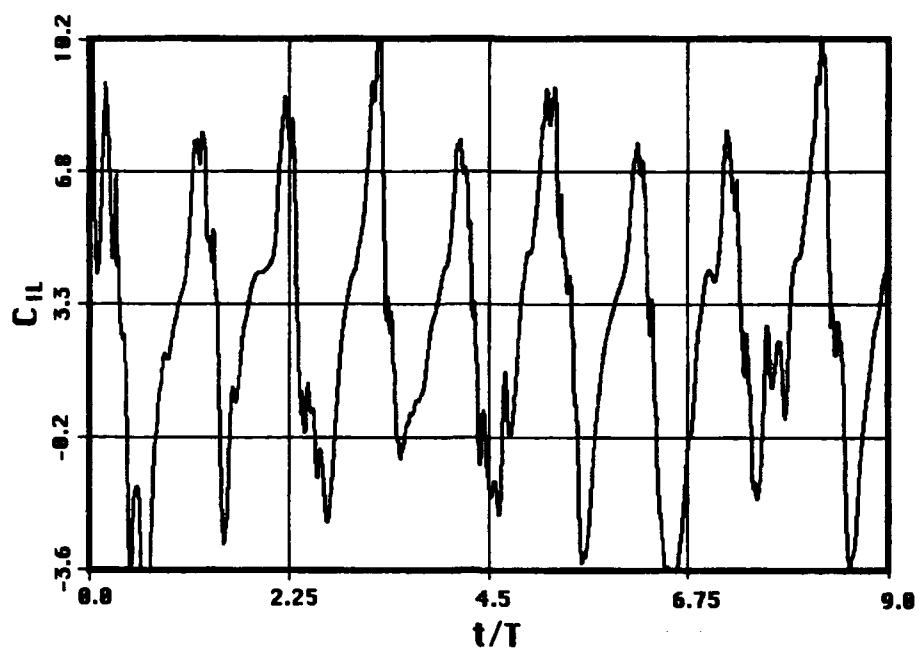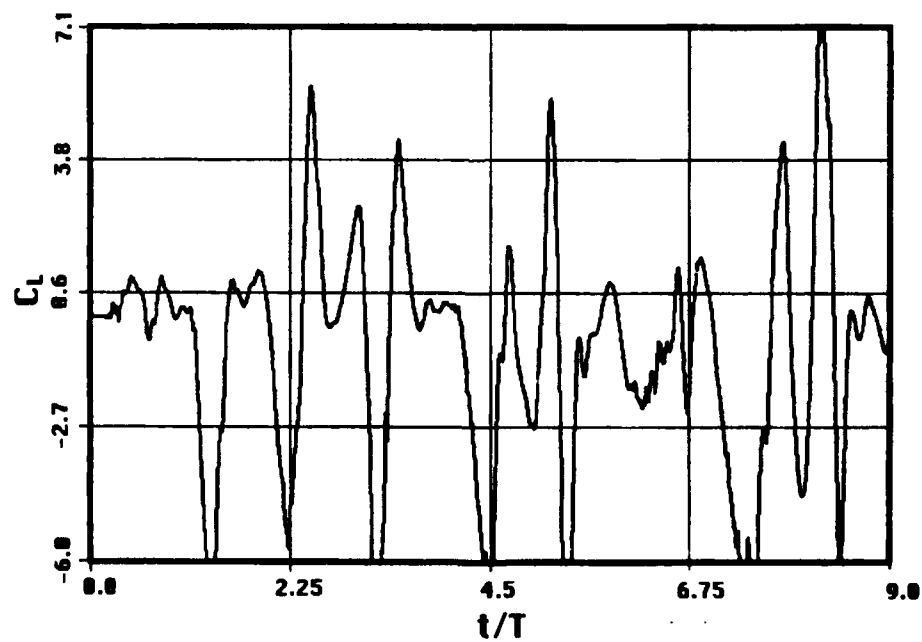
Figure 46. Inline Force Coefficient, K = 6, Re = 1200, V_r = 0.7

Figure 47. Tranverse Force Coefficient, K = 6, Re = 1200, V_r = 0.7

61

Figure 48. Closeup View of Streaklines, K = 6, Re = 1200, V_r = 0.7, t/T = 9.0

Figure 49. Streaklines, K = 6, Re = 1200, V_r = 0.7, t/T = 9.0
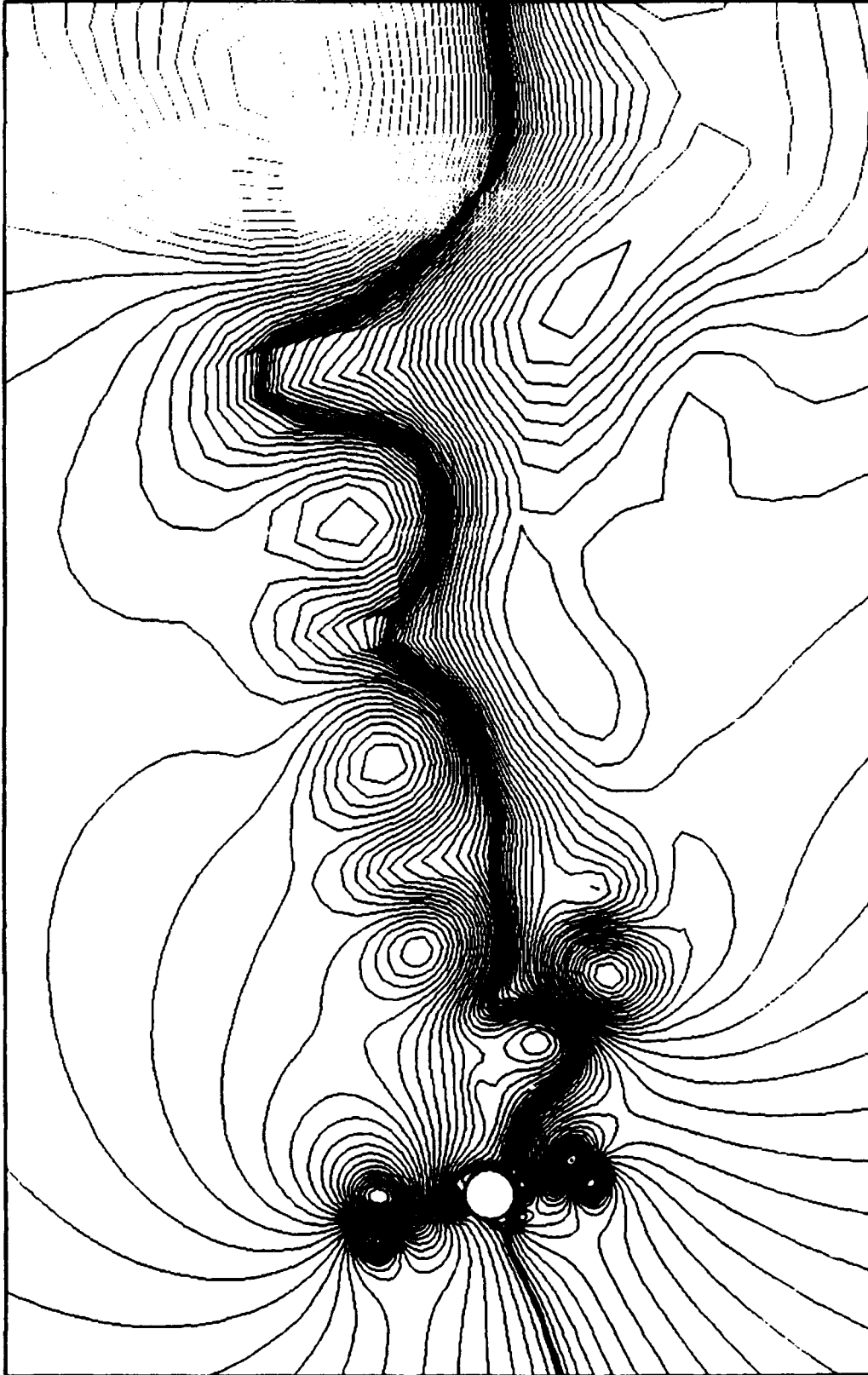
Figure 50. Streamlines, $K = 6$, $Re = 1200$, $V_r = 0.7$, $t/T = 9.0$

64

Figure 51. Vorticity Contours, K = 6, Re = 1200, V_r = 0.7, t/T = 9.0
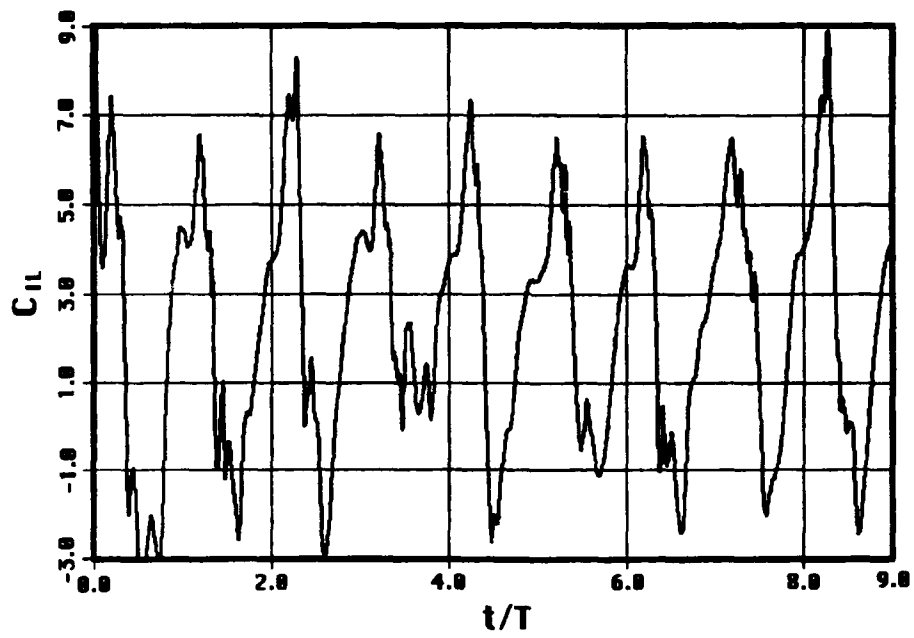
Figure 52. Inline Force Coefficient, K = 6, Re = 1200, V_r = 1.0
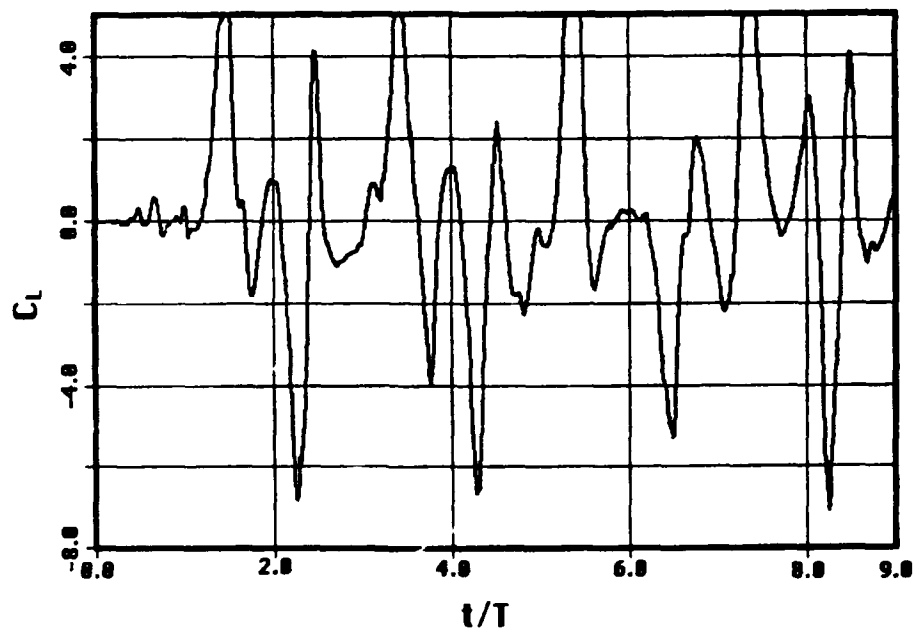
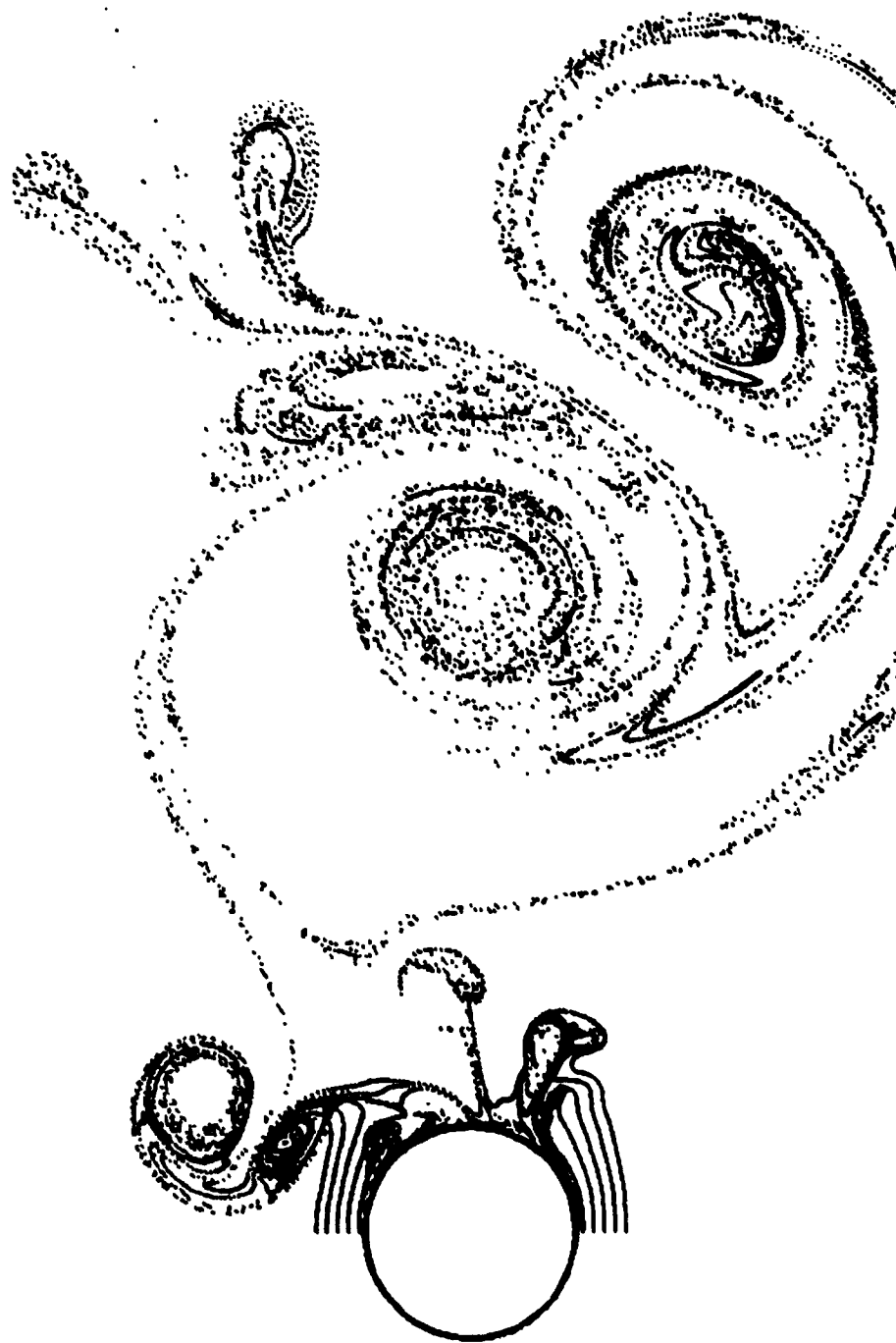Figure 53. Transverse Force Coefficient, K = 6, Re = 1200, V_r = 1.0

66

Figure 54. Closeup View of Streaklines, K = 6, Re = 1200, V_r = 1.0, t/T = 9.0

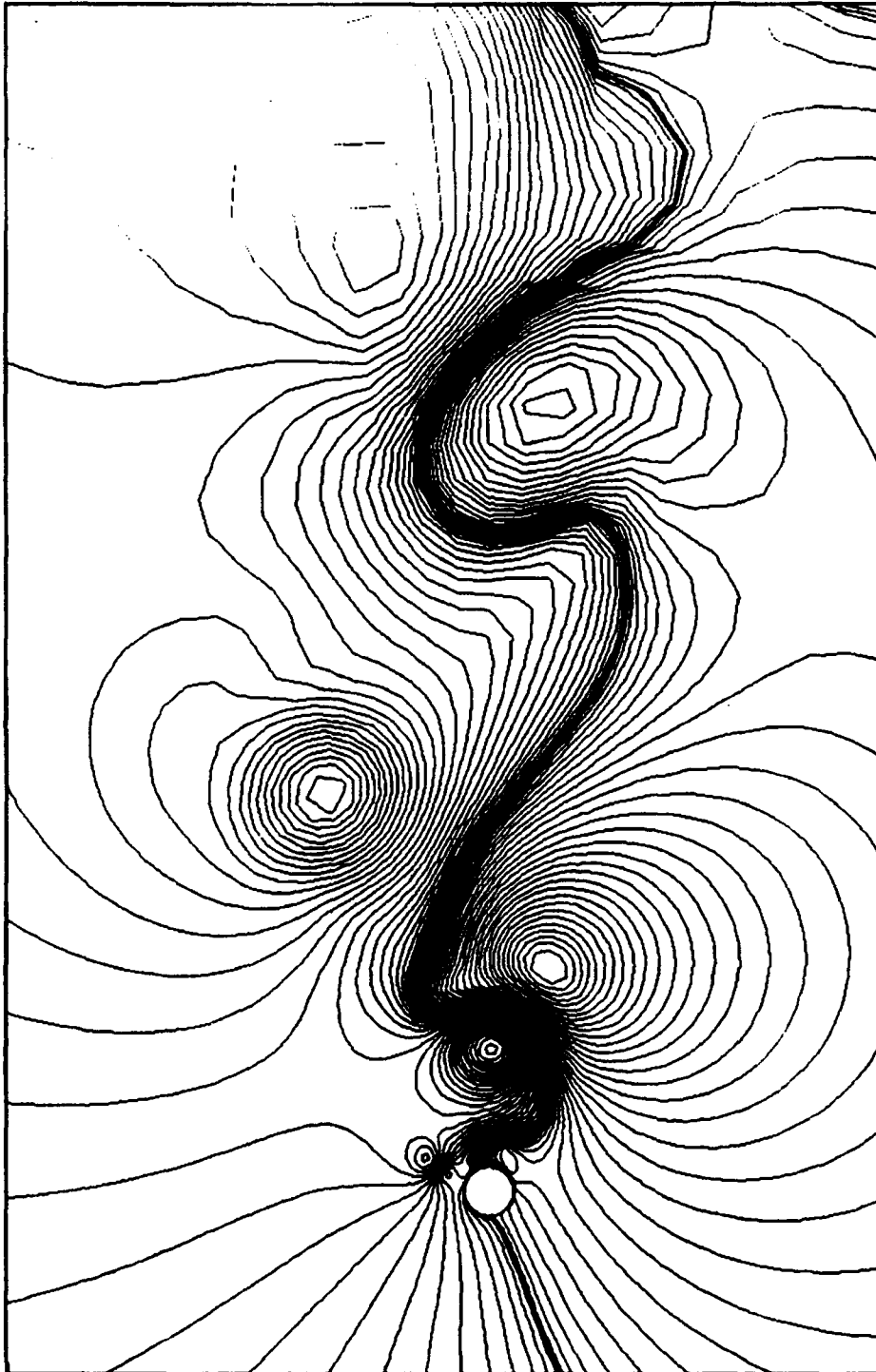Figure 55. Streaklines, K = 6, Re = 1200, V_r = 1.0, t/T = 9.0

Figure 56. Streamlines, $K = 6$, $Re = 1200$, $V_r = 1.0$, $t/T = 9.0$

69

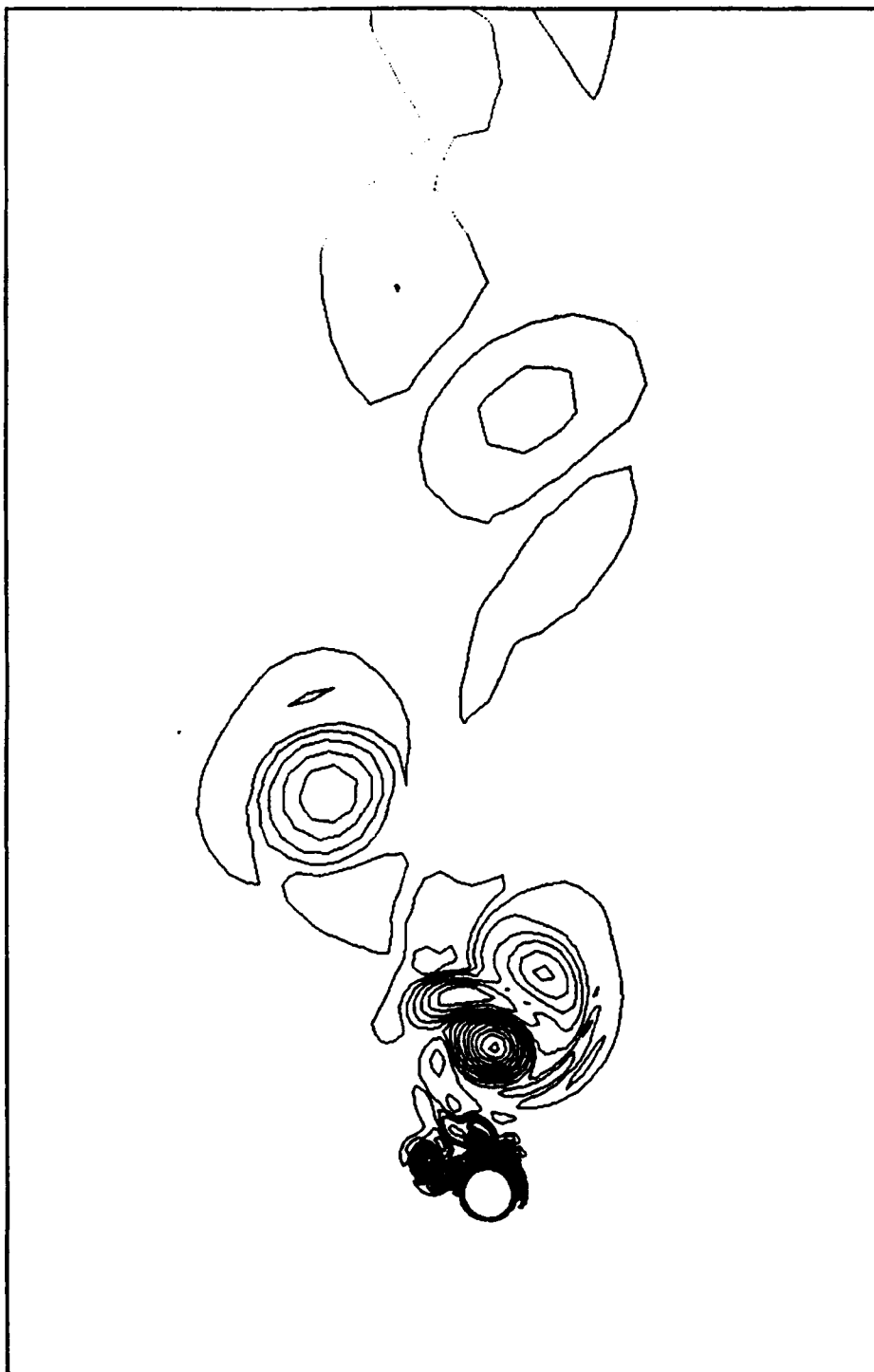Figure 57. Vorticity Contours, K = 6, Re = 1200, V_r = 1.0, t/T = 9.0

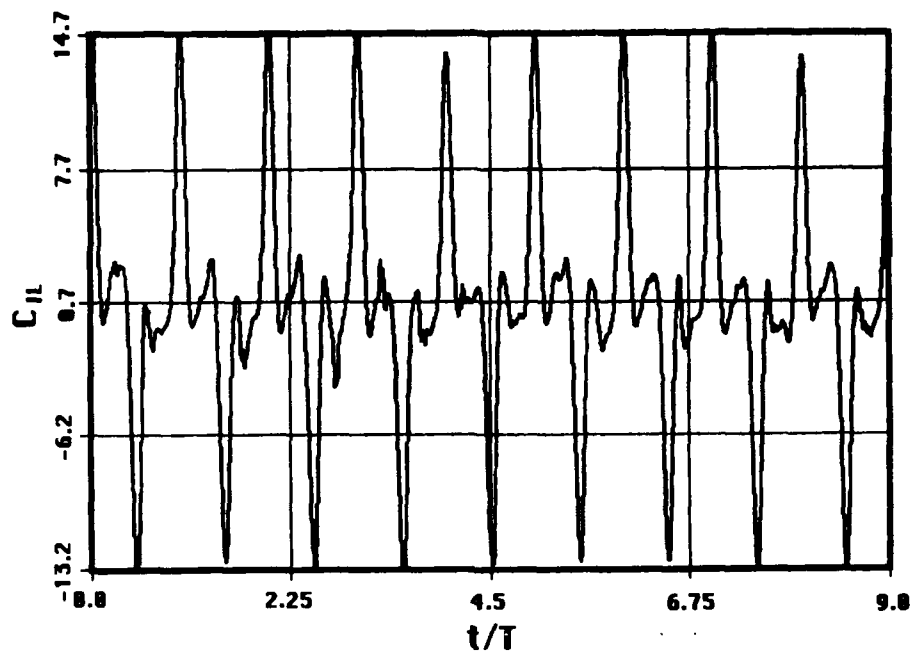Figure 58. Inline Force Coefficient, K = 6, Re = 1200, V_r = 1.2

Figure 59. Transverse Force Coefficient, K = 6, Re = 1200, V_r = 1.2

71

Figure 60. Closeup View of Streaklines, K = 6, Re = 1200, V_r = 1.2, t/T = 9.0

Figure 61. Streaklines, K = 6, Re = 1200, V_r = 1.2, t/T = 9.0

Figure 62. Streamlines, K = 6, Re = 1200, V_r = 1.2, t/T = 9.0

74

Figure 63. Vorticity Contours, K = 6, Re = 1200, V_r = 1.2, t/T = 9.0

Figure 64. Inline Force Coefficient, K = 4, Re = 800, V_r = 0.6
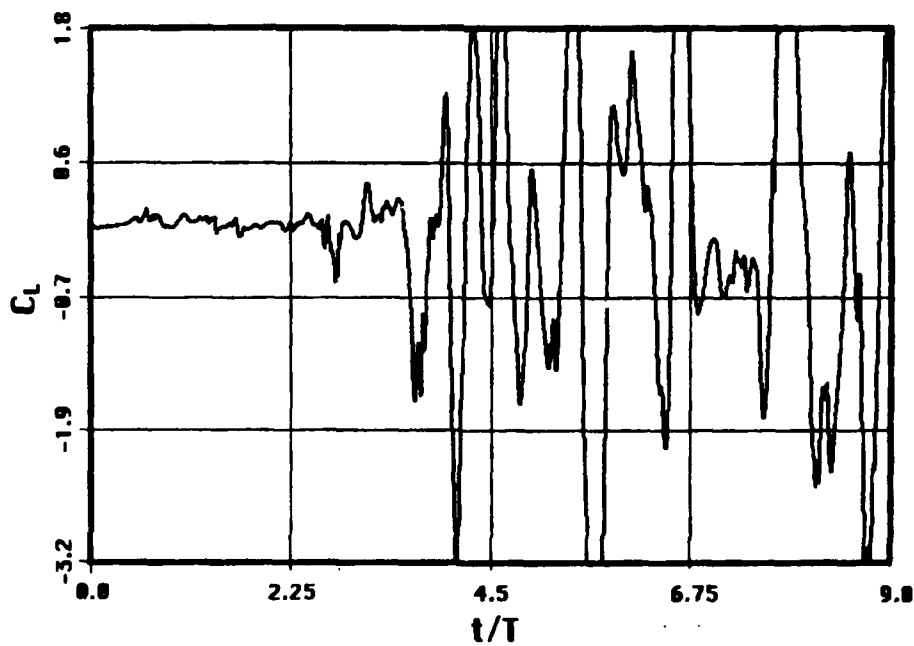("Steep Sine" Oscillation)

Figure 65. Transverse Force Coefficient, K = 4, Re = 800, V_r = 0.6
("Steep Sine" Oscillation)

76

Figure 66. Closeup View of Streaklines, K = 4, Re = 800, V_r = 0.6, t/T = 9.0
("Steep Sine" Oscillation)

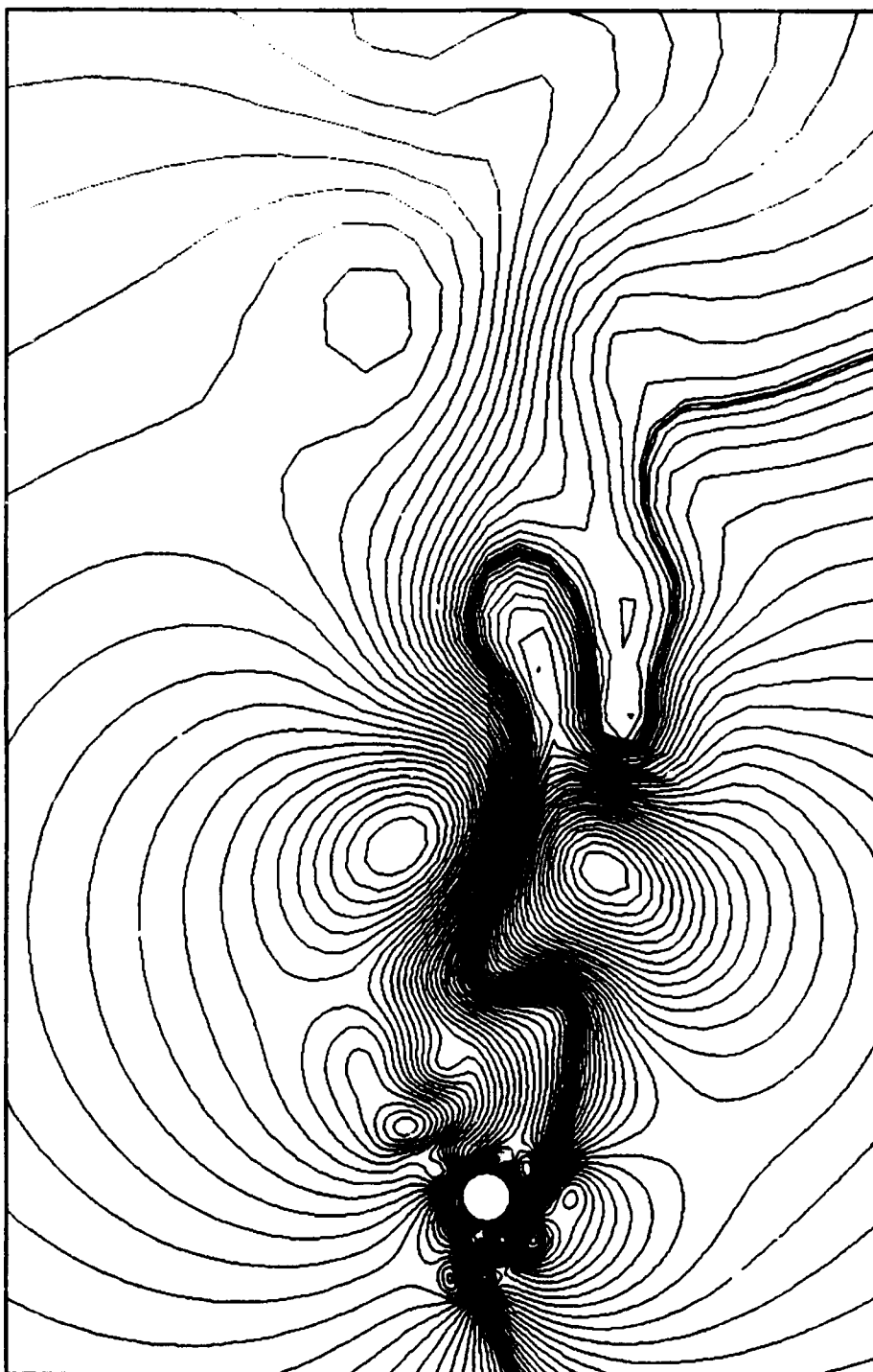Figure 67. Streaklines, K = 4, Re = 800, V_r = 0.6, t/T = 9.0
("Steep Sine" Oscillation)

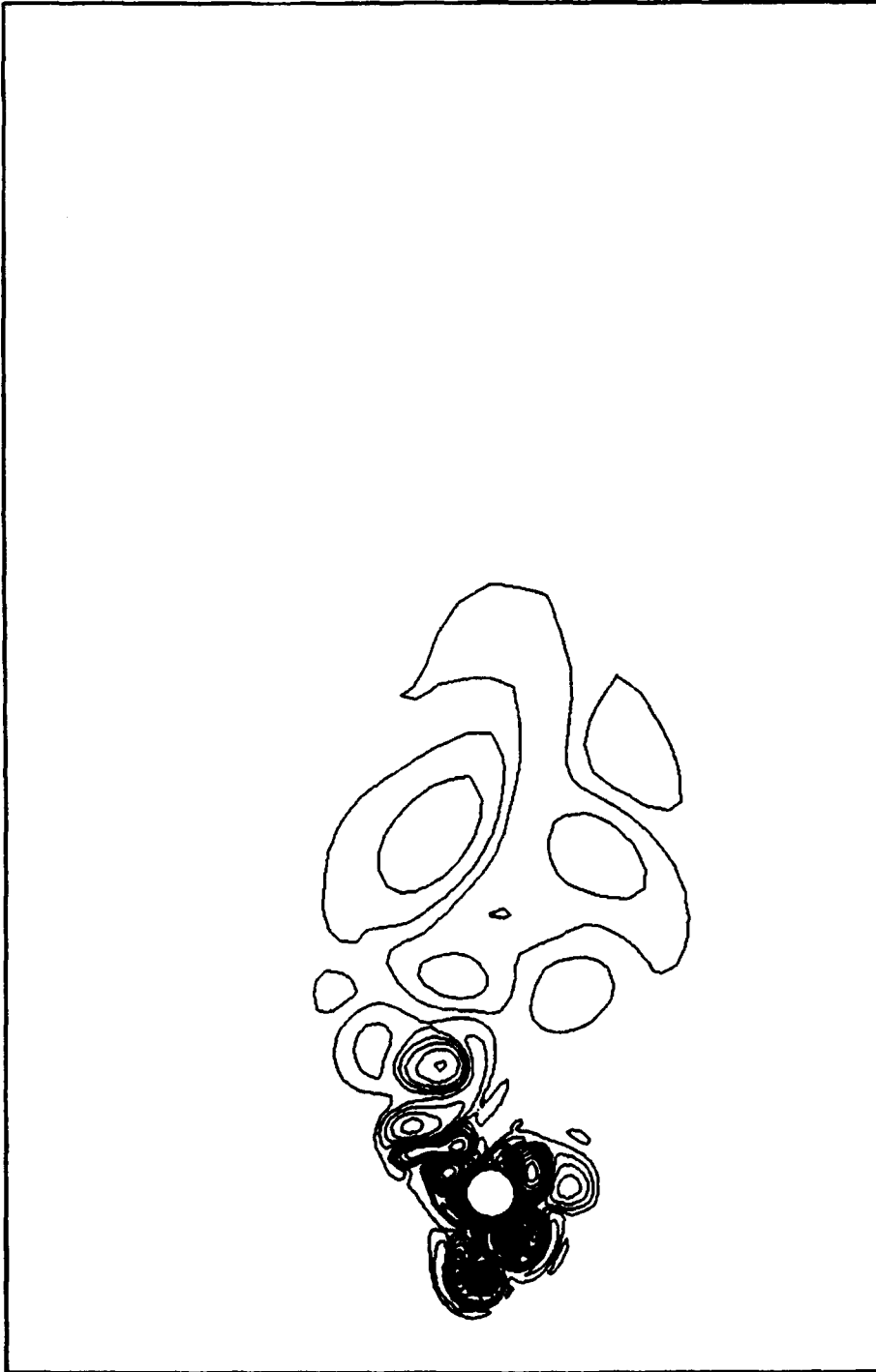Figure 68. Streamlines, K = 4, Re = 800, V_r = 0.6, t/T = 9.0
("Steep Sine" Oscillation)

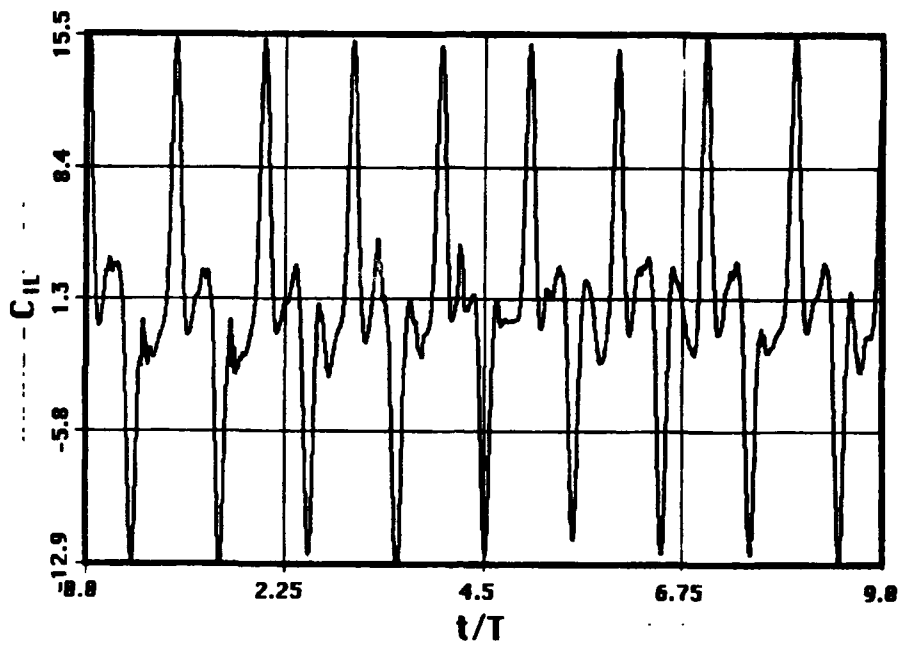Figure 69. Vorticity Contours, $K = 4$, $Re = 800$, $V_r = 0.6$, $t/T = 9.0$ ("Steep Sine" Oscillation)

Figure 70. Inline Force Coefficient, K = 4, Re = 800, V_r = 0.7
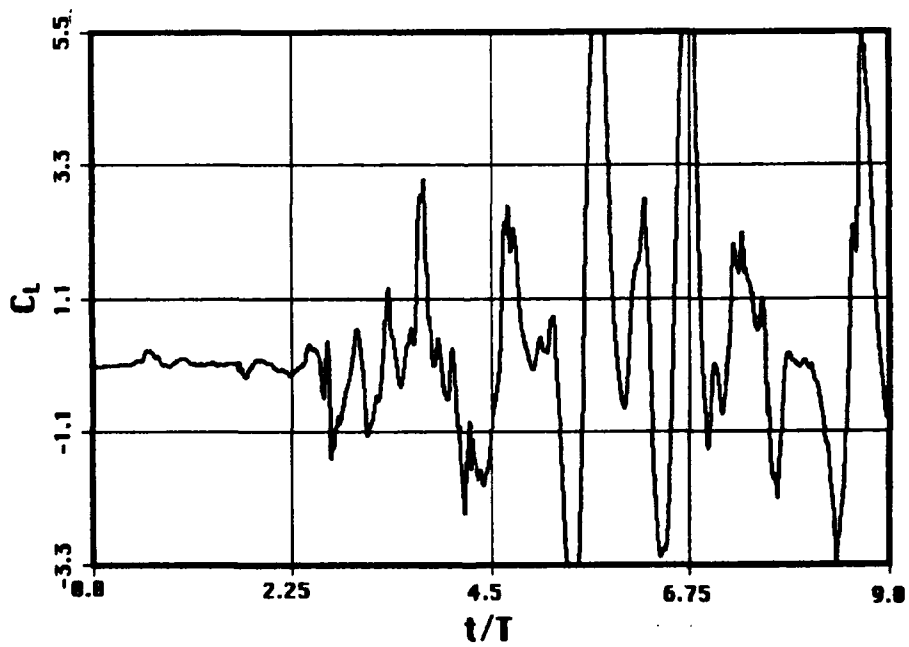("Steep Sine" Oscillation)

Figure 71. Transverse Force Coefficient, K = 4, Re = 800, V_r = 0.7
("Steep Sine" Oscillation)

81

Figure 72. Closeup View of Streaklines, K = 4, Re = 800, V_r = 0.7, t/T = 9.0 ("Steep Sine" Oscillation)

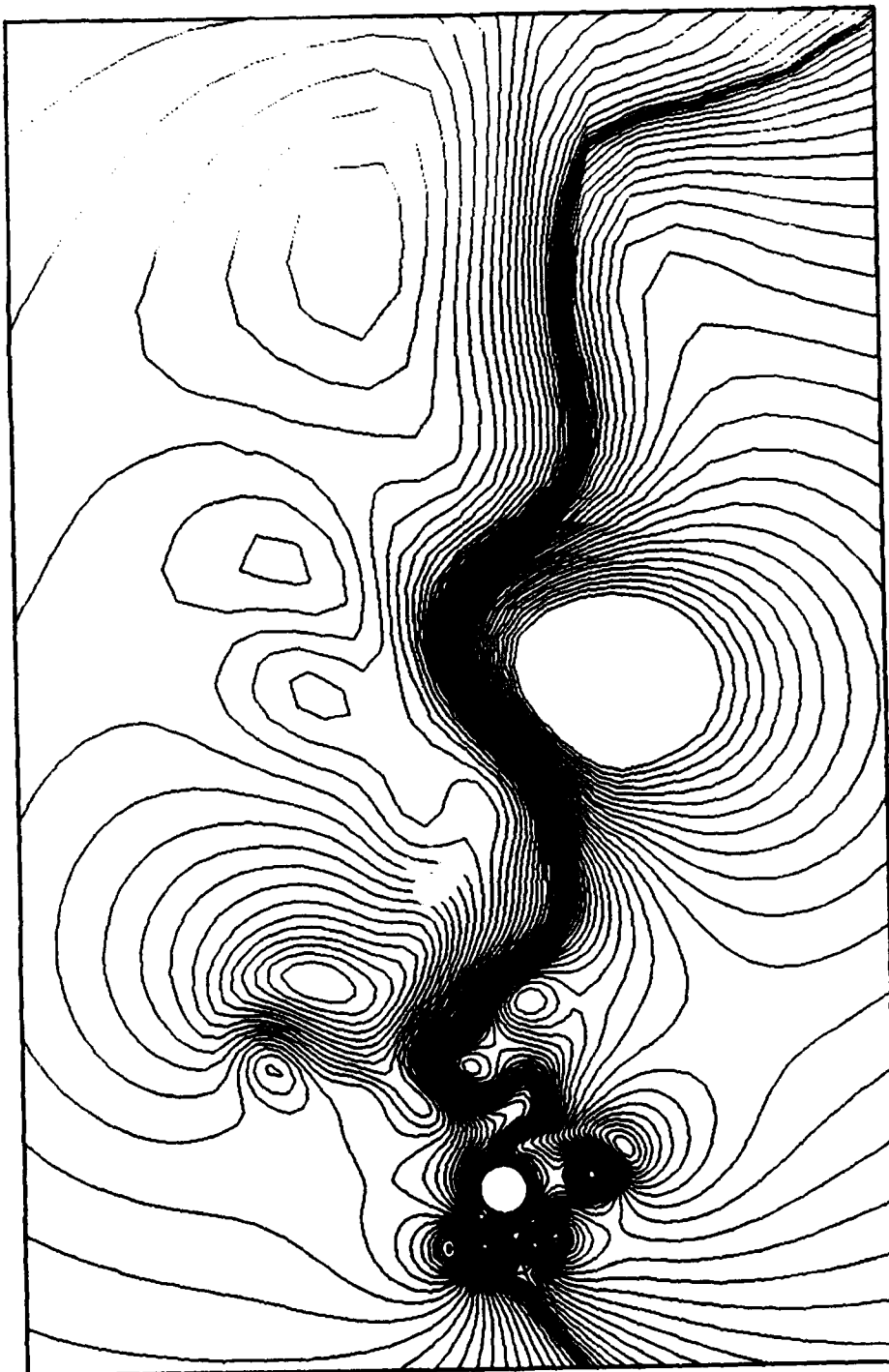Figure 73. Streaklines, K = 4, Re = 800, V_r = 0.7, t/T = 9.0 ("Steep Sine" Oscillation)

Figure 74. Streamlines, K = 4, Re = 800, V_r = 0.7, t/T = 9.0 ("Steep Sine" Oscillation)

Figure 75. Vorticity Contours, K = 4, Re = 800, V_r = 0.7, t/T = 9.0
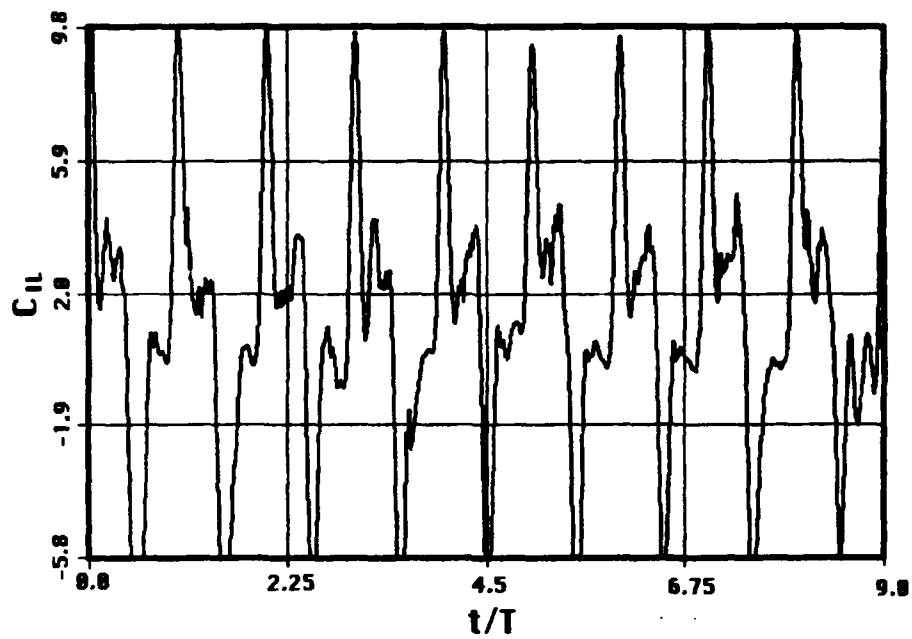("Steep Sine" Oscillation)

Figure 76. Inline Force Coefficient, K = 6, Re = 1200, V_r = 0.6
("Steep Sine" Oscillation)

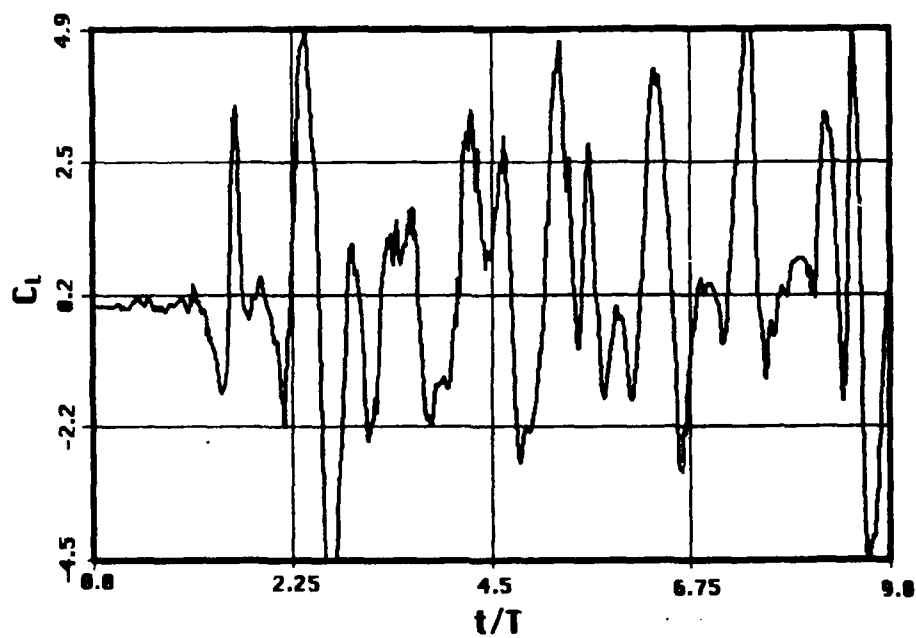Figure 77. Transverse Force Coefficient, K = 6, Re = 1200, V_r = 0.6
("Steep Sine" Oscillation)

Figure 78. Closeup View of Streaklines, $K = 6$, $Re = 1200$, $V_r = 0.6$, $t/T = 9.0$ ("Steep Sine" Oscillation)

87

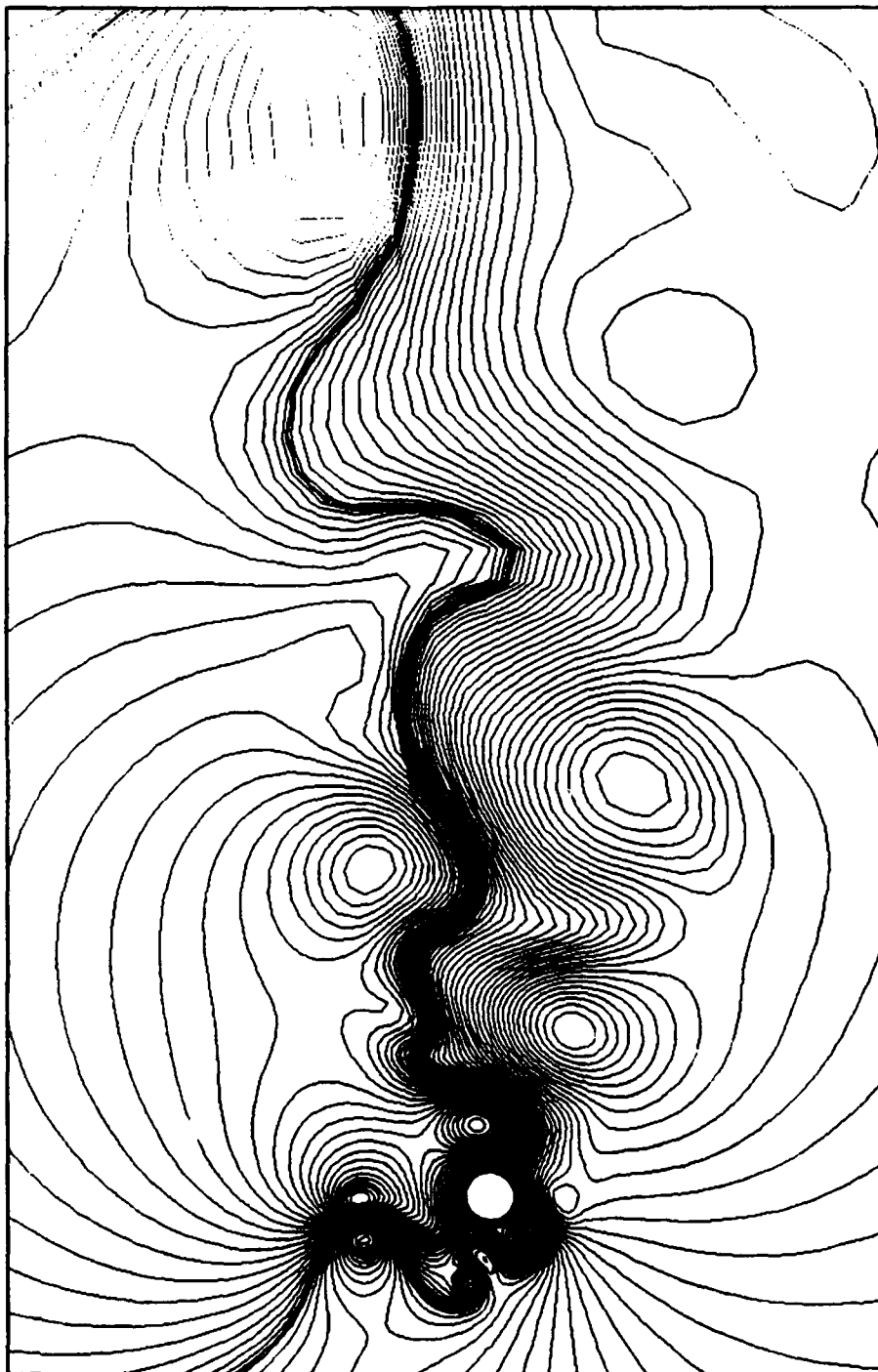Figure 79. Streaklines, $K = 6$, $Re = 1200$, $V_r = 0.6$, $t/T = 9.0$ ("Steep Sine" Oscillation)

Figure 80. Streamlines, K = 6, Re = 1200, V_r = 0.6, t/T = 9.0 ("Steep Sine" Oscillation)

89

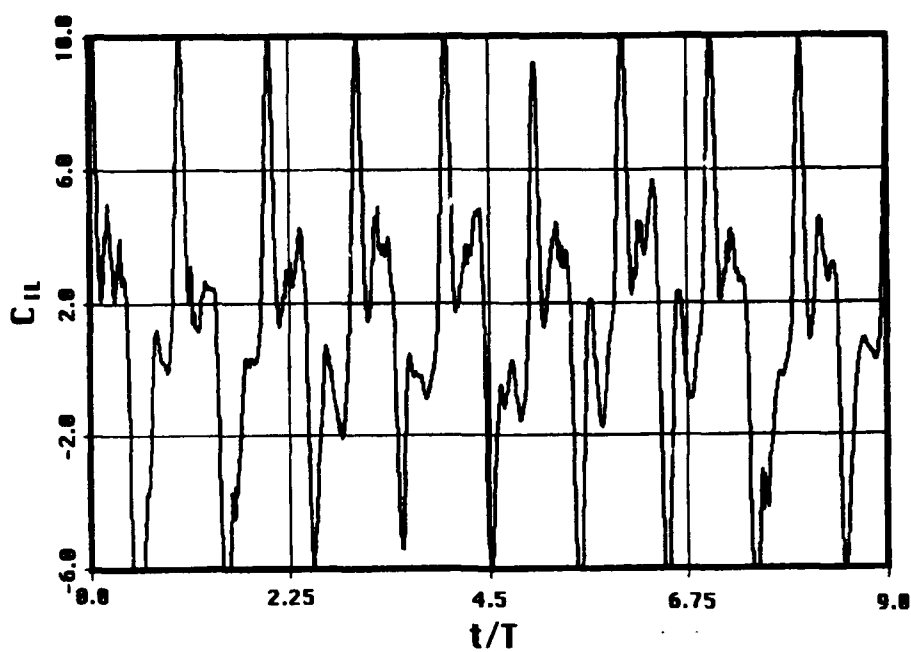Figure 81. Vorticity Contours, K = 6, Re = 1200, V_r = 0.6, t/T = 9.0 ("Steep Sine" Oscillation)

Figure 82. Inline Force Coefficient, K = 6, Re = 1200, V_r = 0.7
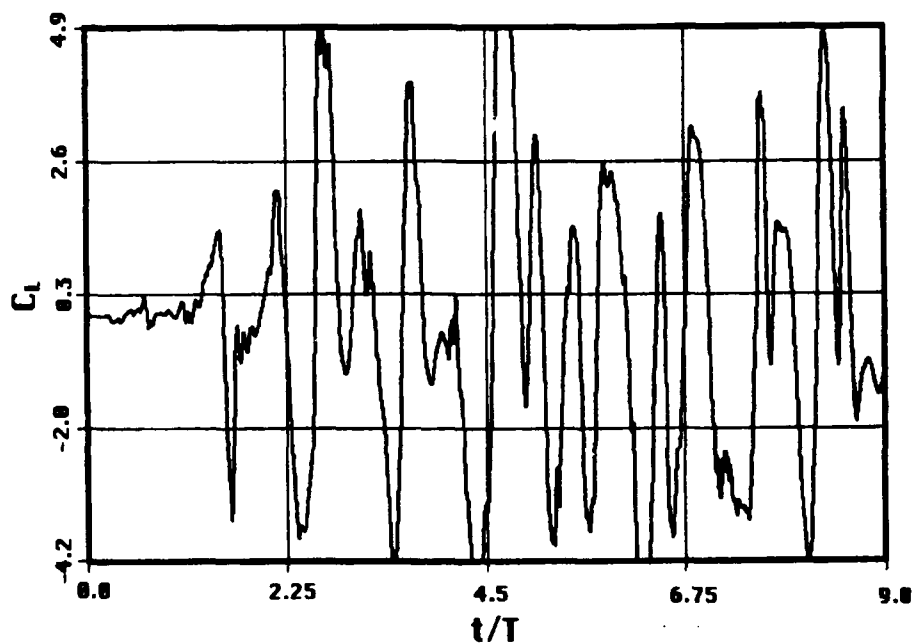("Steep Sine" Oscillation)

Figure 83. Transverse Force Coefficient, K = 6, Re = 1200, V_r = 0.7
("Steep Sine" Oscillation)

91

Figure 84. Streaklines, K = 6, Re = 1200, V_r = 0.7, t/T = 9.0
("Steep Sine" Oscillation)
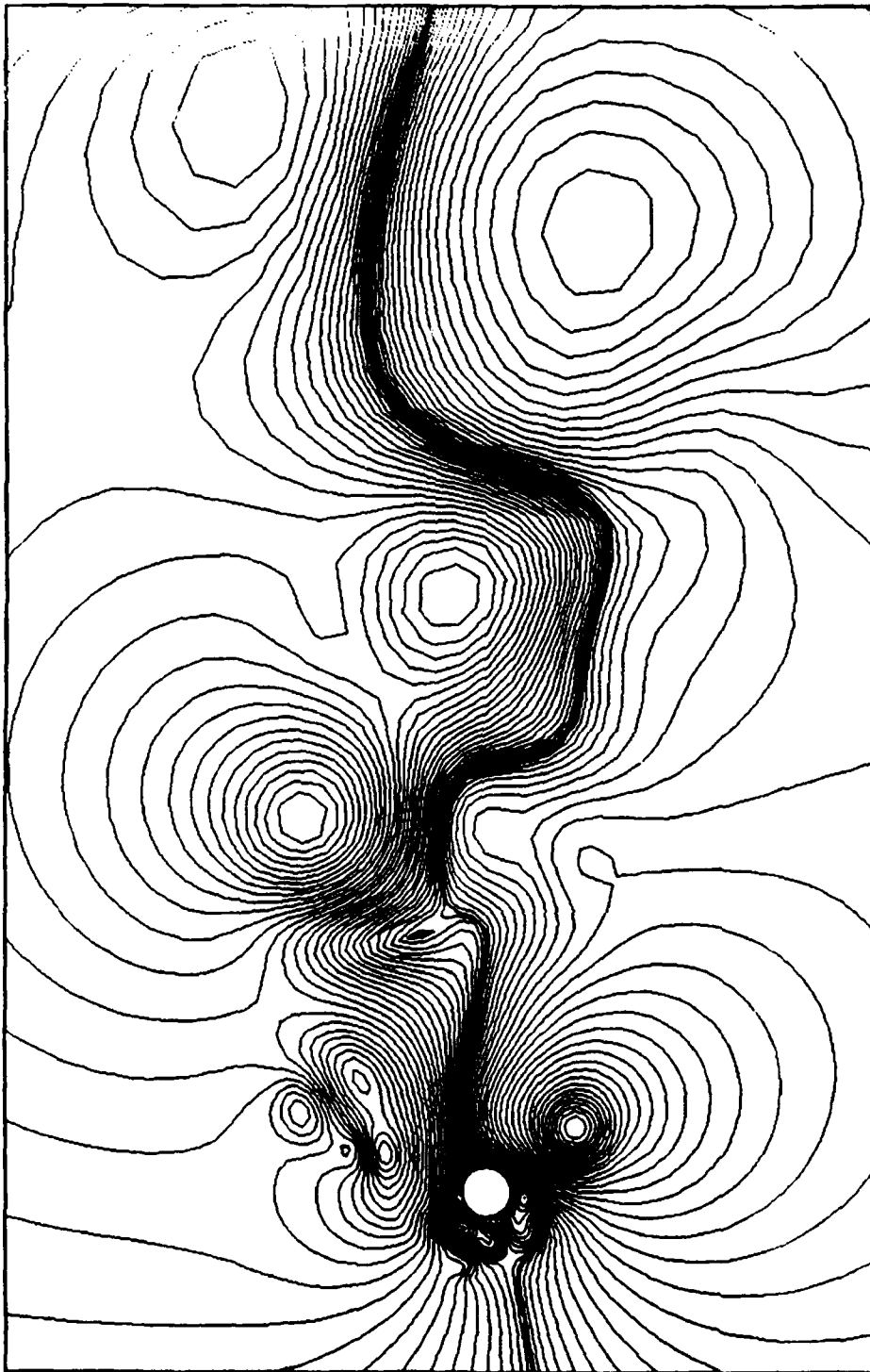
Figure 85. Streamlines, K = 6, Re = 1200, V_r = 0.7, t/T = 9.0
("Steep Sine" Oscillation)

Figure 86. Vorticity Contours, K = 6, Re = 1200, V_r = 0.7, t/T = 9.0
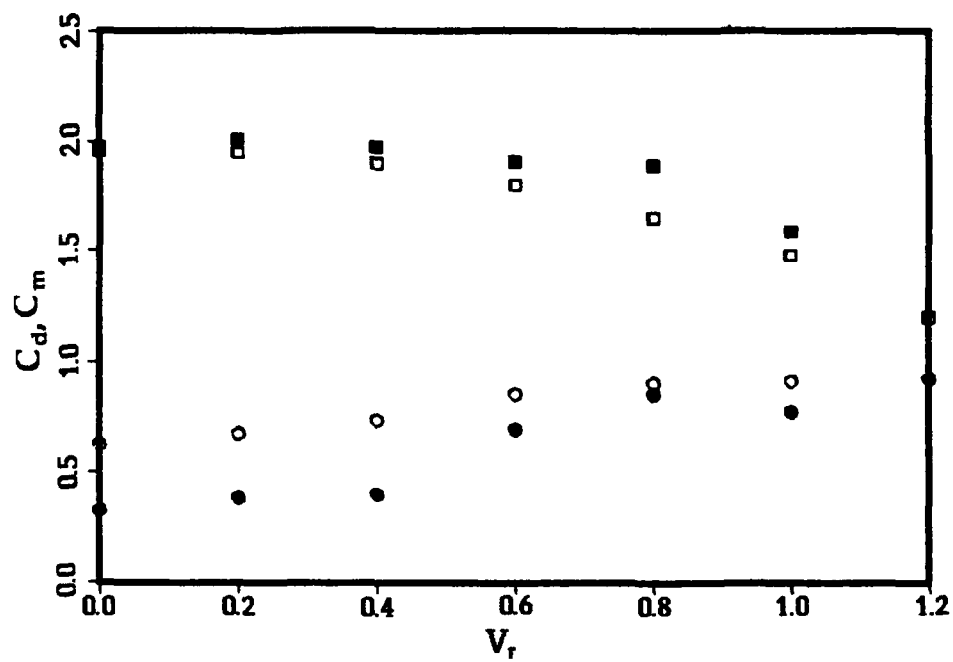("Steep Sine" Oscillation)

Figure 87. C_d and C_m versus V_r, K = 4, b = 200, n = 8.
C_d numerical (solid circles), C_m numerical (solid squares)
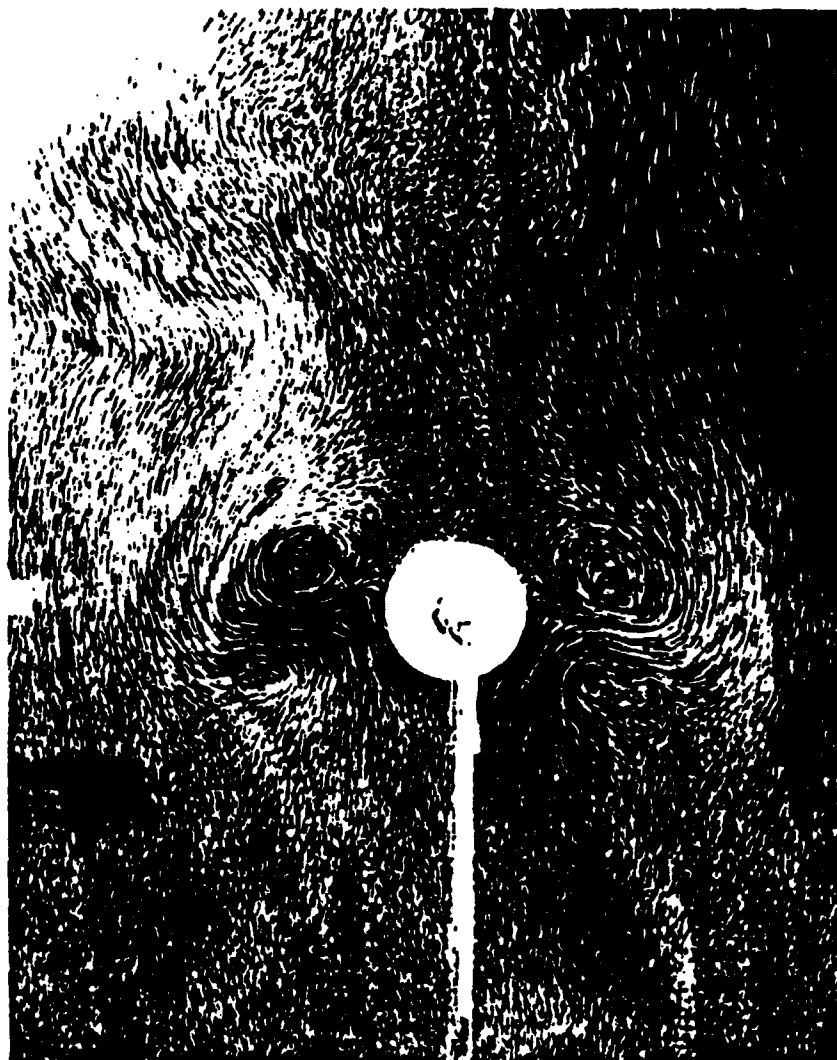C_d experimental (open circles), C_m experimental (open squares)

95

Figure 88. Flow Visualization for K = 4, V_r = 0.8, t/T = 8-7/8

REFERENCES

1. Baba, N. and Miyata, 1987, H., "Higher-Order Accurate Difference Solutions of Vortex Generation from a Circular Cylinder in an Oscillatory Flow," *Journal of Computational Physics*, Vol. 69, pp. 362-396.

2. Fredrickson, K., 1990, *Numerical Study of Non-impulsively Started Flow Around a Circular Cylinder*, M.S. Thesis, Naval Postgraduate School, Monterey, CA.

3. Justesen, P., 1991, "A Numerical Study of Oscillating Flow Around a Circular Cylinder," *Journal of Fluid Mechanics*, Vol. 222, pp. 157-196.

4. Justesen, P., and Spalart, P. R., 1990, "Two-Equation Turbulence Modeling of Oscillatory Boundary Layers," AIAA Paper No. 90-0496.

5 Lecointe, Y., and Piquet, J., 1984, "On the Use of Several Compact Methods for the Study of Unsteady Incompressible Viscous Flow Round a Circular Cylinder," *Computers &Fluids*, Vol. 12, No. 4, pp. 255-280.

6. Murashige, S., Hinatsu, M., and Kinoshita, T., 1989, "Direct Calculations of the Navier-Stokes Equations for Forces Acting on a Cylinder in Oscillatory Flow," In Proceedings of the Eight International Conference on Offshore Mechanics and Arctic Engineering, The Hague, Vol. 2, pp. 411-418.

7. Putzig, C. J., 1991, "Numerical Experiments in Unsteady Flows through the use of Full Navier-Stokes Equations," M.S. Thesis, Naval Postgraduate School, Monterey, CA.

8. Sarpkaya, T. and Butterworth, W., 1991, "Separation Points on a Cylinder in Oscillating Flow," In *Proc. Ninth Intl. Conf. Offshore Mech. and Arctic Engng. Stavanger* (in Press in the *Journal of Offshore Mechanics and Arctic Engineering*, ASME).

9. Sarpkaya, T. and Isaacson, 1981, M., *Mechanics of Wave Forces on Offshore Structures*, Van Nostrand Reinhold, New York, NY.

10. Sarpkaya, T. and Storm, M., 1985, "In-line Force on a Cylinder Translating in Oscillating Flow," *Applied Ocean Research*, Vol. 7, No. 4, pp. 188-196.

11. Wang, X., 1989, *A Numerical Study of Unsteady Flows Past A Circular Cylinder*, Ph.D. Dissertation, University of Houston, Houston, TX.